THE ROLE OF DYNAMIN IN CELL-CELL

FUSION

by
Nathalie Gerassimov

A dissertation submitted to Johns Hopkins University in conformity with the
requirements for the degree of Doctor of Philosophy

Baltimore, Maryland

June 2018

Abstract

Myoblast fusion leads to the formation of multinucleated muscle fibers and is essential for muscle development and regeneration. *Drosophila* embryonic muscle development has been an instrumental *in vivo* system to uncover evolutionarily conserved cellular and molecular mechanisms of myoblast fusion. Work from our lab has shown that myoblast fusion is promoted by a cell type-specific, F-actin-enriched podosome-like structure (PLS) that invades the apposing fusion partner with multiple finger-like protrusions at the fusogenic synapse. Here, we shown that the conserved large GTPase Dynamin (Dyn), best known for its function in endocytosis, is a critical component of myoblast fusion *in vivo*. Interference with Dyn function during myoblast fusion using two different temperature-sensitive alleles of *Drosophila* Dyn, *shibire*^{ts} (*shi*^{ts}), leads to a severe myoblast fusion defect, which can be rescued by overexpressing wild-type Dyn. Furthermore, RNAi knockdown of Dyn in cultured cells that are induced to fuse also results in a fusion defect, suggesting a general role for Dyn in cell-cell fusion. We show that Dyn is enriched within the F-actin foci at the fusogenic synapse in wild-type embryos and that the F-actin foci exhibit abnormal morphology in *shi*^{ts} mutant embryos at restrictive temperature, indicating a function of Dyn in organizing these actin-enriched structures. Interestingly, electron microscopy analysis revealed no endocytic vesicles at the fusogenic synapse where Dyn is enriched in wild-type embryos, and no collared pits indicative of blocked endocytosis are observed at the fusogenic synapse in *shi*^{ts}

mutant embryos at restrictive temperature, suggesting that endocytosis may not play a direct role in myoblast fusion. Together, our findings strongly support a novel endocytosis-independent function of Dyn in regulating F-actin organization during cell-cell fusion.

Faculty Sponsor: Elizabeth H. Chen, Ph.D.

Reader: Deborah Andrew, Ph.D.

Acknowledgements

"Our power lies in our small daily choices, one after another, to create eternal ripples of a life well lived." - Mollie Marti

First and foremost I want to thank the three female mentors who have guided me in my scientific maturation. Your advice has accompanied me from my first PCR to my most crucial experiments.

Dr. Gudrun Ihrke was the first scientist that I got to know well and my first research mentor prior to graduate school. From her I learned the joy of research and through her I gained the confidence to attempt this journey. These are only a few of the reasons why I will never be able to express sufficiently how grateful I am to have had the honor of working with her.

I would like to thank my advisor, Dr. Elizabeth Chen, for her patience and support in my pursuit of scientific studies. She has supported me through the ups and downs of scientific research and through personal and professional maturation process. I have learned many things from Dr. Chen that will help me approach the future more fearlessly.

Dr. Erika Matunis was so gracious to accept me in her lab once the Chen lab relocated to another university so I could continue my thesis research. I will always be grateful for that. Additionally, having the chance to experience her energetic approach to life/science/mentorship has strongly influence my own approach to these matters.

"It takes a whole village to raise a child." - Igbo and Yoruba (Nigeria) Proverb

Next, I want to thank my thesis committee members who have supported me through their thoughtful advice, namely, Dr. Geraldine Seydoux, Dr. Debbie

Andrew, Dr. Doug Robinson, and Dr. Carolyn Machamer. It is an honor to have had the benefit of your experience.

"We speak not only to tell other people what we think, but to tell ourselves what we think. Speech is a part of thought." - Oliver Sacks

I was fortunate to have been part of two excellent labs during my studies, both of which have left their mark on me. In the Chen lab I have benefited from the advice of many experienced scientists. In our lab meetings I have practiced scientific thought and experimental design. In the Matunis lab I have found many friends who reminded me how much more fun it is to work surrounded by friends. I have also learned a lot from the Matunis Lab members.

"If I have seen a little further it is by standing on the shoulders of Giants." - Isaac Newton

Dr. SangJoon Kim laid the foundation for my dissertation research by initiating this project and generating many of the mutant versions of the gene I used in my experiments. Dr. JiHoon Kim was also instrumental in guiding me towards the completion of my research. I am grateful to both of them for their support.

"Family is not an important thing. It's everything." - Michael J. Fox

I would also like to thank my family, my mother Nadja Ulbrich and my aunt and uncle Nataliya and Vitalik Prytkov, for their support of my ambitions. My academic path started with those reading and writing lessons in my childhood. Additionally, my husband Manpreet Bumra played an instrumental role in me achieving this milestone. It is true that he deserves an honorary Ph.D. for the amount of time he spent waiting while I was finishing experiments.

Table of Contents

List of Tables

List of Figures

Chapter 1: Introduction

Summary

This chapter serves as an introduction to myoblast fusion in the *Drosophila melanogaster* embryo. Emphasis is given to the F-actin rich focus mediating myoblast fusion at contact site of fusing cells (fusogenic synapse). Furthermore, Dynamin (Dyn), a large GTPase best known for its role in endocytosis, is discussed.

Cell-cell fusion

Cell-cell fusion is a fundamental process during which two or more cells form a multinucleated syncytium by merging their cell membranes and cytoplasm (reviewed in Chen and Olson, 2005). This process is fundamental to fertilization, development, physiological maintenance and in particular: placenta formation, osteogenesis, immune response, myogenesis and muscle maintenance.

The merging of membranes is an energetically unfavorable process frequently accompanied by the use of a fusogen - a protein that when expressed in normally non-fusing cells can lead to cell-cell fusion - to force the two membranes to merge. To date, the *Drosophila* fusogen remains unknown. However, unbiased genetic screens uncovered the critical role of F-actin polymerization at the fusogenic synapse as a crucial component of myoblast fusion. There is emerging evidence that the role of F-actin in cell-cell fusion is conserved.

Drosophila body-wall musculature as an _in vivo_ system to study cell-cell fusion

Morphology of larval body-wall musculature

Larval body-wall musculature (also called somatic musculature) has served as a prime model system for studying the mechanism underlying myogenesis because of the molecular and genetic tools available. A *Drosophila* larva has a head followed by 11 segments – three of which make up the thorax (T) and eight make up the abdomen (A) - numbered starting from the head

(Figure 1.1 A). For orientation, each segment can be divided midsagittally into two hemisegments. Underneath the surface made of the cuticle and the epidermis lies the larval body-wall musculature (Figure 1.1 B). Hemisegments A2 through A7 each have a precise pattern of 30 muscle fibers (the muscle pattern is modified slightly in A1 and more significantly in A8 and the thorax; Figure 1.1 C; Bate, 1990). *Drosophila* muscle fibers are comprised of a single myotube with relatively few nuclei (3 to 30) unlike their more complex vertebrate counterpart, the skeletal muscles. Each muscle has a stereotypical position, shape, attachment, and nuclei number and can be grouped by its respective position into dorsal (D), lateral (L), or ventral (V) muscle groups (Figure 1.1 C). This precise muscle fiber arrangement is well suited for scientific studies investigating cell specification, attachment and myoblast fusion.

Embryonic progression of the early mesoderm to somatic progenitors

Larval body-wall musculature is derived from a portion of the mesoderm during embryogenesis. Early on, the mesoderm is specified on the ventral site of the embryo and is invaginated during gastrulation. The cells of the mesoderm then dissipate during an epithelial-to-mesenchymal transition and migrate dorsally along the ectoderm to form a layer under the epidermis. As the embryo undergoes germ band extension, the mesoderm is patterned into the precursors of somatic and visceral muscles as well as the heart. The key determinant in this process is the level of Twist (Twi), a basic Helix-Loop-Helix transcription factor.
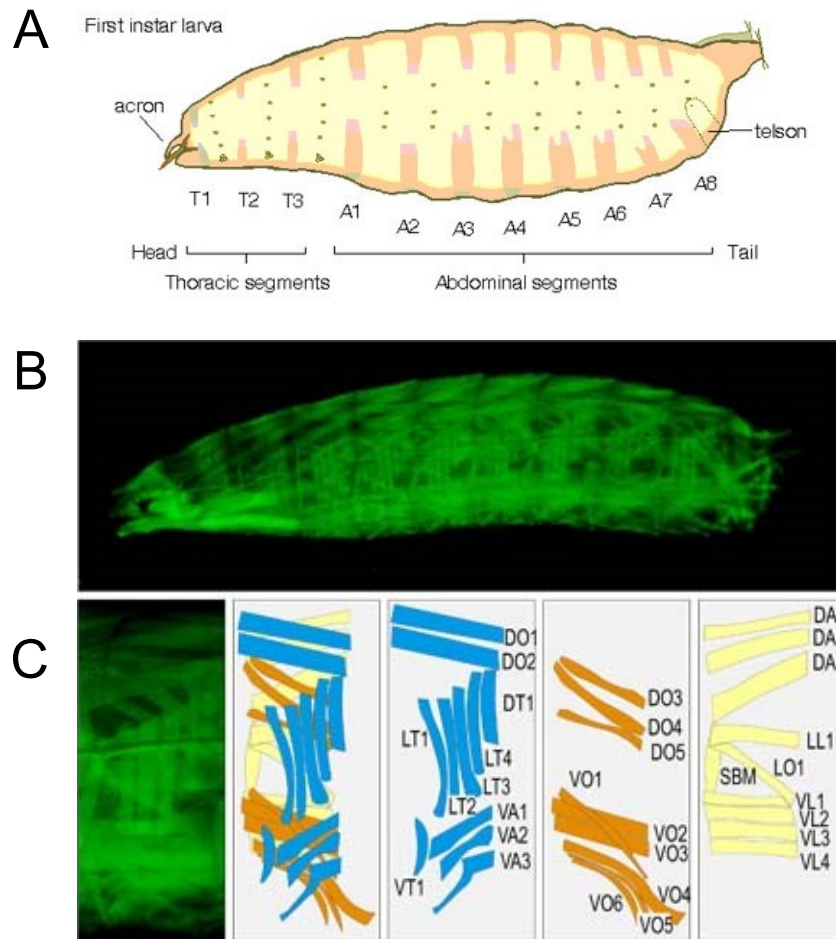
Figure 1.1 *Drosophila* body wall musculature has a precisely repeated pattern.

(A) The larva consists of a head followed by thoracic and abdominal segments.

(B) Larval body wall musculature was visualized using an encoded muscle-specific GFP construct. This view shows the muscle pattern of each hemisegments.

(C) The muscle arrangement of the 30 muscle fibers of an abdominal hemi-segment is represented. Each muscle can be grouped by its respective position into dorsal (D), lateral (L), or ventral (V) muscle groups. Muscles closest to the epidermis are shown in blue.

Image source:
http://www.mun.ca/biology/desmid/brian/BIOL3530/DB_02/fig2_7.jpg
http://www3.mpibpc.mpg.de/groups/vorbrueggen/pages/Myogenesis_intro.html

The mesoderm has alternating regions of high and low Twist expression; high levels of twist drive cells into somatic myogenesis, whereas low Twist expression allows for differentiation of other mesoderm derivatives (Baylies and Bate, 1996). Thus, high Twist expression is the key determinant for somatic myogenesis.

<u>Somatic musculature formation requires the specification of two cell types - founder cells and fusion competent myoblasts (FCMs)</u>

Midway through embryogenesis, muscle precursors - small syncytia containing two to three nuclei - appear (Bate, 1990). These precursors establish their attachments to the epidermis and undergo subsequent rounds of myoblast fusion to form larger myotubes. Preceding precursor formation is the specification of two distinct cell types, muscle founder cells and FCMs (Bate 1990; Dohrmann *et al*. 1990). The myoblast fusion defect in *myoblast city* (*mbc)* provided the first genetic evidence for the founder cell hypothesis (Rushton *et al*., 1995). Because of an almost complete absence of myoblast fusion, founder cells remain mononucleated but establish correct position, orientation and innervation of their respective myotubes – leading to the appearance of long, stretched out, mononucleated muscle fibers (Figure 1.2 B shows an example of a fusion defect which is not *mbc*). The surrounding FCMs remain as a generic pool of dispersed round mononucleated single cells (Figure 1.2 B and C).
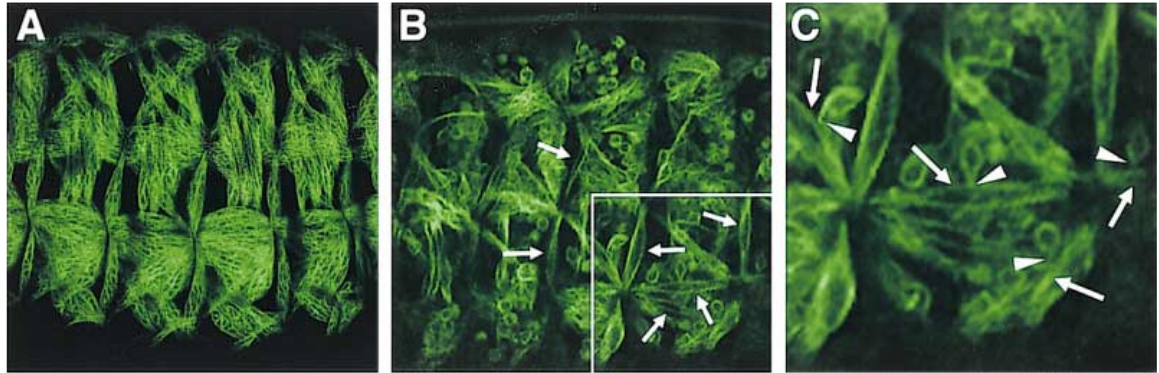
Figure 1.2 Forward genetic screens for myoblast fusion-defective mutants formed the basis for investigating the cellular and molecular mechanisms of myoblast fusion.

  (A-B) Four hemisegments with their muscle fibers were visualized by microtubule-bound GFP. Embryos are oriented with dorsal up and anterior to the left.

  (A) Wildtype (wt) body-wall musculature

  (B) One representative fusion defect phenotype with elongated mononucleated muscle founder cells (long arrows). GFP signal is restricted to the cytosol and excluded from nuclei.

  (C) The boxed region in B was magnified to emphasize round mononucleated FCMs attached to stretched out founder cells (arrow heads)

Image Source: Chen and Olson, 2001.

The founder cells/muscle precursors/myotubes express one or more "muscle identity" proteins such as Even skipped (Eve), Slouch (Slou) and Ladybird (Lb) and act as "seeds" that establish the identity of the muscle (most identity proteins are typically expressed in a few muscle fibers; Figure 1.3). The surrounding FCMs also have cell-type specific markers such as Lame duck (Lmd), a Gli superfamily transcription factor, required for the specification and differentiation of FCMs (Figure 1.4 A and B; Duan *et al*., 2001). Myoblast fusion leads to the incorporation of the FCM nucleus into the founder cell/muscle precursor. The newly incorporated nucleus adopts the expression profile of the founder cell/muscle precursor shortly thereafter.

Cell-type specific recognition and adhesion

Once the founder cells and FCM are specified, they need to recognize each other and adhere to each other prior to cell-cell fusion. These processes are mediated by the interaction of cell-type specific Immunoglobulin (Ig)-domain containing cell adhesion molecules (CAMs).

The founder cells have two functionally redundant Ig-CAMs, Dumbfounded (Duf) and Roughest (Rst) (Ruiz-Gomez *et al*., 2000; Strünkelnberg *et al*., 2001). In the absence of both, no myoblast fusion occurs. Additionally, when Duf or Rst are ectopically expressed in the epidermis, they each attract FCMs to that location possibly by a mechanism involving myoblasts randomly exploring their surrounding space via filopodia (Ruiz-Gomez *et al*., 2000).
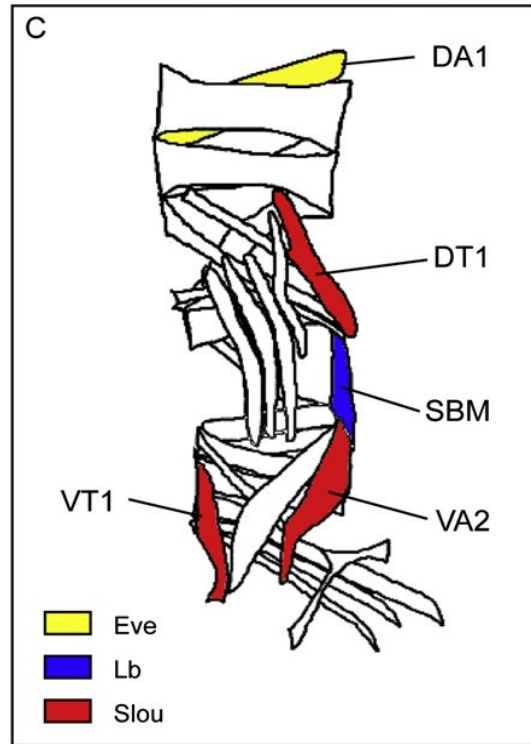
Figure 1.3 Muscle identity proteins characterize specific myotubes

Schematic of a hemisegment's muscle pattern with colored in myotubes expressing specific muscle identity proteins – Eve, Ladybird (Lb or Lbe) and Slou. On average, DA1 muscle has 11 Eve-positive nuclei, segment border muscle (SBM) has 7 Lb-positive nuclei, and DT1, Vt1 and VA2 have 8, 4 and 9 Slou-positive nuclei, respectively.

Image Source: Bataillé *et al*. 2010.

Alternatively, founder-cell specific CAMs may undergo ectodomain shedding where the extracellular portion is cleaved off and acts as a diffusible attractant (Ruiz-Gomez *et al*., 2000; Chen and Olson 2001).

FCMs also have two cell-type specific Ig-CAMs, Sticks and stones (Sns) and Hibris (Hbs) (Bour *et al*., 2000; Artero *et al*., 2001). Sns is the major CAM since *sns* null mutants have a severe fusion defect whereas *hbs* null mutants have only a mild fusion defect (Artero *et al*., 2001). The severity of the fusion defect in *sns hbs* double mutants is not noticeably different from the *sns* mutant (Artero *et al*., 2001). However, myoblast fusion is slightly improved when Hbs is overexpressed in a *sns* null embryos indicating a partial redundancy in function (Shelton *et al*., 2009). Thus, Sns is the essential Ig-CAM in FCMs for myoblast fusion and Hbs is a less efficient paralog.

The Ig-CAMs interact in a cell-type specific manner with each other to form an attachment between founder cells and FCMs. Specifically, the most N-terminal Ig-domains of Duf and Sns interact with each other directly, and the resulting complex places the two extracellular domains in a $90°$ to $110°$ angle to each other (Özkan *et al*., 2014). The engagement of the cell-type specific CAMs in *trans* initiates the signaling that recruits the actin machinery to the contact site in both cells, which ultimately leads to myoblast fusion.

An F-actin focus, also known as a podosome-like structure (PLS), mediates
myoblast fusion

Following engagement of Duf and Sns, F-actin rich structures – called F-actin foci – can be observed at the contact site of the founder cell/muscle precursor and FCM (Figure 1.4 A-C; Kim *et al*., 2007; Kesper *et. al*; 2007, Richardson *et al*., 2007). These foci had an average size of 1.9 μm^2 (ranging from 0.7-4.5 μm^2; Richardson *et al*., 2007). Using live-imaging, it was shown that an F-actin focus marks the fusion site, and that it dissolves prior to FCM nucleus entry into the myotube (Richardson *et al*., 2007). The life span of F-actin foci was 11.9 minutes (ranging from 5.7– 29.5 minutes; Richardson *et al*., 2007). Further studies revealed that the dense F-actin focus resides exclusively in the FCM (Sens *et al*., 2010). The F-actin focus is seen as a protrusion that invades into the founder cell/muscle precursor membrane causing an inward curvature or "dimple" in the receiving cell (Figure 1.4 B). Ultrastructural investigation using electron microscopy (EM) revealed that the F-actin focus can contain invasive finger-like structures that protrude into the founder cell/muscle precursor (Figure 1.4 D). This structure is called a podosome-like structure (PLS) based on several similarities with podosomes – F-actin-rich structures in monocyte-derived cells such as osteoclasts and macrophages (reviewed in McNiven *et al*., 2004). Both structures have a dense F-actin core surrounded by CAMs (Figure 1.4 C), a similar size and life span and both are protrusive (Sens *et al*., 2010).

A

| A phalloidin | A' β-Gal Lmd | A" merge |

B

| α–Duf | phalloidin | merge |

C

| α–Duf | α–Sns | phalloidin | merge |

11
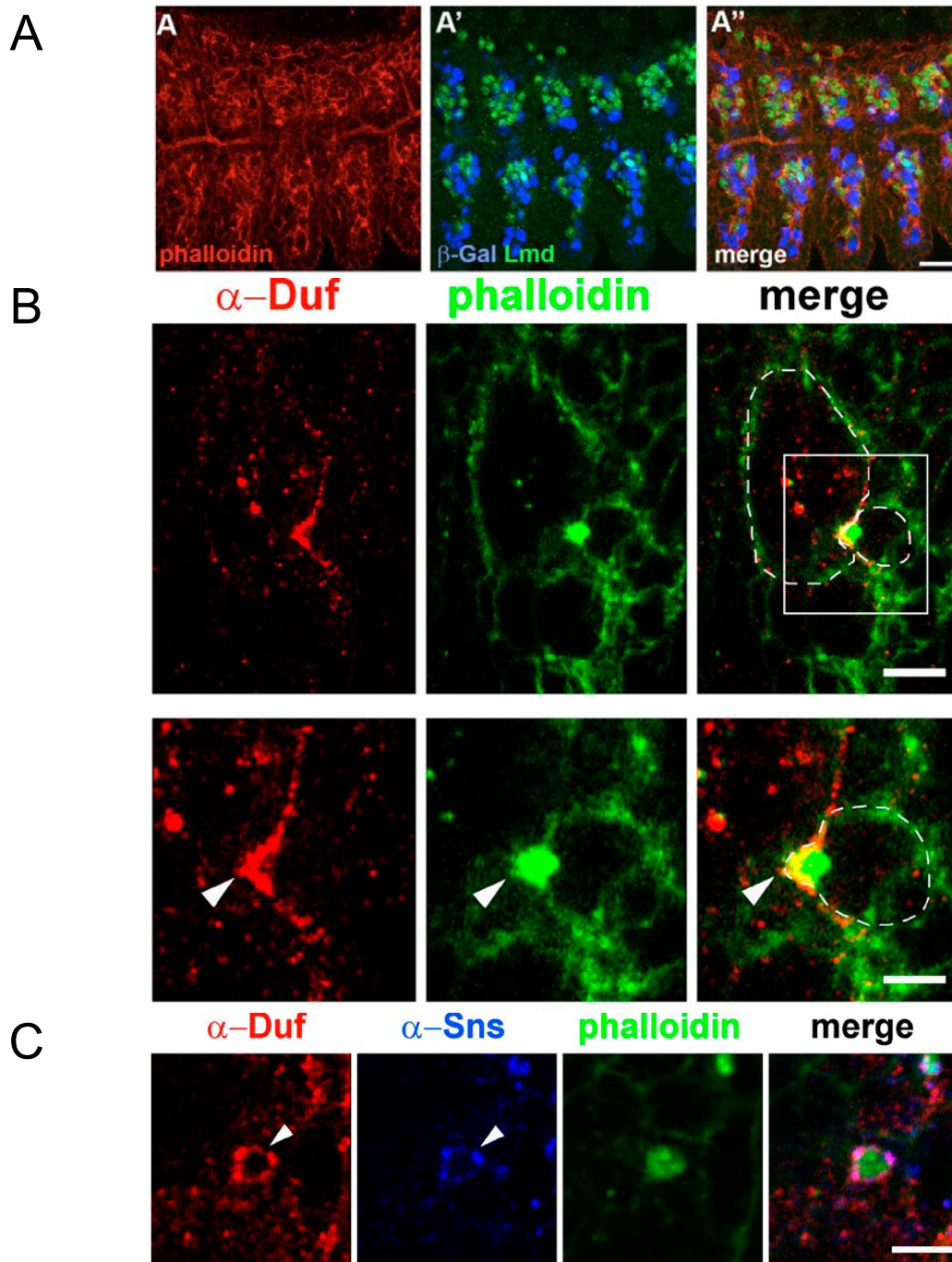
D
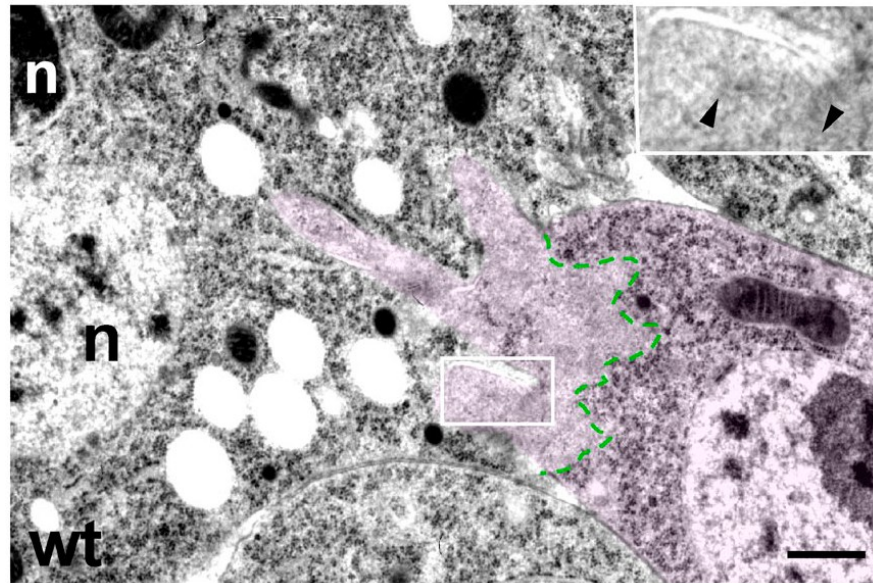
E
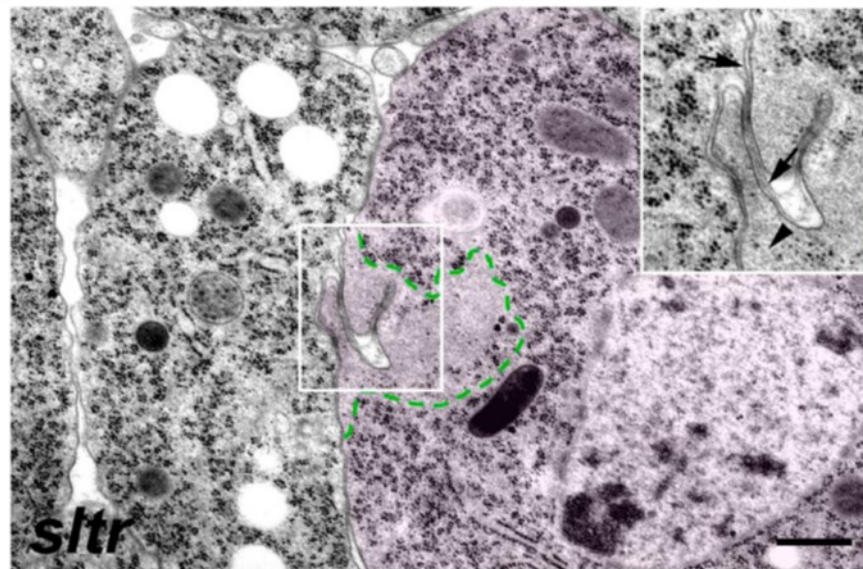
Figure 1.4 F-actin foci mark the site of myoblast fusion

(A) Phalloidin staining of a stage 14 embryo shows many F-actin foci at the contact site of the Lmd-positive FCMs (green) and muscle precursors expressing β-Gal (blue). Scale bar: 20 μm

(B) F-actin focus resides in the round FCM and invades into the muscle precursor at the fusion synapse marked by founder cell specific CAM, Duf. This invasion creates an invagination or a "dimple" in the muscle precursor marked by an arrow head. Scale bar: 10 μm in top and 5 μm in bottom panel.

(C) When the fusion synapse is visualized such that the invasion axis reached out perpendicularly from the plane, the F-actin focus appears as a dense F-actin circle surrounded by Duf and Sns. Scale bar: 5 μm

(D) F-actin focus – also named PLS - is an asymmetric structure mainly residing in the FCM. In EM micrographs the F-actin is denoted by an absence of small black dots (ribosomes). The PLS consists of a "palm" with on average 4 "fingers" that invade into the multinucleated muscle precursors. Scale bar: 500 nm

(E) Myoblast fusion mutants display aberration in this structure. For example *sltr* has an inability to invade into the muscle precursor. Scale bar: 500 nm

Image Sources: Richardson *et al*. 2007 for (A); Sens *et al*., 2010 for (B-D).

Cell-type specific signaling cascades required for myoblast fusion

Small GTPase Rac

Even before the crucial role of F-actin foci was established, several lines of evidence pointed to the importance of actin for myoblast fusion. The overexpression of either dominant-negative or constitutively-active Rac 1 – a member of the Rho family of small GTPase known to regulate cytoskeleton-membrane interactions – caused myoblast fusion defects (Luo *et al*., 1994). *Drosophila* has two Rac genes, *rac1* and *rac2* which are both required for myoblast fusion, since fusion is defective in *rac1 rac2* double mutants but not in either single mutant (Hakeda-Suzuki *et al*., 2002). The fusion defects in *rac1 rac2* double mutants can be rescued by specific expression of Rac1 in either FCMs or founder cells, but rescue is more significant when it is expressed in FCMs (Haralalka *et al*., 2011). Furthermore, two more genes implicated the Rac pathway, namely *mbc*, the *Drosophila* homologue of Dock180, and *ELMO/Ced-12* - which together form a Rac GTPase specific bipartide guanine exchange factor (GEF) (Erickson *et al*., 1997; Nolan *et al*., 1998; Geisbrecht *et al*., 2008). Later studies using cell-type specific rescue experiments in *mbc* mutant embryos showed that MBC is required in the FCMs and not in the founder cells (Haralalka *et al*., 2011). Activation of Rac by certain members of the Dock180 family and ELMO occurs by at least three different mechanisms: ELMO can stabilize the Dock180/Rac (nucleotide-free) complex formation or relieve steric inhibition of Dock180 or facilitate translocation of Dock180-ELMO complex to the plasma membrane (Lu and Ravichandran, 2006). It is unclear which of the three is

utilized in the FCMs during *Drosophila* myoblast fusion. It appears that Rac activation in the founder cell is independent of the Mbc/ELMO complex and probably relies on a different GEF. Rac activation is essential for myoblast fusion because it contributes to the downstream activation of the Arp2/3 complex which is required in both cell types. However, signaling upstream of Arp2/3 in the two cell-types is different and is thought to underlie the asymmetric nature of the F-actin focus.

Arp2/3 complex and its activators, WASp and SCAR/WAVE

Arp2/3 complex is a seven-subunit protein complex which nucleates F-actin polymerization on existing filaments resulting in formation of branched actin filaments that underlie F-actin focus formation. Arp2/3 complex requires activation by the members of the Wiskott-Aldrich syndrome protein (WASp) family which has two major branches based on their distinct domains: WASp and SCAR/WAVE (reviewed in Pollitt and Insall, 2009). The N-termini of WASp proteins have a WASp homology 1 (WH1) domain and CRIB domain. SCAR/WAVE proteins have on their N-termini a SCAR homology domain (SHD). Both branches have the VCA domain which includes a WASp homology 2 domain (WH2), which binds monomeric actin; and a central (C) region; and an acidic (A) domain, which together binds the Arp2/3 complex. In *Drosophila* there is one WASp gene and one SCAR/WAVE gene, and both have been implicated in myoblast fusion.

SCAR/WAVE is required in both cell types during myoblast fusion and is activated by Rac. SCAR/WAVE proteins, when inactive, exist in a five protein complex: SCAR/WAVE, Sra1/PIR, Kette/Nap1, Abi, HSPC 300. Activated Rac interacts directly with the Sra1/PIR subunit, thereby dissociating the complex and activating SCAR. Zygotic deletion of SCAR leads to a mild fusion defect (Richardson *et al*., 2007). This fusion defect can be made more severe when the maternal contribution of SCAR is reduced (Richardson *et al*., 2007). Furthermore, zygotic mutant of *kette* displays a severe fusion defect (Schröter *et al*., 2004). Interestingly, F-actin foci form in *scar* maternal/zygotic mutants and *kette* mutants and appear to have similar invasion depths as wildtype F-actin foci indicating that SCAR is not required for F-actin foci invasiveness (Figure 1.5; Sens *et al*., 2010). Zygotic loss-of-function of an essential component of the Arp2/3 complex, Arp66B, has only a mild fusion defect likely because of maternal contribution (Richardson *et al*., 2007). Taken together the following signaling cascade emerges (Figure 1.6): the engagement of cell-type specific CAMs leads to the downstream activation of Rac, SCAR and Arp2/3 in founder cells/muscle precursors and FCMs.

An alternative interpretation of the small rescue of fusion by founder cell specific Rac expression in *rac1 rac2* mutant embryos is that the driver used (rP298-GAL4) has a ~8-10% leaky expression in FCMs (Sens *et al*. 2010). In this model, Rac and Mbc don't function in the founder cells and SCAR in the founder cells is activated by something other than Rac (Figure 1.6)
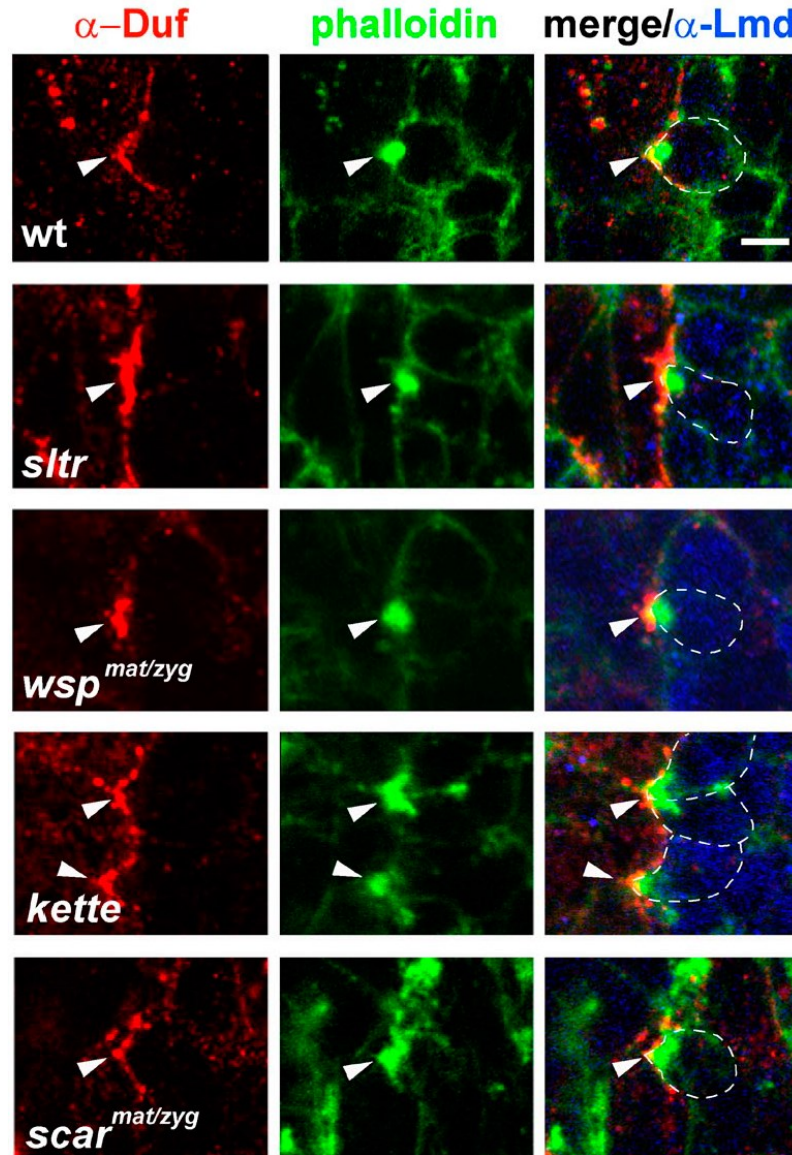
Figure 1.5 The F-actin focus invasiveness requires WASp but not SCAR

In wt embryo the F-actin focus (visualized by phalloidin staining in green) pushes into the founder cell and creates a dimple (visualized by anti-Duf staining). The invasiveness of the F-Actin foci is compromised in *sltr* and *wasp^mat/zyg* mutant implicating the crucial role of WASp in this process. The invasiveness of the F-actin focus seems unaffected in *kette* and *scar^mat/zyg* mutants.

Image Source: Sens *et al*., 2010.

The F-actin at the fusogenic synapse is asymmetric with a dense oval-shaped F-actin focus residing in the FCM and a thin sheath of F-actin residing in the founder cell. This may be explained by FCM-specific activity of another Arp2/3 complex activator, WASp. WASp is required for fusion: maternal/zygotic *WASp* null embryos have a severe myoblast fusion defect (Kim *et al*., 2007, Massarwa *et al*., 2007). Furthermore, the expression of a dominant-negative form of WASp in the *Drosophila* embryo mesoderm causes a severe fusion defect, but expressing it in the founder cells alone doesn't cause a fusion defect, implying that wildtype WASp acts in the FCMs during fusion (Schäfer *et al*., 2007). Same study showed that WASp-GFP is enriched at the fusogenic synapse when expressed in the mesoderm. There was no FCM-specific Gal4 driver at the time of this study to confirm this conclusion.

WASp is autoinhibited by its own N-terminus and is activated by the small GTPase Cdc42. However, Cdc42 is not essential for WASp activation during *Drosophila* myoblast fusion, since *cdc42* loss of function alleles or expression of a dominant-negative form do not cause a fusion defect (Schäfer *et al*., 2007).

Another known regulator of WASp activity is WASp-interacting protein (WIP), called Solitary (Sltr) in *Drosophila*. *sltr* mutants have a severe fusion defect, and Sltr protein co-localizes with F-actin foci and is exclusively detected in the cytoplasm of the FCMs, further supporting FCM-specific function of WASp (Kim *et al*., 2007). WASp/WIP complex is further regulated by another FCM-specific protein, Blown fuse (Blow), which is also enriched at the F-actin foci (Jin *et al*., 2011).
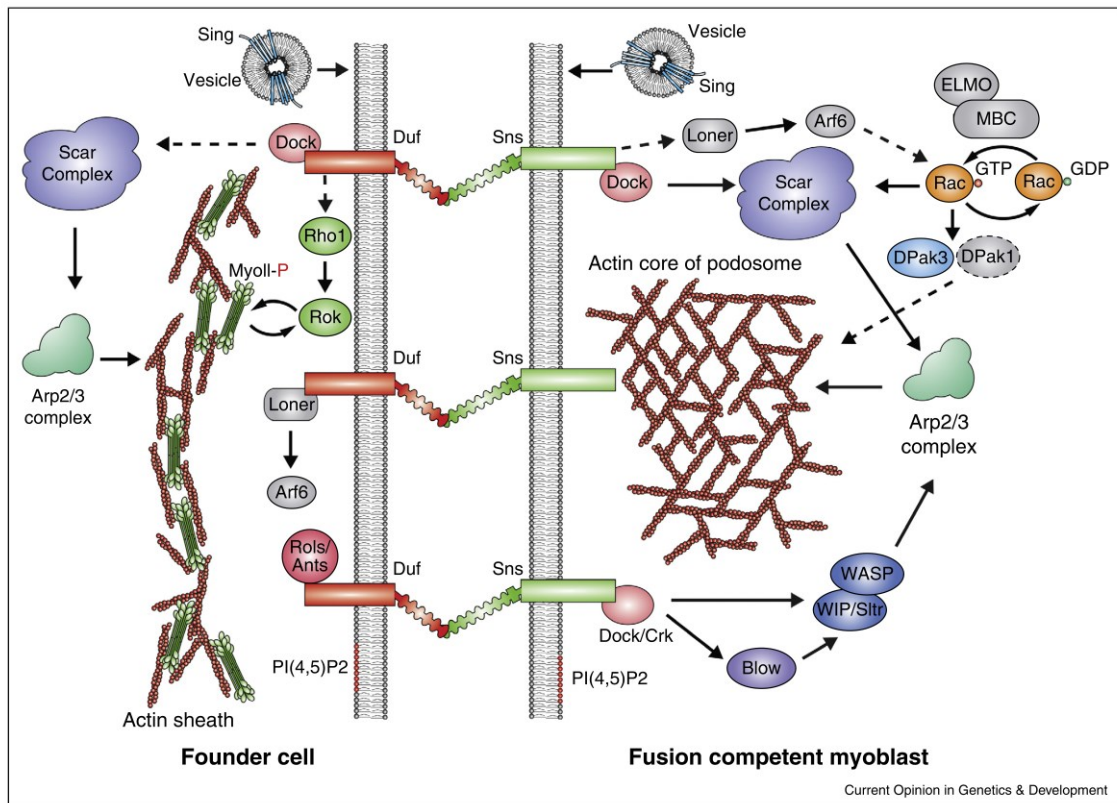
Figure 1.6 Cell-cell recognition between a founder cell/muscle precursor and FCM initiates the signaling cascades that lead to myoblast fusion

Engagement of cell-type specific CAMs – Duf in founder cell and Sns in FCM –initiates the signaling cascade that leads to myoblast fusion. Arp2/3 complex-mediated F-Actin polymerization is essential for the formation of the asymmetric F-actin focus that marks the fusion site. Notably, two Arp2/3 complex activators, SACR –present in both cell types- and WASp – present in the FCMs, are thought to underlie the asymmetric nature of the F-actin focus.

Image Source: Kim *et al*., 2016.

Blow competes with WASp for WIP binding and affects F-actin polymerization at the fusogenic synapse (Jin *et al*., 2011). The invasion depth of F-actin foci in *sltr*, *wasp*^{maternal/zygotic} (*wasp*^{mat/zyg}) and *blow* single mutants is greatly reduced, indicating that WASp and its regulators WIP/Sltr and Blow are required for the invasiveness of the PLS (Figure 1.5; Sens *et al*., 2010, Jin *et al*., 2011).

F-actin foci formation in the FCM requires either SCAR or WASp, since foci are present in either single mutant, but not in a *scar wasp*^{mat/zyg} double mutant. Invasiveness of the PLS is only affected by loss of WASp but not SCAR and functional foci require both Arp2/3 activators.

SH2-SH3 domain-containing adaptor proteins Crk, drk, and dock

The engagement of the cell-type specific CAMs at the fusogenic synapse needs to be relayed to WASp, SCAR and Arp2/3, and this process is hypothesized to occur via SH2-SH3 adaptor proteins. There are three SH2-SH3 domain-containing proteins in *Drosophila*: Crk oncogene (Crk), downstream of receptor kinase (drk; homologue of Grb2) and dreadlocks (dock; homologue of Nck). Among these, Crk and dock have been implicated in myoblast fusion.

The *dock* null allele does not have a fusion defect. Maternally loaded dock mRNA can be detected until almost the completion of myoblast fusion, precluding its loss-of-function analysis (Kaipa *et al*., 2012). Maternal/zygotic *dock* mutants has been generated and appeared to have normal musculature (Desai *et al*., 1999). Furthermore, *dock drk* double mutants also have normal myoblast fusion, but it has not been possible to test the *dock drk Crk* triple mutant or *Crk* single

mutant due to *Crk*'s location on the fourth chromosome. In the absence of

mutant phenotype analysis, there remain localization, genetic and biochemical

interaction studies. Dock is expressed in FCMs and founder cells (Kaipa *et al*.,

2012). It interacts genetically with WASp and WIP/Sltr, genetically and

biochemically with Sns and Hbs, and biochemically with Duf and SCAR.

Crk on the other hand has been shown to physically interact with Blow and

Sns tying the Sns activation all the way to Arp2/3 complex activation via

Blow/WIP/WASP pathway. Taken together Dock is thought to be the adaptor

protein in both cell types and to physically interact with Duf and Sns, whereas

Crk is hypothesized to be specific to the FCMs.

Many more components of the *Drosophila* myoblast fusion have been

identified and described but go beyond the scope of this introduction (Figure 1.6;

reviewed in Kim *et al*., 2015).

F-actin and Myosin II are critical for myoblast fusion in the founder cell/muscle
precursor

The CAM engagement at the fusogenic synapse leads to the formation of

a thin F-actin sheath in the founder cell/muscle precursor (Sens *et al*., 2010).

Furthermore, the mechanical force that the invading PLS exerts on the founder

cell/muscle precursor leads to an accumulation of activated Myosin II (MyoII) in

the receiving partner (Kim *et al*., 2015). This MyoII accumulation was largely

independent of the chemical signaling through Duf/Rst since it also occurred in

duf rst mutant embryos expressing Duf lacking the intracellular domain required

21

for signaling. MyoII acts as a mechanosensor that accumulates at the fusion synapse due to its intrinsic ability to sense cortical stress at the fusion synapse. However, the maintenance of MyoII accumulation at the fusogenic synapse does require CAM-dependent chemical signaling via Rho kinase (Rok) pathway (Figure 1.6). The MyoII accumulation and activation at the fusogenic synapse leads to an increase of cortical tension which aids myoblast fusion by providing the resisting force necessary to force the two bilayer in close apposition. In absence of these resisting forces, the PLS invades deeper into the receiving cell but cell-cell fusion efficiency is decreased. Therefore, in wt embryos the protrusive and resisting forces between FCM and founder cell/muscle precursor put fusion synapse under high mechanical tension and facilitate the close apposition of the two cell membranes required for fusion.

Model of events at the fusogenic synapse leading to myoblast fusion

Myoblast fusion is preceded by recognition and attachment of a founder cell/muscle precursor and FCM, which is mediated by the cell-type specific CAMs, Duf and Sns (Figure 1.7). The engagement of the two CAMs triggers a signaling cascade which leads to F-actin polymerization in both cell types. The F-actin focus forms in the FCM and pushes into the founder cell/muscle precursor which in turn forms a thin F-actin sheath at the fusogenic synapse. As the F-actin focus matures it forms protrusive finger-like structures that invade into the
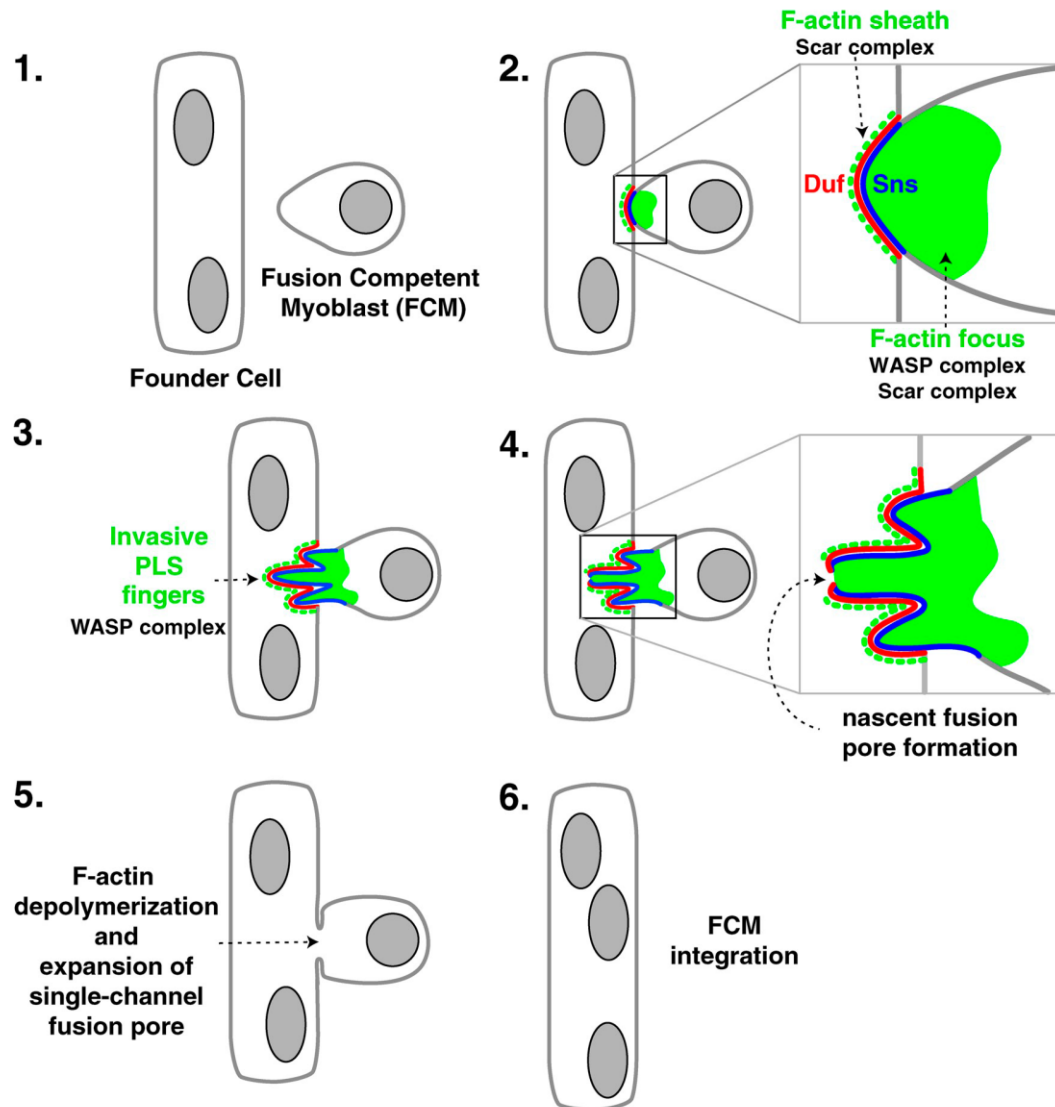
Figure 1.7 Model of cellular events during *Drosophila* embryonic myoblast fusion

Engagement of cell-type specific CAMs – Duf in founder cell and Sns in FCM –initiates the

signaling cascade that leads to myoblast fusion.

Image Source: Sens *et al*., 2010.

founder cell/muscle precursor forcing the apposing cell membranes close together and promoting fusing pore formation. Then the F-actin depolymerizes and the nucleus and cytoplasm of the FCM are incorporated into the growing myotube.

Cell culture system to study cell-cell fusion

Studies of cell-cell fusion in cultured cells are a good complement to *Drosophila* genetics to investigate the molecular mechanism. The Chen lab uses *Drosophila* S2R+ cells which are normally non-fusing but can be induced to fuse upon co-expression of the FCM-specific cell adhesion molecule, Sns, and a *Caenorhabditis elegans* (*C. elegans*) fusogen Eff-1 (Shilagardi *et al*., 2013). Interestingly, the PLS that mediates Sns-Eff-1-induced cell-cell fusion in S2R+ cells resembles the one seen in *Drosophila* embryonic myoblast fusion (Shilagardi *et al.,* 2013).

***Drosophila* vs. mammalian cell-cell fusion**

The cellular mechanism that we have identified in *Drosophila* is conserved across diverse cell fusion processes in vertebrate systems. For example, mouse myoblast and osteoclast fusion are both mediated by a PLS structure that is similar to the one seen in *Drosophila* cell-cell fusion (Shin *et al.,* 2014). However, it is still unclear if there are two different cell-types in vertebrate muscle fusion (reviewed in Kim *et al*., 2015).

Dynamin (Dyn)

The invasive PLS mediating myoblast fusion shares many similarities with podosomes. The implication of Dyn in podosome formation (Ochoa *et al*., 2000) prompted us to examine the potential function of the only *Drosophila* Dyn gene, *shibire*, in myoblast fusion.

Structure and molecular properties

Dyn is a large GTPase, which has an N-terminal GTPase domain followed by several other domains (Figure 1.8 A; reviewed in Antonny *et al*., 2016). On its C-terminus, Dyn has a pleckstrin homology (PH) domain which can interact with phosphoinositide-4,5-biphosphate (PIP_2) on the plasma membrane and a proline-rich domain (PRD) which can interact with proteins containing SH3 domains. Additionally, Dyn has a GTPase effector domain (GED) between the PH and PRD domains. This domain was discovered by its ability to affect the GTP hydrolysis rate of the GTPase domain; this interaction relies on the fact that the GED domain and middle domain (situated between the GTPase domain and PH domain) form a coiled coil - also named the stalk - which brings the PRD domain adjacent to the GTPase domain. The N- and C-terminal α-helices of the GTPase domain form a bundle with the C-terminal α-helix of the GED domain, and together they form the bundle signaling element (BSE) - an intramolecular signaling module critical for Dyn's structural stability.

Dyn exists in an equilibrium of dimers/tetramers in the cell (Figure 1.8 B).
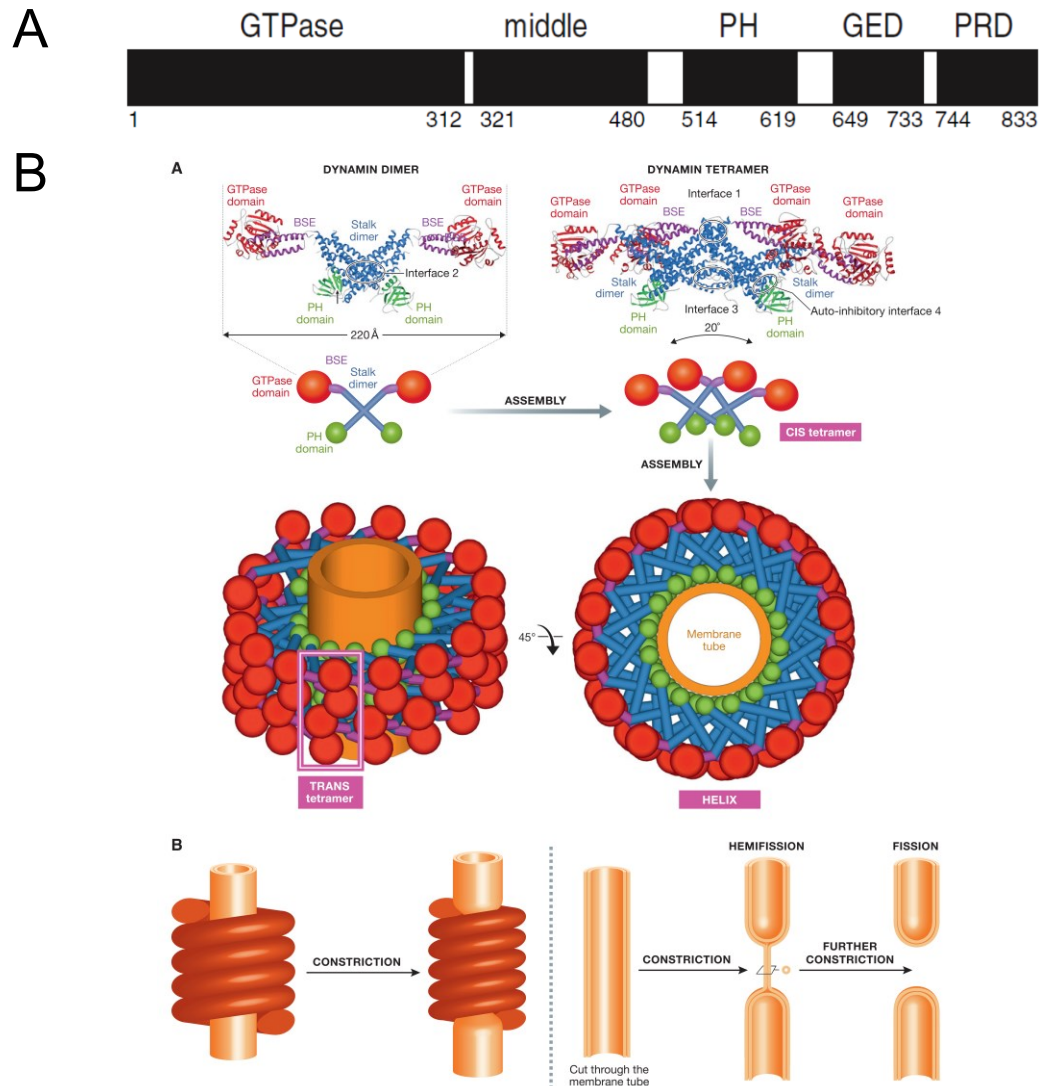
Figure 1.8 Dyn dimers/tetramers can assemble into helices or rings

(A) A schematic of Dyn's domains. GED and middle domain form a coiled coil which is also called the stalk. Numbering denotes *Drosophila* Dyn domains.

(B) Illustration of Dyn dimers/tetramers and their assembly into a helix. Nucleotide dependent constriction of the helix mediates vesicle fission.

Image Source: Kim *et al*., 2016
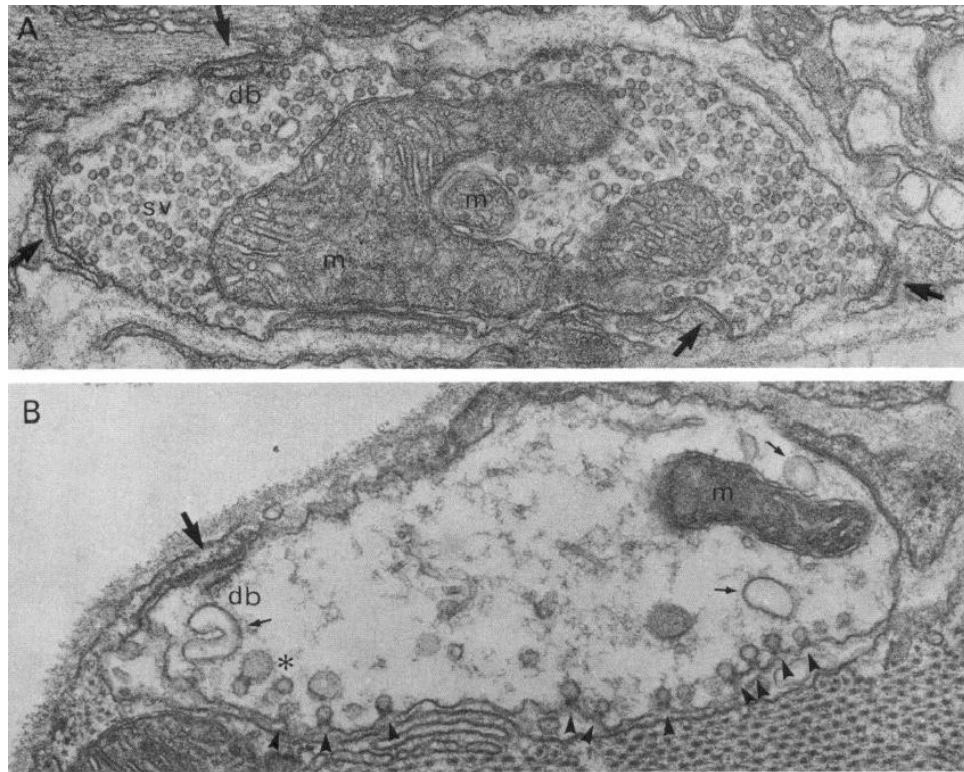
Figure 1.9 Endocytosis is blocked in _shi^ts1_ mutant at restrictive temperature

Drosophila neuromuscular junction is visualized with EM microscopy.

(A) In wt flies, the nerve terminal is filled with vesicles containing neurotransmitters.

(B) In _shi^ts1_ at restrictive temperature, the vesicles secreted during muscle movement can't be reformed because of blocked endocytosis leading to a depletion of vesicles and paralysis. Furthermore, invaginated pits with constricted necks are observed on the plasma membrane.

Image Source: Koenig and Ikeda, 1989

For its physiological function Dyn assembles into higher order oligomers such as spirals or rings (Figure 1.8 B). This assembly is known to drastically increase Dyn's GTP hydrolysis rate (up to 100 fold) by allowing the GTPase domains of adjacent tetramers to physically interact. Dyn assembly into oligomers causes conformational change in the GTPase domain that makes it more efficient for GTP hydrolysis and requires the BSE element (Chappie *et al*., 2009).

Dyn and endocytosis

Dyn was first discovered as an ATP-dependent mechanochemical enzyme that bundles microtubules into a hexagonal arrangement (Shpetner and Vallee, 1989). Later studies uncovered a completely different GTP-dependent physiological role for Dyn – endocytosis – the process by which cells can internalize extracellular fluid, membrane proteins and extracellular ligands. Several different forms of endocytosis exist (discussed in the next section), but for the purposes of this section endocytosis refers to clathrin and Dyn-dependent endocytosis also called receptor-mediated endocytosis. Briefly, upon binding its ligands membrane receptors accumulate to a local area of the plasma membrane which is invaginated via the clathrin coat. As the vesicle matures, it becomes constricted at the neck and is than severed from the plasma membrane forming an endocytic vesicle.

This insight was preceded by discovery of temperature-sensitive alleles of *Drosophila* Dyn, called *shibire* (*shi*), in a screen for reversible adult paralysis (Grigliatti *et al*., 1973). Adult flies were mutagenized and screened for paralysis at restrictive temperature (29℃). The paralyzed flies were then returned to

permissive temperature (22℃) and screened for recovery. Six temperature-sensitive *shi* alleles were discovered in this screen and numbered 1-6. The first allele, *shi^ts1^*, is the most severe allele, so much so that it has to be kept over a balancer at room temperature. Two more *shi* alleles from the original study are still available: *shi^ts2^* and the less severe *shi^ts4^*. Many early studies focused on *shi^ts1^*. The major breakthrough in understanding Dyn's function came when the neuromuscular junctions of *shi^ts1^* flies were imaged with electron microscopy (EM) and many invaginated pits where observed at the plasma membrane of the nerve terminal (Kosaka and Ikeda, 1982). At the same time a collar-like cytoplasmic electron dense material, about 10 nm thick, was observed at the neck of the invaginated vesicles which we now known to have been a Dyn oligomer (Kosaka and Ikeda, 1982). Further evidence supporting the idea that *shi^ts1^* blocks endocytosis came from EM images of the vesicle-depleted terminals of *shi^ts1^* after 8 min at 29℃ (Figure 1.9; Koenig and Ikeda, 1989). Furthermore, the same paper showed a recovery of vesicle numbers and an absence of collared pits in the nerve terminals of *shi^ts1^* after 30 min at 19℃. Taken together these findings strongly implicated Dyn as essential for endocytic vesicle separation from the plasma membrane.

Additional evidence for the role of Dyn in endocytosis came from exposure of rat nerve terminals (more specifically synaptosomes resulting from a mild homogenization of the brain which subsequent fractionation) to GTP-γS, a non-hydrolyzable analogue of GTP. This experiment revealed tubular invaginations with transverse electron-dense rings that were also positive for dyn EM gold-

immunoreactivity (Takei *et al.*, 1995). Later studies using cultured cells further supported the observation that a Dyn higher order structure can be found at the neck of invaginated pits.

Although not all endocytic events require the contribution of F-actin polymerization, it is likely to play a role in mammalian endocytosis in some contexts since pharmacologic disruption of F-actin by Cytochalasin D and Latrunculin A significantly reduce clathrin-mediated endocytosis (reviewed in Loebrich, 2014). One emerging principle is that cell membrane tension may affect whether F-actin is needed for endocytosis, with high tension membranes utilizing F-action polymerization to aid with vesicle fission.

Almost 30 years of research have cemented Dyn as a crucial component for endocytic vesicle fission from the plasma membrane (reviewed in Antonny *et al.*, 2016). Experts agree that self-oligomerization of Dyn into helices at the neck of the vesicle is required. Additionally, Dyn helix constriction – a reduction in the oligomer diameter - is driven by nucleotide-driven conformational changes, and vesicle fission is dependent on GTP hydrolysis. It is likely that Dyn oligomerization promotes membrane curvature, since without Dyn the necks of the clathrin coated pits are larger. Furthermore, biochemical studies and EM imaging of purified Dyn have shown that non-hydrolyzable GTP analogues favor Dyn oligomerization and that GTP hydrolysis favors disassembly of the Dyn oligomer. Despite extensive research, there is still some mystery surrounding the endocytic process.

<u>Mammalian and *Drosophila* endocytosis</u>

Mammalian cells have many different pathways of internalization which can also be divided into Dyn-dependent and -independent endocytosis (Figure 1.10; reviewed in Mayor *et al.*, 2014). Among the Dyn-dependent pathways are clathrin- and caveolin-dependent endocytosis as well as a RhoA-dependent pathway without a known vesicle coating protein. The clathrin- and Dyn-independent pathways include Cdc42 and Arf1-dependent pathway where nascent **cl**athrin-**i**ndependent **c**arriers (CLICs) fuse to form early endosomal intermediates called Glycosylphosphatidylinositol-anchored protein (GPI-AP) **e**nriched **c**ompartments (GEECs). This pathway is cholesterol-sensitive and relies on F-actin polymerization.

There is significantly less evidence for different types of endocytosis in *Drosophila*. *Drosophila melanogaster* appears to only have the clathrin and GEEC (clathrin- and Dyn-independent) pathways, and there is no evidence of caveolin in *Drosophila* genome (Gupta *et al.*, 2009). Hence, it seems that there is only one Dyn-dependent pathway of endocytosis which is also clathrin-dependent.

Drosophila clathrin-dependent and receptor-mediated endocytosis can be studied either using endogenous or mammalian receptors. Studies using the endogenous *Drosophila* scavenger receptors (receptors with broad ligand specificity found in immune cells) have been conducted *in vivo* and *ex vivo* and have shown that the *shi^{ts1}* and *shi^{ts2}* block receptor-mediated/clathrin-dependent

31
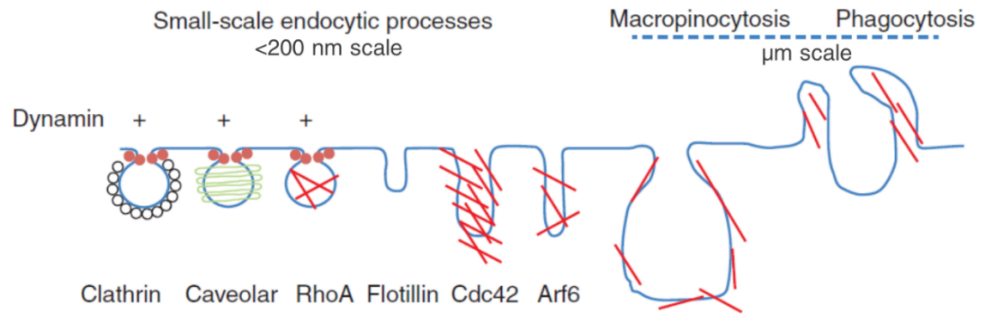
Figure 1.10 Different endocytic pathways

Mammalian endocytic pathways have two major categorizations based on clathrin and/or Dyn dependency. Several clathrin- and Dyn-independent pathways exist. There are only 2 known *Drosophila* endocytic pathways: clathrin- and Dyn-dependent endocytosis and the Cdc42-dependent GEEC pathway.

Images Source: Mayor *et al*., 2014

endocytosis at restrictive temperature (Abrams *et al*., 1992; Guha *et al*., 2003). Alternatively, receptor-mediated endocytosis can be studied by the expression of the mammalian Transferrin receptor – normally used for iron import into the cell (Gupta *et al*., 2009). This approach relies on the pulse-chase approach of a fluorescently labeled Transferrin (Tf) ligand which is internalized upon binding to its receptor via clathrin-mediated endocytosis.

Dyn endocytosis-independent functions

Dyn localizes with numerous actin-dependent structures such as lamellipodia, phagocytic cups, circular dorsal ruffles, actin comets and podosomes/invadopodia and Dyn perturbation affects their morphology and function. These processes are considered to be Dyn's endocytosis-independent functions (reviewed in Sever *et al*., 2013). One emerging idea is that Dyn is a regulator of the F-actin cytoskeleton via direct and indirect interactions.

Here, Dyn's role in two processes will be reviewed: formation of F-actin comet tails by *Listeria* or specialized intracellular vesicles, and formation and function of podosomes/invadopodia. Evidence to implicate Dyn's function in F-actin regulation came from experiments with a dominant-negative point mutant, Dyn^{K44A}, which can't bind GTP.

Listeria, a pathogenic bacterium found in contaminated food, can travel through a host's cells by F-actin polymerization in its comet tail. A similar F-actin comet tail can be observed - independent of *Listeria* infection - on some vesicles upon overexpression of a type I phosphatidylinositol 5-phosphate kinase in cells

(Rozelle *et al.*, 2000). Both tails rely on F-actin polymerization to propel through the cytosol. Overexpression of Dyn^{K44A} significantly reduces the formation of these comet tails and the velocity of vesicles (Orth *et al.*, 2002). Furthermore, Dyn is strongly enriched along the entire length of the F-actin tail, suggesting that it is involved in F-actin regulation (Orth *et al.*, 2002).

Dyn has also been implicated in the formation of podosomes and invadopodia (reviewed in McNiven *et al.*, 2004). Cells of the monocytic lineage form podosomes whereas cancer cells (or transformed cells) form invadopodia that also are sites of localized metalloprotease-mediated degradation of extracellular matrix (ECM). Some investigators do not consider the two structures as distinct and use the term invadosome for both (Destaing *et al.*, 2013). Dyn has been shown to localize to both structures. Overexpression of the dominant-negative point mutant, Dyn^{K44A}, affects F-actin dynamics in podosomes and affects the ECM degradation and morphology of invadopodia. The PRD domain of Dyn is sufficient to localize Dyn to the podosome, and expression of DynΔPRD almost completely disrupts podosome formation (Lee and De Camilli, 2001 [loss of podosome rosettes in Fig. 4B]). Addition evidence supporting an essential role of Dyn in invadosome formation is the almost complete absence of these structures in Dyn1 and Dyn2 knockout (KO) mouse embryonic fibroblasts that have been transformed with v-Src, which are normally very rich in invadopodia (Destaing *et al.*, 2013). The ability of Dyn1 and Dyn2 KO cells to degrade the ECM and to invade into the matrigel is also dramatically decreased as compared to transformed MEF with wt Dyn. Furthermore, acute disruption of Dyn in the

same cells by photo-inactivation leads to a distinct morphological change in the invadopodia's F-actin network further supporting a direct effect.

It was proposed that Dyn's PRD domain-mediated interactions with other F-actin regulators are involved in comets tails and podosomes/invadopodia. Such interactions are typically proposed to involve cortactin which also localizes to these F-actin rich structures, but the functional evidence is sparse. An alternative view emerged with the report that Dyn can bind F-actin directly.

Direct interaction of Dyn and F-actin

Actin monomers can bind and hydrolyze ATP to ADP and assemble into filaments. The F-actin filament is polar: one end (the pointed end) is composed of Actin-ADP and is disassembling; the other end (the barbed end) is composed of newly added actin monomers bound to ATP and is elongating, unless it is bound by a barbed end specific capping protein. Dyn can directly bind F-actin throughout the filament, and this binding is diminished when several positively charged residues in the middle domain are replaced with negatively charged residues (Gu *et al*., 2010, reviewed in Sever *et al*., 2013). The same study showed that short F-actin filaments promote Dyn oligomerization, that Dyn oligomers can bundle F-actin filaments, and that Dyn can effect F-actin polymerization. Dyn has been shown to prevent the action of the severing and capping protein Gelsolin on the barbed ends of the F-actin and thereby promote F-actin polymerization *in vitro*. Taken together the following model was proposed (Figure 1.11): Gelsolin severs longer F-actin filaments into shorter ones and caps

them. Dyn dimers/tetramers bind these short filaments, promoting Dyn oligomerization and F-actin bundling; this in turn leads to a displacement of Gelsolin from the barbed ends which are now available for further extension. In summary, Dyn can affect F-actin polymerization by antagonizing Gelsolin binding to barbed ends.

Dyn and cell-cell fusion

Dyn was shown to be essential for mouse osteoclast and myoblast fusion in that the deletion of Dyn1 and Dyn2 prevented fusion and reduced the formation of invadosome-like actin-rich protrusions similar to *Drosophila* PLS (Shin *et al*., 2014). In EM micrographs F-actin rich protrusions were associated with clathrin-coated pits in the receiving cell, so Dyn's endocytosis-dependent function in the receiving cell appeared to be involved. To further test requirement of endocytosis for cell-cell fusion, Dyn-independent perturbations of endocytosis (depletion of clathrin heavy chain [clathrin monomer consist of one heavy and one light chain] or expression of truncated and dominant-negative form of amphiphysin [a membrane bending protein critical for endocytosis]) were examined and also impaired fusion. Taken together the investigators proposed a mechanism in which actin-rich protrusions in the attacking cell and clathrin-coated pits in the receiving cell mediate cell-cell recognition leading to cell-cell fusion.
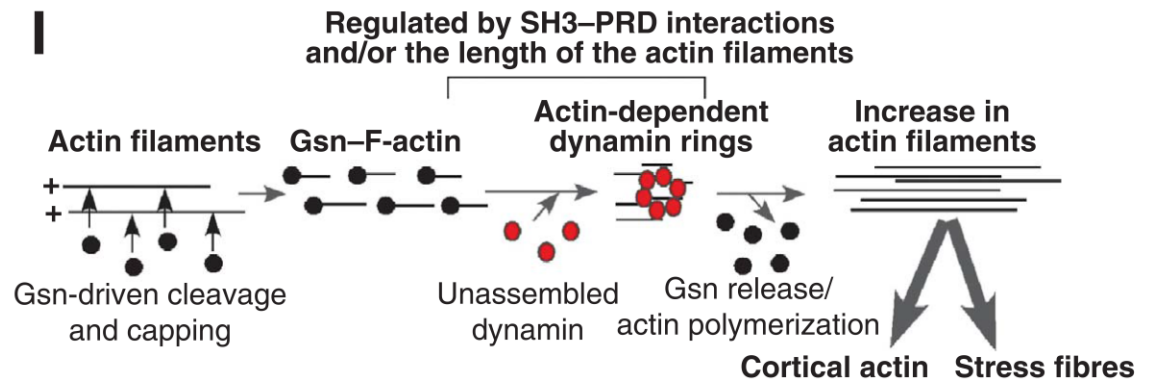
Figure 1.11 Model of Dyn's direct interaction with F-actin filaments

The severing and capping protein gelsolin (Gsn) severs longer F-actin filaments into shorter ones and caps them. Dyn dimers/tetramers bind these short filaments which in turn promotes Dyn oligomerization and F-actin bundling which leads to a displacement of Gelsolin from the barbed ends which are now available for further extension.

Images Source: Gu *et al*., 2010

<u>Dyn and human disease</u>

Human Dyn 2 has been implicated in two autosomal-dominant diseases: centronuclear myopathy (CNM) and Charcot-Marie-Tooth disease (CMT). CNM is a congenital disease involving muscle weakness which can range from severe neonatal to mild late-onset forms, and Dyn2 mutations are associated with 50% of all CNM cases. As the name suggests, one hallmark of CNM is centrally located nuclei in muscle fibers. CMT is a peripheral neuropathy with muscular weakness of the extremities and defects in neuronal axon conduction (Ferguson and De Camilli, 2012). The disease etiology is completely unknown.

The reported CNM and CMT mutations affect the middle, PH and GED domains and are heterozygous missense or small deletion mutations. Several studies have focused on investigating the molecular and cellular phenotypes of patients' mutations but no clear genotype/phenotype relationship has emerged (reviewed in Durieux *et al*., 2010). In CNM, there is some evidence to implicate Dyn's function in endocytosis, because CNM can also be caused by mutations in Amphiphysin 2 which also functions in endocytosis. However, one crucial issue with this hypothesis is why CNM is so tissue-specific. Dyn's endocytosis-independent functions have also been hypothesized as possible mechanism for these diseases. Specifically, Dyn 2 has been reported to localize to the centrosomes and to interact with γ-tubulin. It was shown that CMN-causing Dyn2 mutants drastically reduce their localization to centrosomes (Bitoun *et al*., 2005). Additionally, CMT-causing Dyn2 mutations can disorganize the microtubule cytoskeleton. Taking together, Dyn2 role's in actin and microtubule cytoskeleton

regulation may suggest that Dyn2 mutations prevent proper positioning of the nuclei. However, cell-cell fusion has not yet been investigated as a possible mechanism for CMN.

Hypothesis

This dissertation reports on the investigation of the role of Dyn during myoblast fusion in *Drosophila* embryo. Evidence will be presented to support Dyn's endocytosis-independent role in fusion. Specifically, we propose that Dyn affects the F-actin cytoskeleton morphology at the fusogenic synapse and aids in the invasiveness of this structure leading to cell-cell fusion.

Significance

A critical step of myogenesis is the formation of multinucleated skeletal muscles through fusion of myoblasts during embryogenesis. Myoblast fusion is also critical for postnatal muscle growth, maintenance and regeneration. Hence, elucidating the mechanisms underlying myoblast fusion will not only contribute to our understanding of skeletal muscle biology, but also lead to improvements in the efficacy of muscle regeneration in the treatment of genetic and acquired muscle disorders.

Chapter 2: Results and Discussion

Summary

In this chapter data are presented to support Dyn's role in cell-cell fusion. Specifically, decrease in Dyn function causes a fusion defect in the *Drosophila* embryo and the S2R+ cell based system.

In the *Drosophila* embryo, Dyn is required for proper morphology and invasiveness of the F-actin foci at the fusogenic synapse. This function is likely to be endocytosis-independent.

I have utilized three different strategies to investigate Dyn's function in cell-cell fusion and endocytosis in S2R+ cells and found that they are highly correlated.

Part 2.1: Dyn is required for *Drosophila* embryonic myoblast fusion.

Effect of temperature-sensitive Dyn alleles on myoblast fusion

The implication of Dyn in podosome formation prompted us to examine

whether the only *Drosophila dyn* gene, *shi*, functions in myoblast fusion. Since

Dyn is required throughout embryonic development, we used temperature-

sensitive (ts) alleles of Dyn, *shi^{ts}*, to test its requirement in embryonic myoblast

fusion. Several *shi^{ts}* alleles exist and they are single residue substitutions in the

GTPase domain or the BSE just downstream of the GTPase domain (Table 1).

We decided to examine the embryonic muscle phenotype of eight of these alleles

and confirmed that all the stocks contained the reported mutations by

sequencing.

Temperature sensitive *shi* embryos were allowed to develop up to mid-

embryogenesis at permissive temperature (18-20℃) and then shifted to

restrictive temperatures (32 - 34℃) just prior to myoblast fusion. We examined

the resulting muscle phenotype at embryonic stage 15 (E15) when myoblast

fusion is complete. Only some of the alleles showed a fusion defect phenotype,

indicated by the presence of round single nucleated FCMs and thin stretched out

muscle fibers; *ts2* mutant had a severe fusion phenotype and *ts4* had a mild

fusion phenotype (Figure 2.1 A). In our initial experiments *ts1* mutant embryos

were a mixture of embryos with normal musculature and embryos with a mild

fusion defect. Since *ts1* is the most severe endocytic allele and the only *shi^{ts}*

stock kept over a balancer at 25℃, I hypothesized that the maternal contribution

Table 1 *Drosophila* temperature-sensitive Dyn alleles, shi, are single residue substitutions in the GTPase domain or the BSE

shi allele name	Mutation
ts1	G268D
ts2	G141S
ts4	P171S
TP1	T104I
TP4	P133L
TP5	Not mapped (M1-P27 ok and D50-L355 ok, mutation most likely between Q28 and K49)
TP9	A268D
TP12	A268D

Table 2 Quantification of the *Drosophila* embryonic fusion defect using 4 different *shi* alleles

	w^{1118}	shi^{ts1}	shi^{ts2}	shi^{ts4}	shi^{TP4}
Mean	9.28	3.22	3.95	7.90	9.04
SD	1.50	1.24	1.45	1.75	1.92
N	298	135	338	336	94

SD: Standard deviation

N represents number of DA1 muscles

A

| anti - TM | anti - Mef2 | merge |

w^{1118}

shi^{ts1}

shi^{ts2}

shi^{ts4}

B

eve+ nuclei in DA1 muscle

w^{1118} shi^{ts1} shi^{ts2} shi^{ts4}

****

****

****

****

****
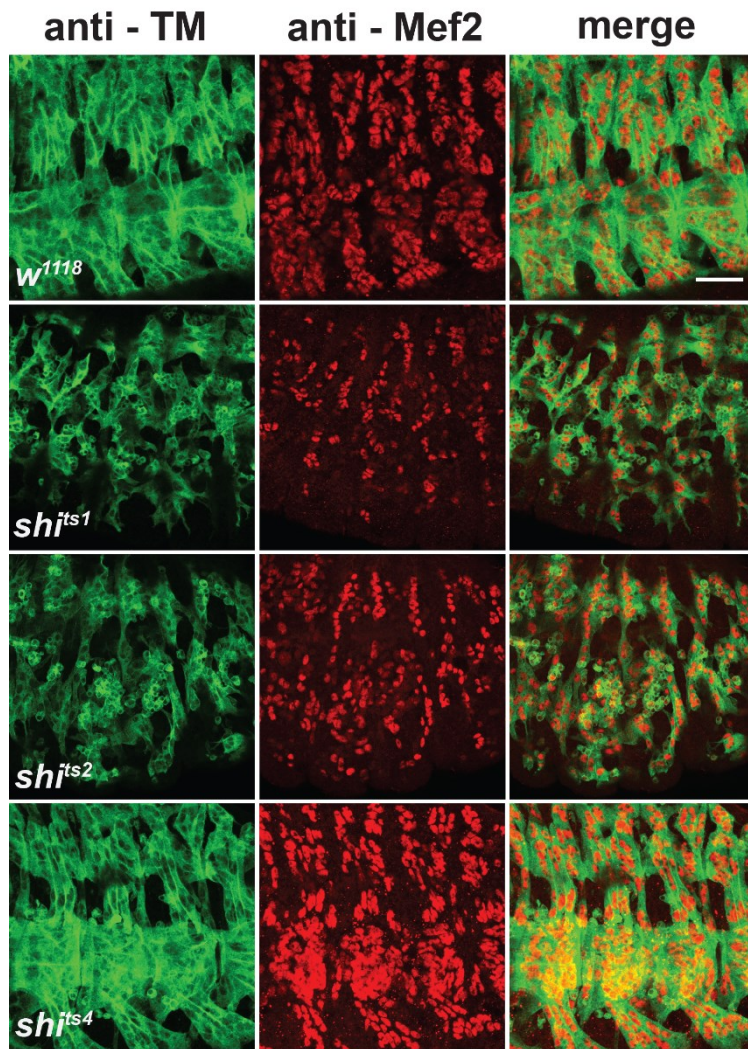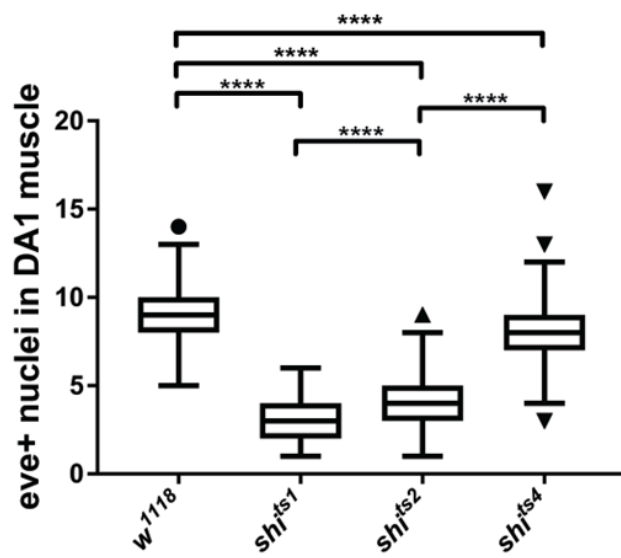
Figure 2.1 Dyn is required for *Drosophila* embryonic myoblast fusion

(A) Ventrolateral view of three to four hemisegments of E15 embryos (dorsal is up and anterior is to the left) whose myoblast fusion occurred at restrictive temperature (32℃). Embryos were stained with anti-Tropomyosin (TM) and anti-Mef2 antibodies to visualize their body-wall musculature. Fusion occurred normally in w^{1118} embryos. In shi^{ts1} and shi^{ts2} embryos many round mono-nucleated cells and thin myotubes were observed which is indicative of a fusion defect. A small fusion defect was observed in shi^{ts4} embryos. Scare bar 20 μm.

Note: In shi^{ts1} and shi^{ts2} embryos we see varying amounts of TM-positive and Dmef2-negative cells which does not correlate with the fusion defect observed.

(B) Number of Eve-positive nuclei in the DA1 muscle were counted to quantify the observed fusion defect; shi^{ts1} and shi^{ts2} had a severe fusion defect and shi^{ts4} had a mild fusion defect and all three were statistically significantly different from w^{1118}. Data is displayed using the Tukey box and whiskers plot. Statistical significance analysis was performed with ANOVA Tukey's multiple comparison test. **** stands for adjusted P-value <0.0001.

of the balanced mother obstructed the *ts1* phenotype. Once embryos were collected from unbalanced females, *ts1* had a pervasive severe fusion defect similar to *ts2* (Figure 2.1 A). *TP1*, *TP5*, *TP9* and *TP12* had normal looking musculature (Kim S. PhD, unpublished). Next, I wanted to quantify the embryonic myoblast fusion phenotype defect by using the eve-positive nuclei count in the DA1 muscle (Figure 2.1 B; Table 2). Wildtype DA1 muscle under these conditions had 9.28 ± 1.50 (N=298) eve-positive nuclei. As expected, *ts1* and *ts2* had a similarly severe fusion defect with 3.22 ± 1.2 (N=135) and 3.95 ± 1.45 (N=338) eve-positive nuclei, respectively. *ts4* had a mild fusion phenotype with 7.90 ± 1.75 (N=336). *TP4* originally was shown to have a medium fusion defect (Kim S. PhD, unpublished) but in my experiments it had a mild fusion defect that was not statistically significant (Table 2). The reason for the discrepancy is unclear, but because of the presence of other *shi* alleles, *TP4* was not further pursued.

A further confirmation that Dyn has a strong maternal contribution is that the null allele, although embryonically lethal, fails to hatch but survived embryonic period long enough to secrete a cuticle (Poodry, 1990). Considering the fundamental role of endocytosis in development, the embryo can only develop this far because of the maternal contribution. I confirmed that *shi*[FL54] which is a null allele (Windler and Bilder, 2010; a frameshift that induced a premature stop codon within the GTPase binding domain) indeed has normal embryonic musculature (data not shown). Furthermore, when two independent Dyn RNAi were expressed in the mesoderm using *twi*-Gal4 driver, myoblast

fusion occurred normally, likely due to insufficient knock-down of the endogenous Dyn (data not shown).

Temperature sensitive alleles of Dyn avoid the issue of maternal contribution because they are homozygous conditional alleles (except *ts1* when it is kept over a balancer). However, it was very surprising that not all *shi^{ts}* alleles had a fusion defect, since all of the alleles were reported to affect endocytosis. I decided to subject the adult flies of all these stocks to the adult paralysis test which is an indirect measure of endocytosis at the neuromuscular junction. First we tested the flies at 37℃ to see a fast effect of the heat. As expected *ts1*, *ts2*, *ts4* alleles became paralyzed within 5 minutes (Figure 2.2 B). All *TP4* and half of *TP5* flies paralyzed within 10 minutes. However, *TP1*, *TP9* and *TP12* did not display adult paralysis at 37℃ (Figure 2.2 A). It is unclear why these alleles didn't display adult paralysis despite harboring the right mutations. I decided to focus on *ts1*, *ts2* and *ts4* alleles in my further investigation. These alleles were also subjected to adult paralysis at 32℃ (Figure 2.2 C) and the allele strength was in order of severity: ts1 ≥ ts2 > ts4.

Prior to investigating these alleles further, I wanted to take a closer look at myoblast fusion of one of the two severe alleles, *ts1* and *ts2*, and in order to avoid the complication of working with a balancer, *ts2* was chosen.

A
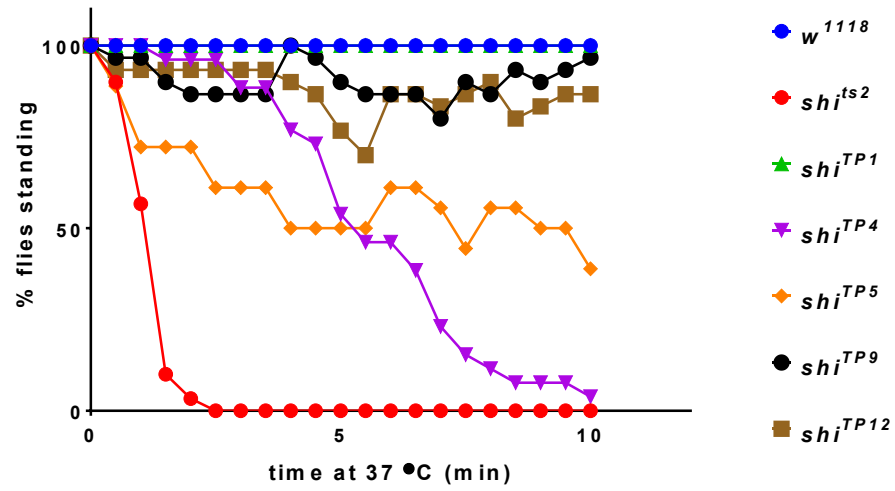
B
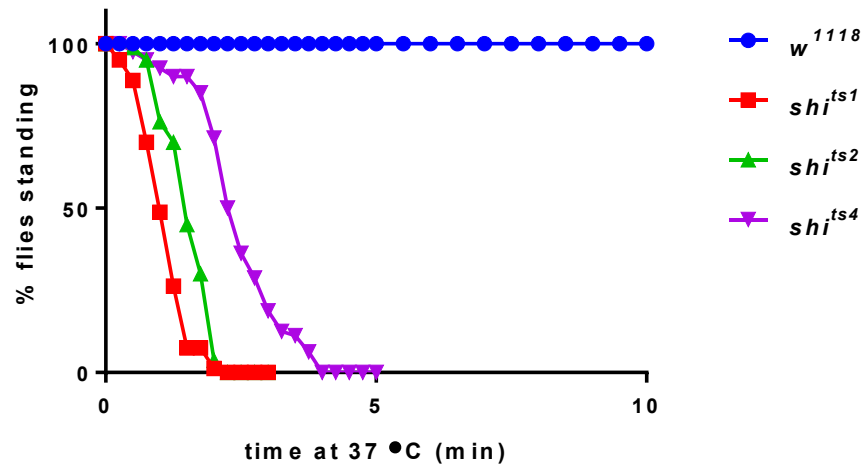
C
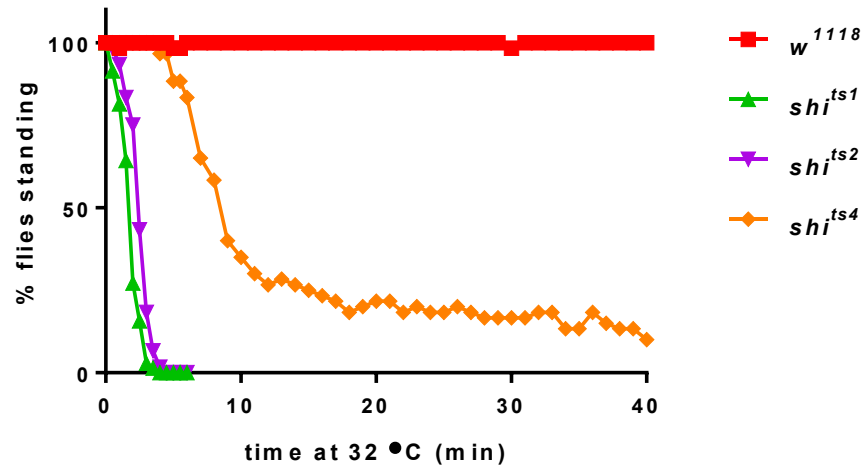
Figure 2.2 Adult fly paralysis of *shi* alleles at restrictive temperature is a reporter of endocytosis blockage at neuromuscular junctions

Flies carrying different *shi* alleles were exposed to restrictive temperatures (37℃ and 32℃) and the number of paralyzed flies over time was scored. Flies were considered paralyzed when they lay on their backs on the ground.

(A) *TP1*, *TP9* and *TP12 shi* alleles did not get paralyzed after 10 minutes at 37℃. TP4 and TP5 are weak *shi* alleles.

(B, C) *ts1*, *ts2* and *ts4* are strong *shi* alleles with all the flies being paralyzed within 5 minutes at 37℃. At 32℃, not all ts4 flies are paralyzed after 40 minutes.

Table 3: Overview of fly paralysis at 32℃ and 37℃

	T (℃)	w^{1118} males	females	shi^{ts1} males	females	shi^{ts2} males	females	shi^{ts4} males	females	shi^{TP4} males	females
Time to min 50% paralysis	32	NA	NA	2 min (33%)	2 min (20%)	2.5 min (43%)	2.5 min (43%)	7 min (33%)	12 min (47%)	20 min (47%)	20 min (50%)
	37	NA	NA	2 min (40%)	2.5 min (27.5%)	3 min (47.5%)	3 min (42.5%)	2.25 min (38%)	5 min (50%)	6 min (50%)	9 min (50%)
Time to 100% paralysis	32	NA	NA	4 min	3 min	4.5 min	4 min	41 min	NA at 70 min 7/30 (23%) standing	NA at 180 min 1/30 (3%) standing	NA at 90 min 8/30 (27%) standing
	37	NA	NA	4.5 min	4 min	5 min	4.5 min	3.25 min	10 min	30 min	39 min
Flies standing at the end of 40 min heat shock	32	30/30	30/30	0/40	0/30	0/30	0/30	1/30 (3%)	5/30 (17%)	5/30 (17%)	11/30 (37%)
	37	40/40	40/40	0/40	0/40	0/40	0/40	0/40	0/40	0/40	0/40

% denotes flies that remained standing

<u>F-actin foci of the *shi^ts2* embryos display an aberrant morphology and decreased invasiveness at restrictive temperature</u>

Myoblast fusion is mediated by F-actin foci that mark the site of fusion. Previous research has shown that the characteristic of the F-actin foci –such as morphology, invasiveness, and F-actin dynamics - correlate with their ability to promote fusion. We decided to look at the F-actin foci in the *shi^ts2* mutant embryos. While the wildtype (wt) F-actin focus is oval shaped and remains so at restrictive temperature, the majority of foci in the *shi^ts2* mutant (60-90%) had a variety of different morphologies that deviated from wt. One striking example are the ring-shaped foci in *shi^ts2* mutant embryos (Figure 2.3 A). When an F-actin focus is observed along its invasion axis, it appears a circle with a dense F-actin core. Approximately 5% (2/41) of the *shi^ts2* mutant foci in this orientation appeared ring-like i.e. they lacked the dense F-actin core. Ring-shaped foci are observed at much lower frequency in heat-shocked wt embryos (less than 0.1%). When founder cell/muscle precursor and FCM are observed side by side, one can see the dimple that the invasive F-actin focus makes in the receiving cell (Figure 2.3 B, C). Furthermore, frequently small F-actin protrusions ("fingers") can be seen extending from the F-actin core (Figure 2.3 C). Vast majority (N=45/50) of F-actin foci in *shi^ts2* embryos at restrictive temperature are flat, lack "fingers" and cause minimal deformation of the receiving cell's plasma membrane (i.e. are less invasive; Figure 2.3 B-D). The invasiveness of F-actin foci including "fingers" was measured. F-actin foci in *w^1118* embryos had an invasion depth

A

Phalloidin	anti-Ants	merge

w^{1118}

shi^{ts2}

B

Phalloidin	anti-Sns	merge
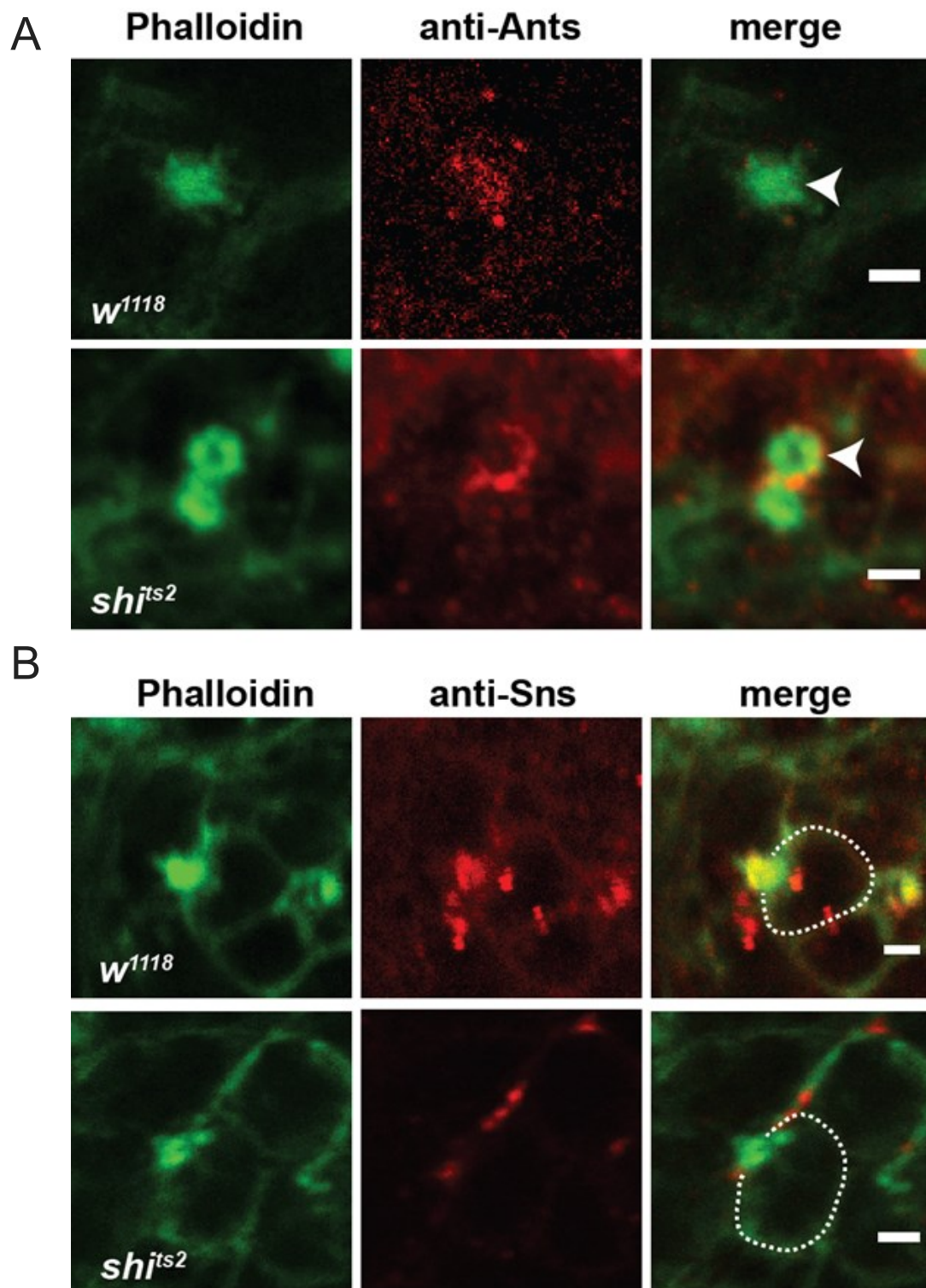
w^{1118}
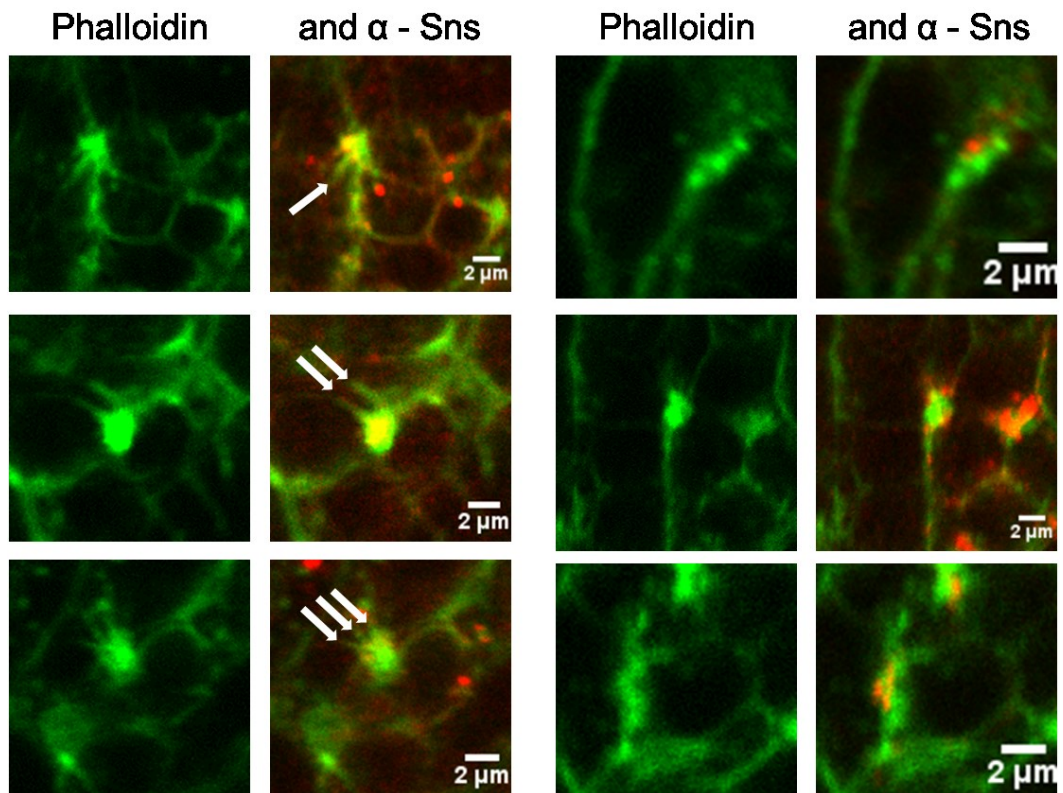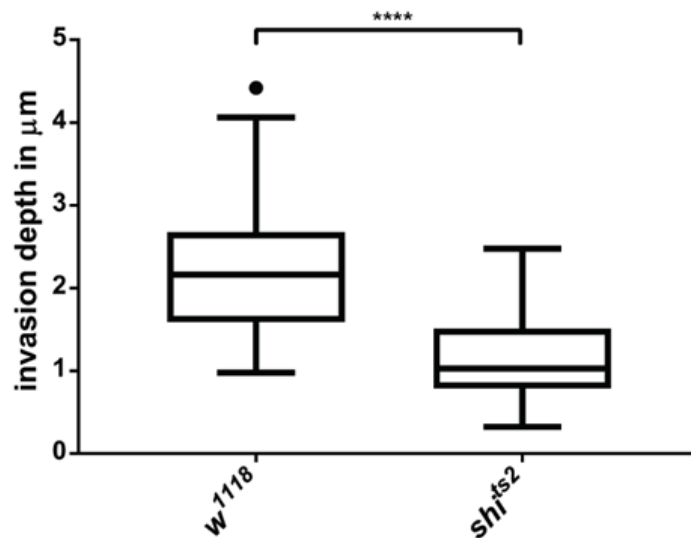
shi^{ts2}

Figure 2.3 Majority of F-actin foci in *shi^ts2* embryos have an aberrant morphology and decreased invasiveness at restrictive temperature

(A) When F-actin foci have their invasion axis perpendicular to the imaging plane, normal foci appear as dense rings (arrow head), however ~5% of *shi^ts2* foci in similar orientation have

a ring-shaped form i.e. lacking the dense F-actin core. Other aberrant forms include flat foci (B)

(B) When the founder cell/muscle precursor and FCM (outlined by dashed line) are aligned side by side, the F-actin focus in seen to protrude into the receiving cell. The invasiveness of a wt F-actin focus (w^{1118}) creates a dimple in the receiving cell's plasma membrane. Furthermore, small extensions ("fingers") can be seen emanating from the F-actin core. Vast majority (N=45/50) of F-actin foci in shi^{ts2} embryos at restrictive temperature are flat, lack "fingers" and cause minimal deformation of the receiving cell's plasma membrane (i.e. less invasive).

(C) More wt and shi^{ts2} F-actin foci showing impaired invasiveness of the mutant. Additionally, arrows denote "fingers" extending from the F-actin core.

(C) The invasiveness of F-actin foci including "fingers" was measured. shi^{ts2} embryos' F-actin foci are significantly less invasive the w^{1118} foci. Data is displayed using the Tukey box and whiskers plot. Statistical significance analysis was performed with Student T-Test. **** stands for P-value <0.0001.

Scale bars 2 μm.

2.2 ± 0.7 μm (N=102). F-actin foci in *shi^{ts2}* embryos were significantly less

invasive with an invasion depth 1.2 ± 0.5 μm (N=76). When the F-actin foci of

heat-shocked *shi^{ts2}* embryos were examined using EM, the PLS lacked long

invasive fingers, had less densely packed F-actin and sometime appeared flat

and elongated (Figure 2.4 A,B). Furthermore, while occasional invaginated pits

were observed in the mesoderm imaged by EM, these did not occur at the

fusogenic synapse, suggesting that endocytosis is not enriched at the fusogenic

synapse (Figure 2.4 B inserts).

Taken together *shi^{ts}* myoblast fusion mutant phenotype is most likely

caused by the aberration of the F-actin foci morphology at the fusogenic synapse

which rendered the F-actin foci less invasive and decreased fusion efficiency.

Dyn enriches at the fusogenic synapse

The observation that the F-actin foci in *shi^{ts2}* mutant at restrictive

temperature have an aberrant F-actin morphology and reduced invasiveness

suggested that Dyn may function at the fusogenic synapse. Therefore, we

wanted to visualize Dyn localization in wt embryo. Dyn is strongly enriched at the

fusogenic synapse as seen by anti-Dyn antibody staining (Kim S. PhD.

unpublished). Furthermore, when F-actin focus formation and dissolution is

visualized by live-imaging Actin-RFP in parallel with Dyn-GFP, Dyn and Actin

have highly correlative special and temporal behavior (Kim S. PhD. unpublished).

Dyn-GFP had a very striking co-localization with the F-actin focus (Figure 2.5 A)
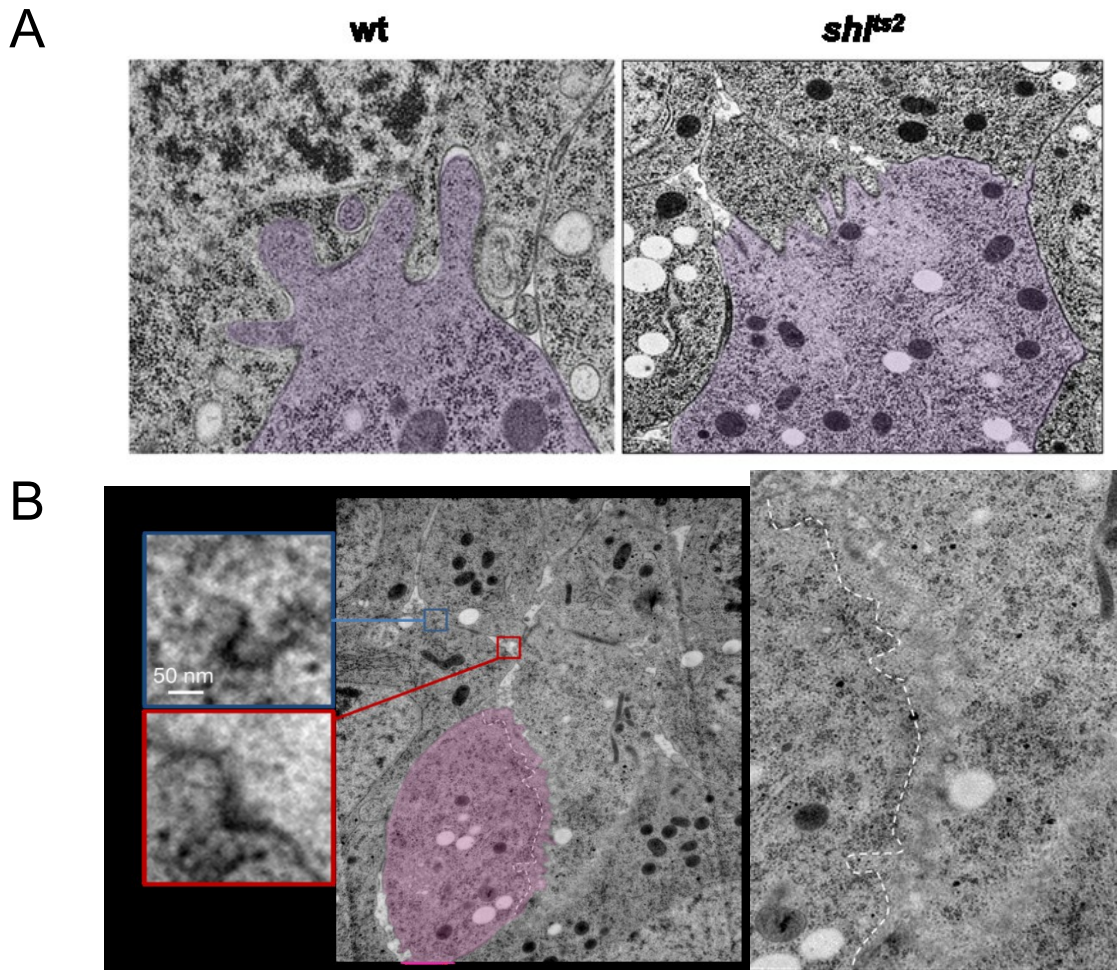
Figure 2.4 PLS in the *shi^ts2* embryos have an aberrant morphology with a lack of invasive fingers when examined by EM micrographs

(A) FCMs are colored in purple. The F-actin in FCMs is denoted by an absence of small black dots (ribosomes). Wt PLS has a "palm" with 4 invasive "fingers" which protrude into the receiving cell (Kim *et al*., 2015). PLS in *shi^ts2* at restrictive temperature lacks long invasive fingers and its F-actin is less dense especially in the middle of the PLS where one can even see an organelle close to the plasma membrane. This PLS morphology is consistent with a ring-shaped focus when the invasion axis is rotated from along the plane to perpendicular to the plane (location, size and absence of small black dots [ribosomes] was used to determine the PLS structures in the mutant embryos).

(B) Another example of *shi^ts2* PLS. Here the shape is more elongated and also lacks invasive fingers. F-actin harboring area is shown magnified on the right, note that the membranes

of attacking and receiving cell are not well resolved, possibly due to fast remodeling of this area. Occasional invaginated pits can be seen (inserts to the left) but not at the fusogenic synapse.

Next, I wanted to see if clathrin also had a colocalization with the F-actin focus by expressing clathrin light chain-GFP (CLC-GFP) in the mesoderm using *twi*-Gal4. Unlike Dyn-GFP, CLC-GFP did not enrich at the fusogenic synapse (Figure 2.5 B). Taken together, Dyn's striking colocalization with the F-actin focus and a lack of enrichment of CLC-GFP suggests that Dyn's endocytosis independent function may contribute to the myoblast fusion.

<u>Dyn is mainly required in the FCMs</u>

In order to confirm that the phenotype observed is specific to Dyn and to assay Dyn's cell-type specificity, we performed rescue experiments with a transgenic line using the Gal4/UAS system (Figure 2.6 A, B; Table 4). When Dyn-GFP was expressed in founder cells/myotubes and FCMs using *twi*-Gal4 driver, the fusion defect was significantly rescued from 3.2 ± 1.6 (N=169) to 8.0 ± 2.0 (N=87) confirming that the fusion defect was due to the temperature-sensitive Dyn mutation. Next we performed cell-type specific rescues. When Dyn-GFP was expressed in founder cells/myotubes using the *rp298*-Gal4 driver, no rescue occurred 3.3 ± 1.2 (N=10). However, when Dyn-GFP was expressed in the FCMs using the *sns*-Gal4, myoblast fusion defect was rescued 6.2 ± 1.5 (N=17) but not as much as with the *twi*-Gal4 driver. This result suggests that Dyn primarily acts on the FCM site in myoblast fusion.
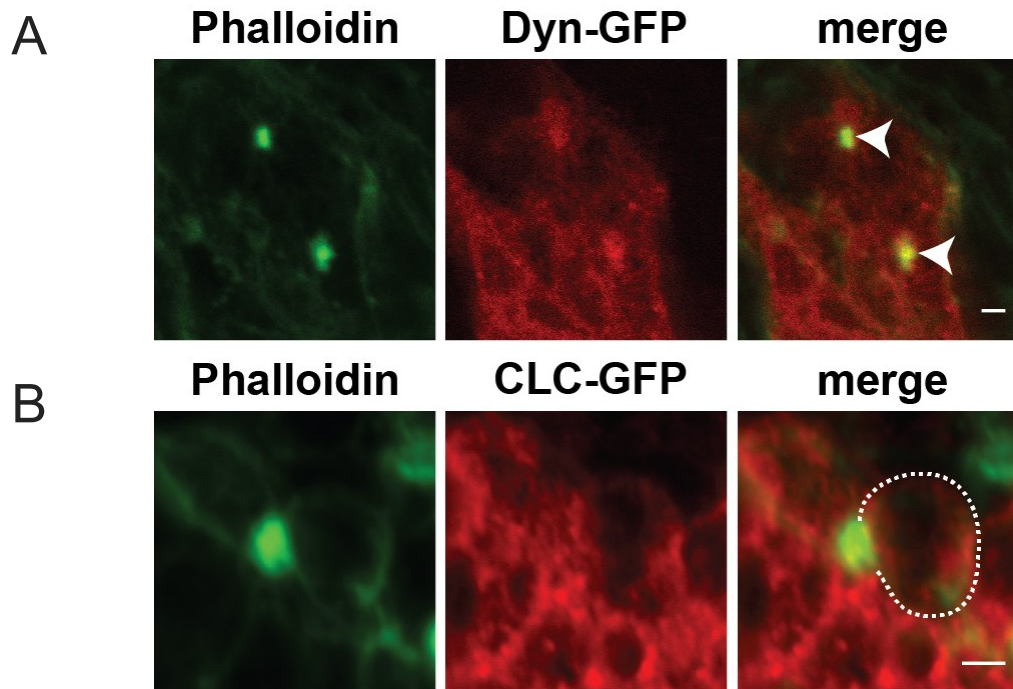
Figure 2.5 Dyn but not clathrin enriches at the fusogenic synapse

(A) Dyn-GFP was expressed in *shi*^{ts2} heat-shocked embryos with *twi*-Gal4 driver. Dyn-GFP
enriches at the fusogenic synapse. Of note here is that this colocalization is best visible
during live-imaging (Lee D. PhD, unpublished), upon fixation with standard protocol
colocalization is only visible in some foci.

(B) Clathrin light chain (CLC) –GFP was expressed in the mesoderm using *twi*-Gal4 and
does not enriched at the fusogenic synapse.

Scale bars 2 µm.

A

| | anti-TM | anti-GFP | merge |

no driver

twi-Gal4 (mesoderm)

rp298-Gal4 (founder cell/ myotube)
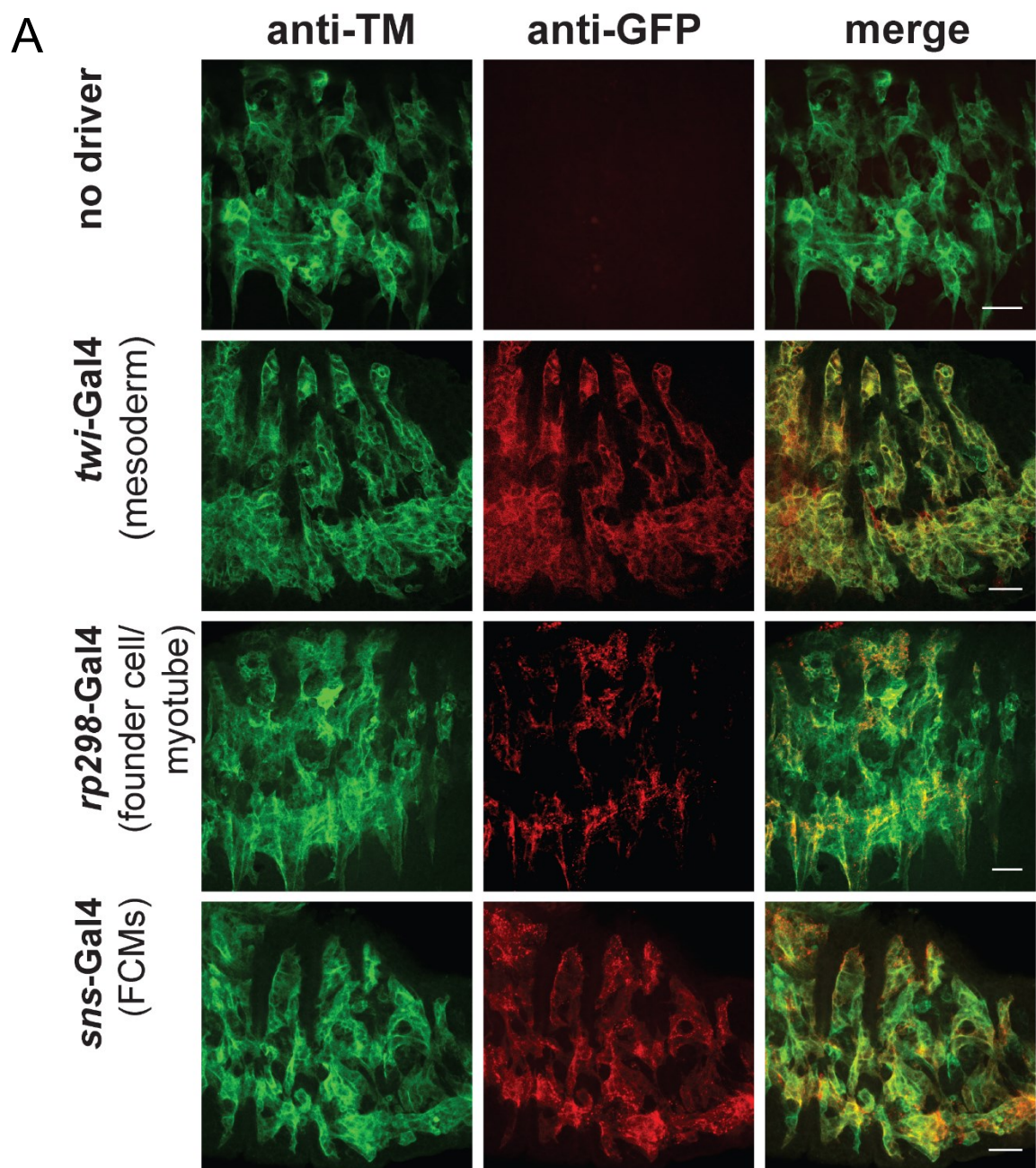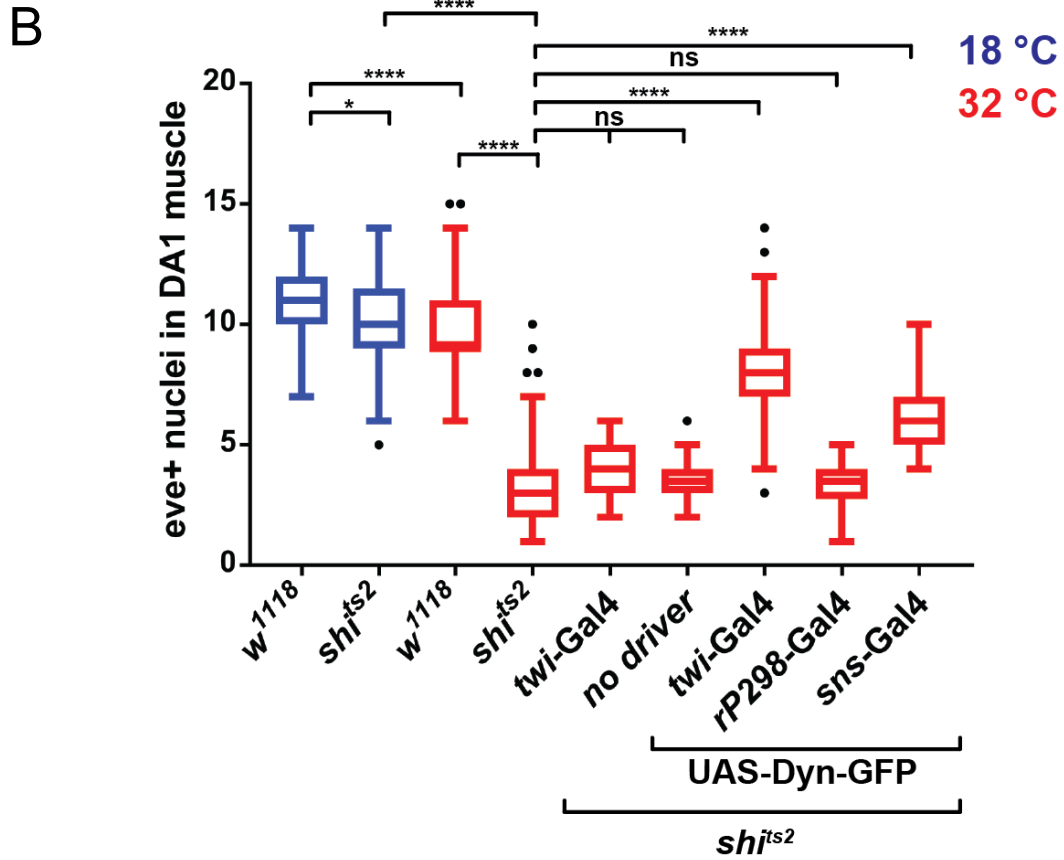
sns-Gal4 (FCMs)

Figure 2.6 *shi^{ts2}* fusion defect can be rescued by UAS-Dyn-GFP expression

(A) Dyn-GFP transgene was expressed in either both cell-types (*twi*-Gal4), in founder
cell/muscle precursor (*rP298*-Ga4) or in FCMs (*sns*-Gal4) in heat-shocked *shi^{ts2}* embryos.
Expression of the transgene was confirmed by anti-GFP staining. When compared to no
driver control, rescue is observed when Dyn is expressed in the mesoderm and, to a
lesser extent in FCMs. Scale bar 20 μm.

(B) Quantification of the *shi^{ts2}* rescue experiments. Data is displayed using the Tukey box
and whiskers plot. Statistical significance analysis was performed with ANOVA Tukey's
multiple comparison test. Adjusted P-values are denoted as follows: * for $p<0.05$, **** for
$p< 0.0001$, ns for non-significant).

Table 4 *shi^ts2* **has a severe fusion defect at restrictive temperature that can be rescued by cell-type specific Dyn transgene expression**

	w^1118 at 18°C	*shi^ts2* at 18°C	*w^1118*	*shi^ts2*	*shi^ts2; twi-Gal4*	*shi^ts2 ; UAS-Dyn-GFP*	*shi^ts2; twi-Gal4 / UAS-Dyn-GFP*	*shi^ts2 ; rP298-Gal4 / UAS-Dyn-GFP*	*shi^ts2 ; sns-Gal4 / UAS-Dyn-GFP*
Mean	11.0	10.3	9.7	3.2	3.9	3.5	8.0	3.3	6.2
SD	1.272	1.6	1.9	1.6	1.1	1.0	2.0	1.2	1.5
N	90	141	122	169	21	30	87	10	17

SD: Standard deviation

N represents number of DA1 muscles

Red: heat-shocked at 34°C

Part 2.2: Dyn is required cell-cell fusion in the S2R+ cells

Dyn enriches at the F-actin foci in fusing S2R+ cells

Cell-based systems allow for more detailed studies of cellular and molecular mechanism, and I wanted to take advantage of the S2R+ based cell-cell fusion system developed in our lab. Normally non-fusing S2R+ cells can be induced to fuse when the *C. elegans* fusogen Eff1 is co-expressed with *Drosophila* FCM-specific CAM Sns.

First I expressed Dyn-RFP and observed its localization. Similar to the *Drosophila* embryo, Dyn strongly enriched with F-actin foci in all low to medium expressing cells (N=40/43) (Figure 2.7 A, A'). The localization is not prominently visible in high expressing cells because the strong cytoplasmic signal (N=3/43). Similar colocalization with F-actin focus was shown with Dyn-3HA showing that localization was not affected by the identity of the tag and if the tag is N- or C-terminal (Figure 2.17).

I also wanted to test if Dyn is mainly localized to the attacking cells as it is the case in the *Drosophila* embryo. For this purpose I created two different populations of cells using transfection. Eff-1 is a fusogen which is required in both fusion partners but on its own it has small cell-cell fusion effect and does not form F-actin foci (Shilagardi *et al*., 2013). Presence of Sns leads to the formation of F-actin foci which make Eff-1 mediated cell-cell fusion up to 8-fold more efficient (Shilagardi *et al*., 2013). One population, called attacking cells, was transfected with Eff1, Sns-GFP, and Dyn-RFP while the other population, called receiving cell, was transfected with Eff1 only.
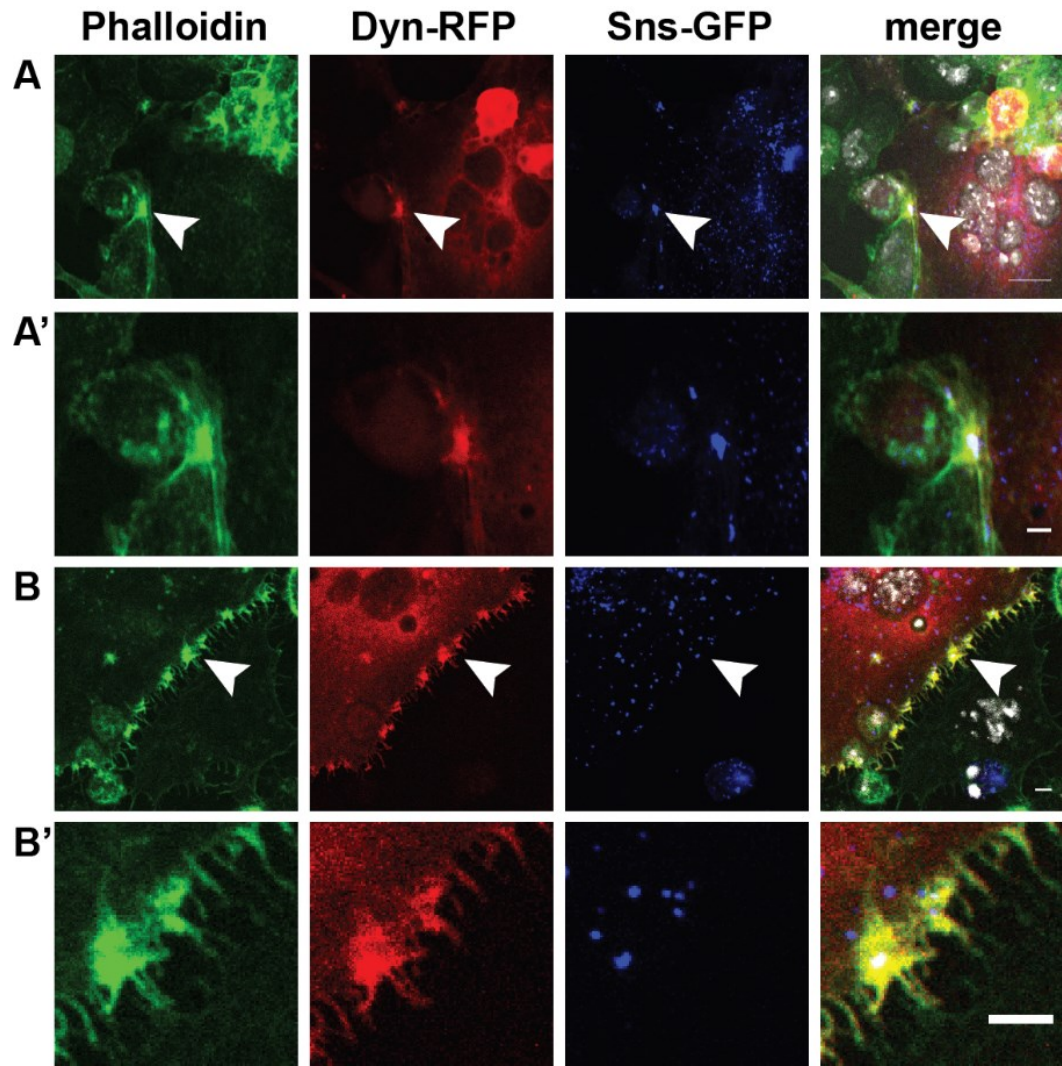
Figure 2.7 Dyn enriches at the F-actin foci in fusing S2R+ cells

(A) Normally non-fusing S2R+ cells can be induced to fuse upon co-expression of *C. elegans* fusogen Eff1 and *Drosophila* CAM Sns. Here a small round cell formed a fusogenic synapse with a larger, flat, 4-nuceli-containing syncytium. Scale bar 20 μm.

(A') F-actin focus in (A) shows a strong enrichment of Dyn at the fusion synapse and a colocalization with F-actin. Scale bar 5 μm.

(B) Two-different cell populations were created using differential transfection to determine the sidedness of the Dyn enrichment. Only one cell population received Sns and Dyn and is capable of functioning at the attacking partner. Here, a multinucleated attacking syncytium formed several foci to invade one single cell lacking Sns and Dyn.

Scale bar 5 μm.

(B') Dyn co-localizes with the F-actin suggesting that it is originating in the attacking cell.

Scale bar 5 μm.

Phalloidin	Dyn-GFP	Eff1-mCherry	merge+Dapi

A

A'

A"

Phalloidin	Dyn-ΔPRD-GFP	Eff1-mCherry	merge+Dapi

B

B'

C

D
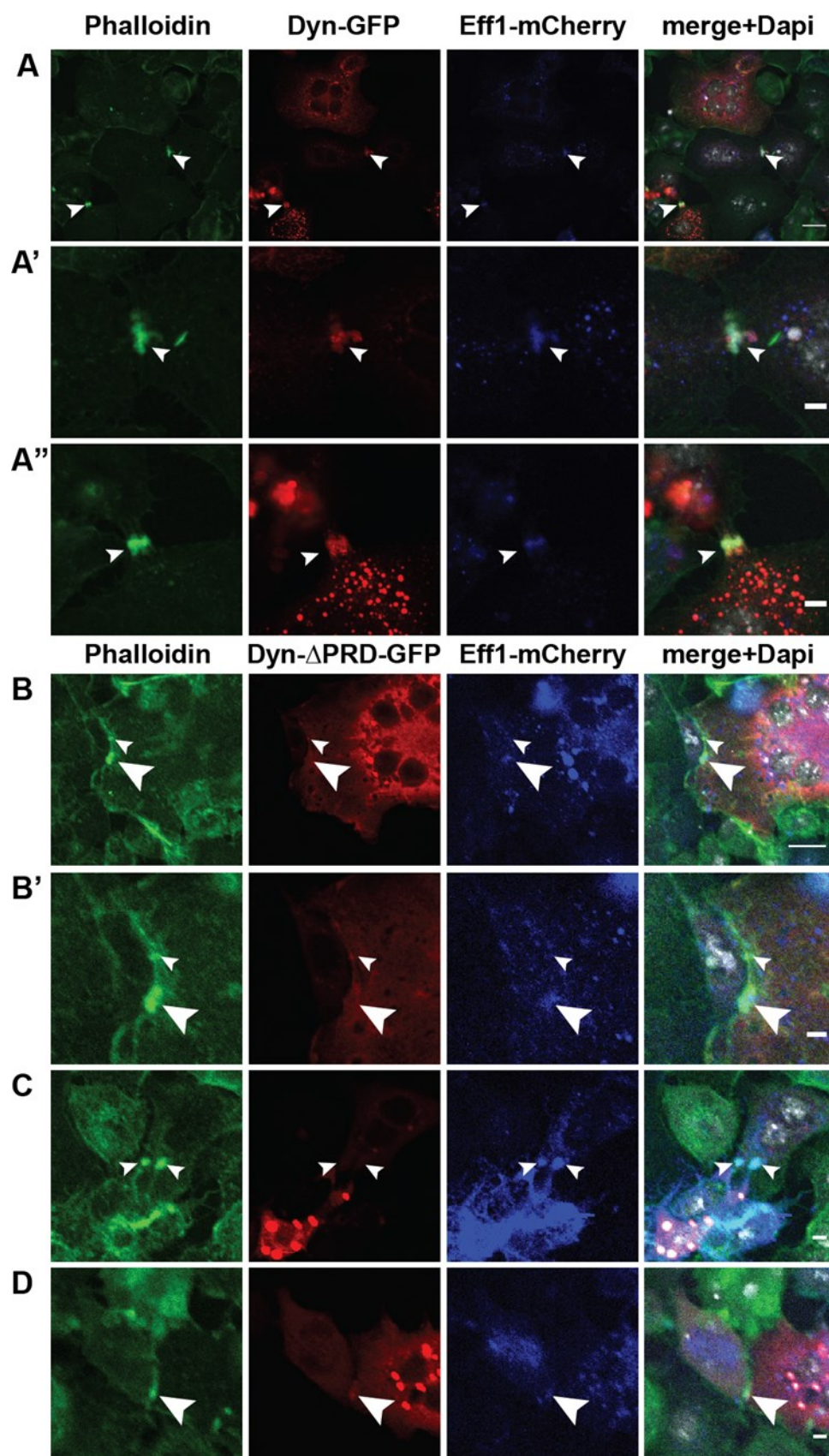
Figure 2.8 Dyn's PRD domain is involved in its localization to the F-actin foci

S2R+ cells were transfected with Eff1-mCherry (blue), Sns and Dyn-GFP (red) or Dyn-ΔPRD-GFP

(A) Dyn-GFP strongly enriches at the foci (small arrow heads). Scale bar 20 μm.

(A', A") Foci from (A) are shown magnified. Because the cytosolic Dyn signal is low, the enrichment of Dyn at the fusogenic synapse is extremely visible. Scale bar 5 μm.

(B-D) Deletion of the PRD domain diminished the Dyn signal at the F-actin foci.

(B-B') Two foci are shown, the larger focus (large arrow head) has almost no Dyn-ΔPRD enrichment whereas the much smaller structure above (small arrow head) has some Dyn-ΔPRD enrichment. Scale bar 20 μm in B and 5 μm in B'.

(C) Two foci showing a complete lack of Dyn-ΔPRD enrichment. Scale bar 5 μm.

(D) One focus showing some Dyn-ΔPRD enrichment. Scale bar 5 μm.

When a Dyn and Sns expressing cell was found to make a fusion synapse with a cell devoid of Dyn and Sns, Dyn-RFP was enriched at the F-actin focus, suggesting that Dyn enriched with the F-actin foci in the attacking cell (Figure 2.7 B).

Dyn localization to sites of its function in endocytosis-dependent and –independent processes via its PRD domain. Dyn-ΔPRD enrichment at the F-actin focus seemed drastically reduced as compared to full length protein (Figure 2.8). Dyn forms oligomers at the site of its function, so it was probably that residual recruitment of Dyn-ΔPRD was due to its incorporation into complexes with wildtype Dyn.

Crk, drk/Grb2 and dock/Nck localize to the F-actin focus and drk and dock interact with Dyn

Our data suggested that Dyn's PRD was important for Dyn recruitment to the F-actin foci. Next, I wanted to see which of the SH2-SH3 adaptor proteins are also enriched at the F-actin foci in S2R+ cells. I expressed tagged versions of Crk, drk/Grb2, and dock/Nck and all three enriched at the F-actin foci (Figure 2.9 A-C) and co-localized with Dyn (Figure 2.9 D-F). Next, I decided to perform co-immunoprecipitation (co-IP) experiments to investigate which of the three adapter proteins can biochemically interact with Dyn. Drk/rb2, and dock/Nck but not Crk interacted with Dyn (Figure 2.10). Furthermore, this interaction was reduced upon PRD deletion.

Phalloidin		Sns	merge

A Crk

A'

B drk

B'

C dock

C'
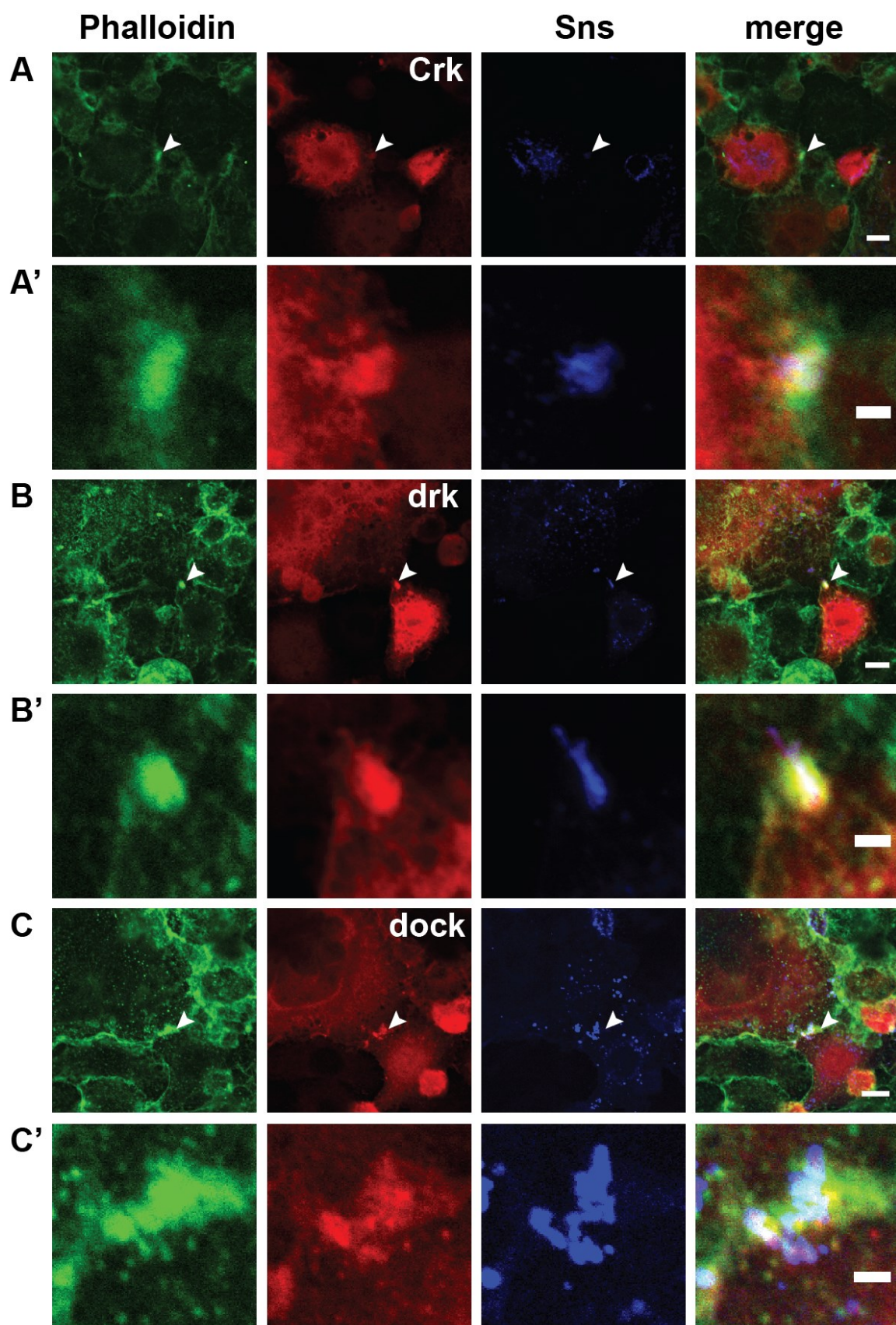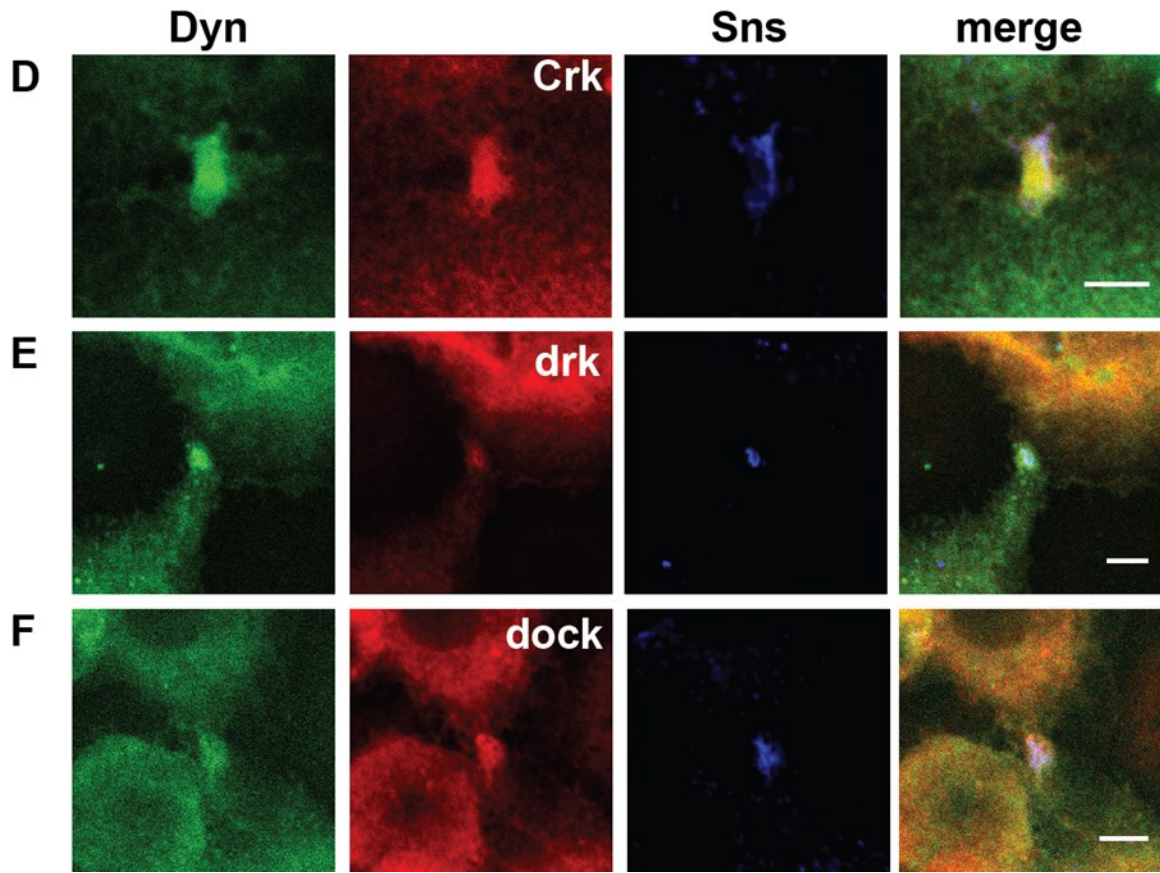
Figure 2.9 All three SH2-SH3 adaptor proteins (Crk, drk/Grb2, dock/Nck) localize to the F-actin foci and colocalize with Dyn

(A-F) S2R+ cells were co-transfected with Eff1, Sns, and one of three adaptor proteins.

(A-C)The fusogenic synapses were visualized by phalloidin enrichment and Sns presence (denoted by arrow heads in A-C and showed enlarged in A'-C'). Crk, drk and dock enrich at the foci. Scale bars 10 μm in A, B, C and 2 μm in A', B', C'.

(D-F) Fusogenic synapses in fusing S2R+ cells were visualized by an enrichment of Dyn and presence of Sns. Crk, drk and dock enrich at the foci. Scale bars 5 μm.

A

Crk-V5 — SH2 — SH3.1 — SH3.2 —

Crk-R38K-V5 — | SH2 — SH3.1 — SH3.2 —

drk-V5 — SH3.1 — SH2 — SH3.2 —

dock-V5 — SH3.1 — SH3.2 — SH3.3 — SH2 —

B

Shi-GFP

Crk-V5   Crk-R38K-V5

In   IP (GFP)   In   IP (GFP)

- 150 kDa

α - GFP   - 100 kDa

- 37 kDa

α – V5

- 20 kDa

C

Drk-V5 Dock-V5   Drk-V5 Dock-V5

shiGFP wt ΔPRD wt ΔPRD   wt ΔPRD wt ΔPRD

- 150 kDa

α-GFP

- 50 kDa

α-V5   - 37 kDa

- 20 kDa
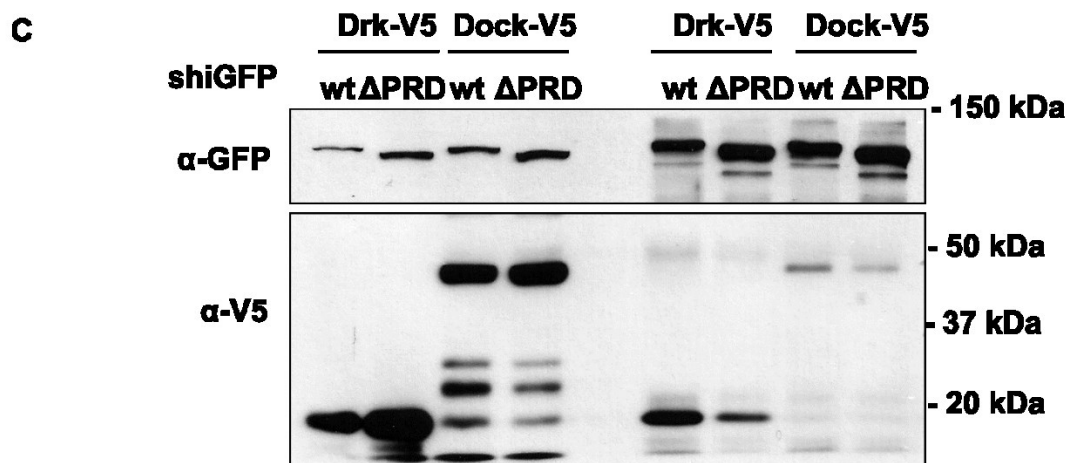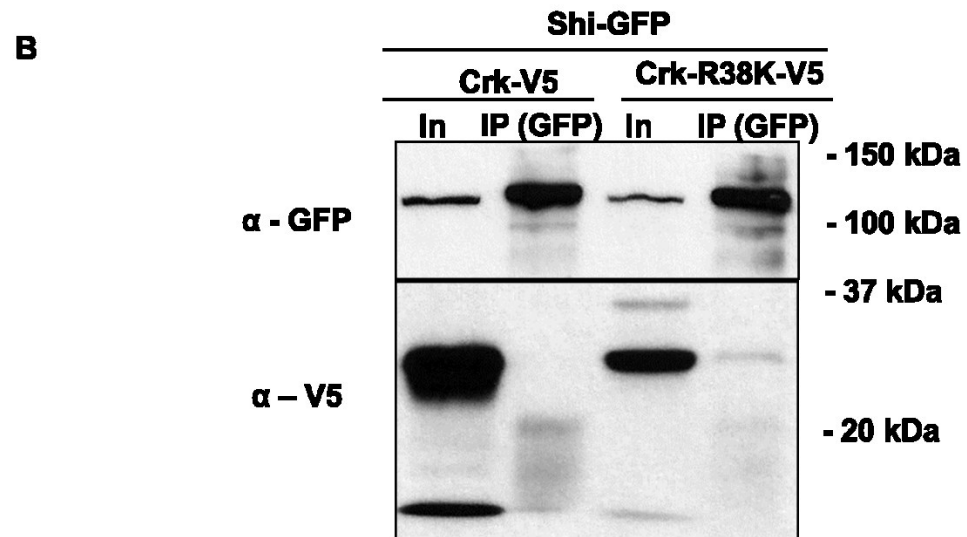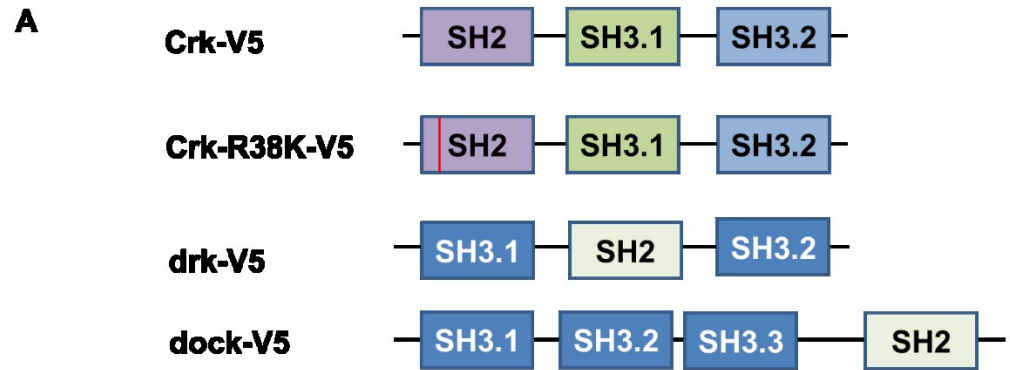
Figure 2.10 Co-IP experiments show that Dyn interacts with drk/Grb2 and dock/Nck but not Crk

Dyn-GFP was co-expressed with V5-tagged adaptor proteins in S2R+ cells. Dyn-GFP or Dyn-ΔPRD-GFP was used as bait.

(A) A schematic of the SH2 and SH3 domains in the three adaptor proteins. Since Crk was shown to interact with Sns, I also included the Crk-R38K mutant which is constitutively inactive into this experiment.

(B) Crk-V5 nor Crk-R38K are not pulled down by Dyn-GFP. "In" stands for Input/cell lysate. IP stands for immunoprecipitate

(C) Lanes on the left show input, lanes on the right show co-IP. Drk-V5 and dock-V5 are pulled down by Dyn-GFP and the amount of drk and dock is diminished when pulled down with Dyn-ΔPRD

Knock-down (KD) of Dyn causes a fusion defect in S2R+ cells

Next, I wanted to see if knocking down Dyn will cause a fusion defect. There are two different ways to knock down mRNA using long dsRNA in *Drosophila* cells. In the first protocol – called soaking - large amount of dsRNA is added to the medium in which the cells are cultured for three to four days and then the cells are transfected for cell fusion experiments with Eff1 and Sns. Alternatively, the cells are co-transfected with Eff1, Sns, and dsRNA at the same time – called transfection KD protocol. The transfection protocol is faster and less harsh on the cells, but the soaking protocol leads to a more robust and pervasive knock-down of the target mRNA.

When S2R+ cells were incubated with long dsRNA targeted against the open reading frame (ORF) using the soaking protocol, Dyn knock down using either mRNA caused a fusion defect (Figure 2.11 D). The knock down of Dyn mRNA was confirmed using RT-PCR (Figure 2.11 A). However, when the same dsRNA was used in the transfection protocol, no fusion defect was observed (Figure 2.11 E) despite the confirmation of KD using RT-PCR. This is most likely due to an insufficient knock-down of Dyn using the transfection protocol. I also tested whether overexpressing Dyn affects fusion which it didn't suggesting that Dyn is not a limiting factor in fusion (Figure 2.11 F).

Next, I wanted to see if this fusion defect can be rescued by Dyn. Since knock-down in *Drosophila* is done by long dsRNA it is not feasible to make a KD-resistant full-length form of Dyn. An alternative approach is to knock down the

72
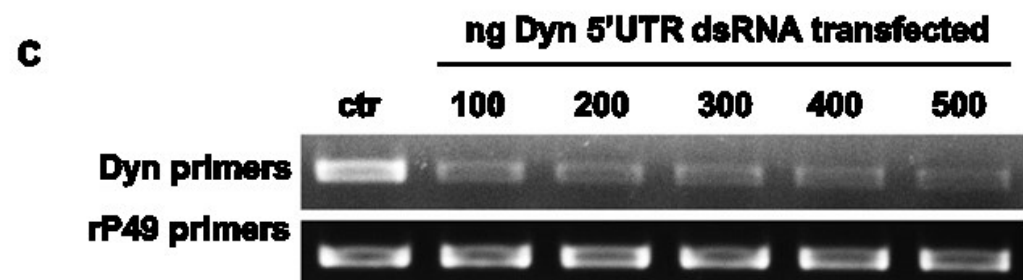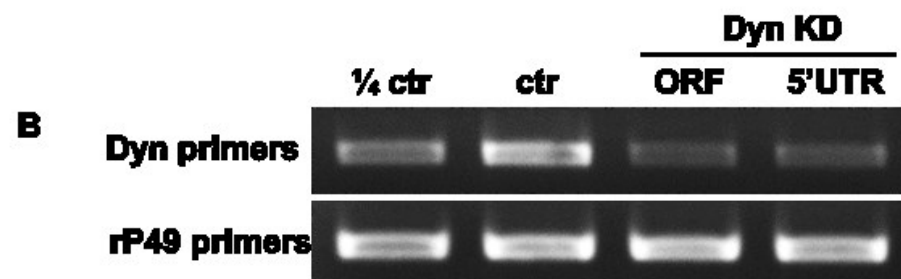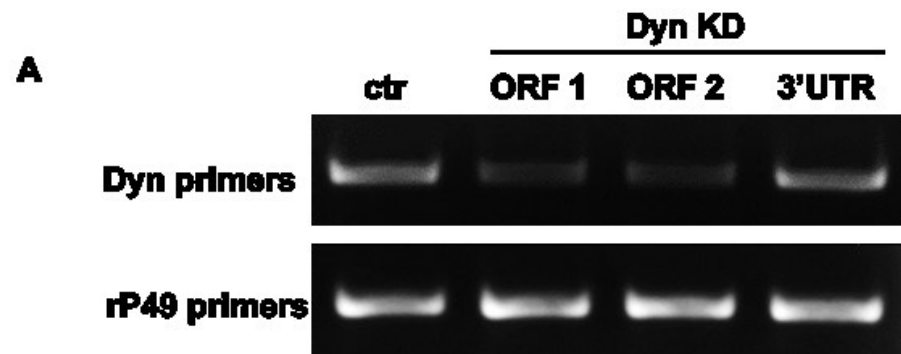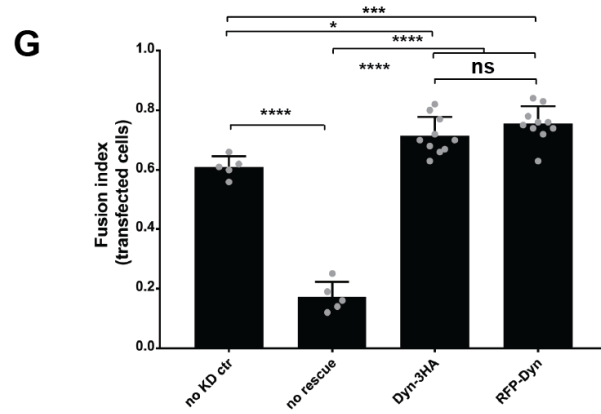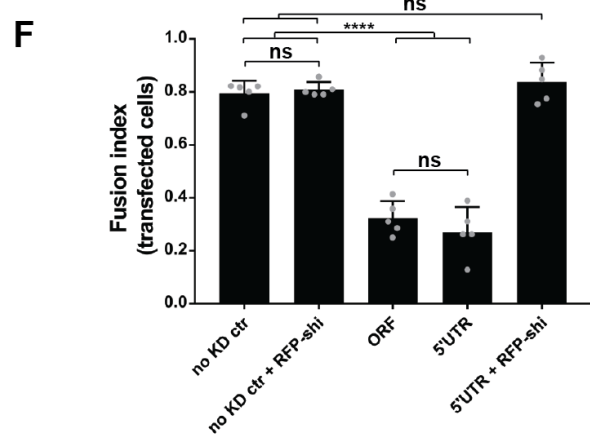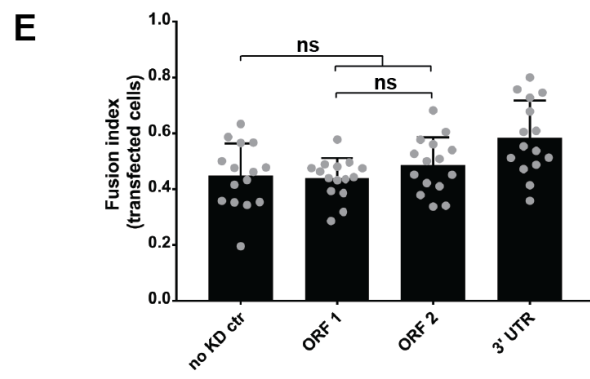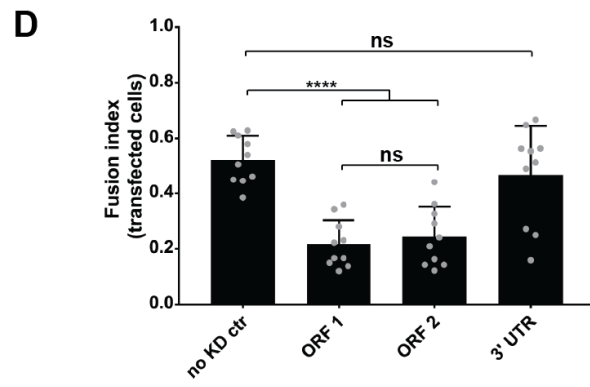
Figure 2.11 Dyn is required for S2R+ cell-cell fusion

(A-C) Total RNA collected from either no KD control cells (ctr) or Dyn KD cells was used for

RT-PCR to assess the knock-down of Dyn mRNA using long dsRNA. Primers against the

ribosomal protein 49 (rP49) were used as a loading control.

(A) Dyn mRNA was successfully decreased using dsRNA against two different regions of the

Dyn ORF but not against the 3'UTR.

(B) Dyn mRNA was successfully decreased using dsRNA against Dyn's 5'UTR. Based on

band signal from ¼ ctr it appears that the Dyn KD is more than 75%.

(C) Increasing amounts of dsRNA against Dyn's 5'UTR were used to decrease Dyn's mRNA

using the transfection protocol.

(D-G) Quantification of the fusion defect caused by dsRNA against either ORF or UTRs of

Dyn. The bar graph shows the mean and standard deviation. Additionally, the grey dots

show each individual value. Statistical significance analysis was performed with ANOVA

Tukey's multiple comparison test. Adjusted P-values are denoted as follows: * for $p<0.05$,

** for $p<0.01$, *** for $p<0.001$, **** for $p< 0.0001$ and ns for non-significant).

Treatment of S2R+cells with DsRNA against two different regions of Dyn caused a fusion

defect using soaking protocol (D), but not the shorter transfection protocol (E). Treatment

against Dyn's 3'UTR didn't cause a fusion defect using either protocol.

(F) Dyn KD using dsRNA against Dyn's 5'URT causes a strong fusion defect. RFP-Dyn

expression in the 5'UTR KD cells rescued the fusion defect completely. Overexpression

of RFP-Dyn in S2R+ cells didn't affect fusion.

(G) The fusion defect caused by dsRNA against Dyn's 5'UTR can be rescued equally well by

RFP-Dyn and Dyn-3HA (this data was obtained at 20℃).

endogenous proteins using the untranslated regions (UTRs). I designed long dsRNA against the 5'UTR and the 3'UTR, but only the dsRNA against the 5'UTR created a successful KD of mRNA (Figure 2.11 A, B) and lead to a significant cell-cell fusion defect (Figure 2.11 D, F). This fusion defect can be rescued by expression of either N- or C-terminally tagged Dyn (Figure 2.11 F, G).

I wanted to revisit the transfection protocol for Dyn knock-down using the dsRNA against Dyn's 5'UTR. The typical amount of dsRNA co-transfected with Eff1 and Sns is 100 ng and did not lead to a fusion defect, despite observable KD of Dyn mRNA (Figure 2.11 C). I attempted to recreate the fusion defect I observed by soaking by transfecting larger amounts of dsRNA. At 500 ng of transfected dsRNA I saw a fusion defect but this fusion defect was not as severe and not as repeatable as the one I saw with soaking (data not shown). Since the KD by soaking is much more robust than that caused by transfection, I used the soaking protocol for the remainder of my experiments.

Since we hypothesized that Dyn is recruited to the fusogenic synapse via its interaction with the SH2-SH3 adaptor proteins, I attempted to disrupt fusion by knocking down all three adaptor proteins individually, either by soaking or transfection. All three were expressed in S2R+ cells (FlyBase, Figure 2.12 C) and RT-PCR of all three KDs showed a reduction in mRNA levels (Figure 2.12 D). However, no effect on fusion was observed with single KDs (Figure 2.12 E). I also used larger amounts of dsRNA (3 fold) and performed multiple KD simultaneously by soaking and transfection (Figure 2.12 E,G). None of the

A

no KD ctr Crk KD drk KD dock KD

B

no KD ctr 3xCrk KD 3xdrk KD all KD

C

Flybase modENCODE S2R+ RNA-seq levels

High expression

Moderate

Crk Drk Dock shi

D

ctr crk KD

Crk primer

rP49 primer

ctr drk KD

drk primer

rP49 primer

ctr dock KD

dock primer

rP49 primer

E

ns

Fusion index (transfected cells)

no KD ctr Crk-KD Drk-KD Dock 3xcrk KD 3x Drk KD all KD all KD

RNA KD by soaking

F

no KD ctr 3xCrk KD 3xdrk KD 3xdock KD all KD all KD

Crk primers

drk primers

dock primers

rP49 primers

G

ns

Fusion index (transfected cells)

no KD ctr 3xcrk KD 3xdrk KD 3xdock KD

RNA KD by transfection

76

Figure 2.12 KD of SH2-SH3 adaptor proteins didn't cause a fusion defect

(A-B) S2R+ cells were treated with dsRNA against Crk, drk, or dock using the soaking with
dsRNA protocol and then co-transfected with Eff1 and Sns to induce fusion. 3x denotes
the three fold larger amount of dsRNA added to the medium in which the S2R+ cells
were cultured. S2R+ cells treated with 1x anti-dock dsRNA or 3x anti-drk dsRNA very
effected in their morphology/cell number.

(C) FlyBase model organisms RNAseq data indicated that Crk, Drk, and Dock are expressed
in S2R+ cells with drk being most abundant.

(D) RT-PCR was used to confirm a successful KD of adaptor protein mRNAs when soaked
with a single dose of respective dsRNA.

(E) Quantification of the fusion defect of cells treated with either single dose or triple dose of
respective dsRNA using the soaking protocol. No fusion defect was observed for any of
the conditions tested.

(F) RT-PCR confirmation of successful KD using transfection protocol

(G) Quantification of fusion index for adaptor protein KDs. No fusion defect was observed.

(E, G) The bar graph shows the mean and standard deviation. Additionally, the grey dots
show each individual value. Statistical significance analysis was performed with ANOVA
Tukey's multiple comparison test. Adjusted P-values are denoted as follows: * for $p<0.05$,
** for $p<0.01$, *** for $p<0.001$, **** for $p< 0.0001$ and ns for non-significant).

conditions tested yielded a fusion defect. In this experiment I observed that cells

soaked for 3-4 days with either a single treatment of anti-dock dsRNA or triple

treatment of anti-drk dsRNA looked less healthy (Figure 2.12 A). This was not

seen using the transfection protocol further confirming that the soaking protocol

is more efficient at KD.

Structure-function studies of Dyn in S2R+ cells treated with dsRNA against Dyn's

5'-UTR

Next, I attempted a rescue of the fusion defect caused by 5'UTR knock

down of Dyn. A complete rescue was achieved using Dyn-3HA and RFP-Dyn

(Figure 2.11 F, G).

This was a critical experiment to allow for structure-function experiments.

My experimental strategy has focused on three main directions:

1. Rescue of fusion defect using shi^{ts} alleles of Dyn at permissive and
   restrictive temperatures
2. Rescue of fusion defect with well-studied alleles of Dyn deficient in
   specific molecular functions which also act as DN in endocytosis
3. Rescue of fusion defect using mutants of Dyn reported to be
   diminished in their ability to bind F-actin directly

Rescue of fusion defect using shi^ts alleles of Dyn at permissive and restrictive temperatures.

S2R+ cells fuse at permissive and restrictive temperatures

My experiments using the *shi^ts* alleles require permissive (18-20℃) and restrictive temperatures (32-34℃). *Drosophila* cell lines are cultured 19-25℃. Cell-cell fusion assays in our lab are performed at room temperature and I first wanted to test that *Drosophila* cells can survive and more importantly fuse at these other temperatures. The S2R cells fused less at 20℃ (Figure 2.13 A, B) but this could be compensated if they were allowed to fuse for one extra day (transfected and cultured at room temperature for one day, than allowed to fuse at 20℃ for 2 days; Figure 2.13 C). S2R+ cells also fused at 32-34℃ but if they were left for two days at 34℃ they died. In summary, S2R+ cells were amenable to fusion assays at permissive and restrictive temperatures.

S2R+ cell-cell fusion rescue with *shi^ts* alleles at permissive and restrictive temperatures

I cloned the temperature-sensitive Dyn alleles (*ts1*, *ts2*, *ts4* and *TP4*) into Dyn-3HA backbone and checked their expression by western blotting (WB) at permissive temperature (20℃) and restrictive temperature (32℃). All four constructed expressed in S2R+ cells in levels similar to wt Dyn-3HA at permissive temperature (Figure 2.14 A). These were then used in conjunction with Dyn 5'UTR KD at permissive temperature (20℃) to assay for their ability to rescue S2R+ cell-cell fusion (Figure 2.14 B).
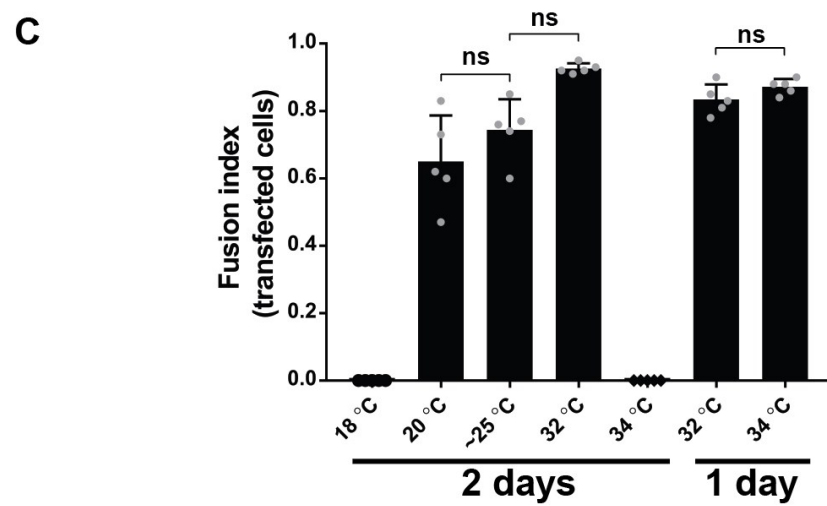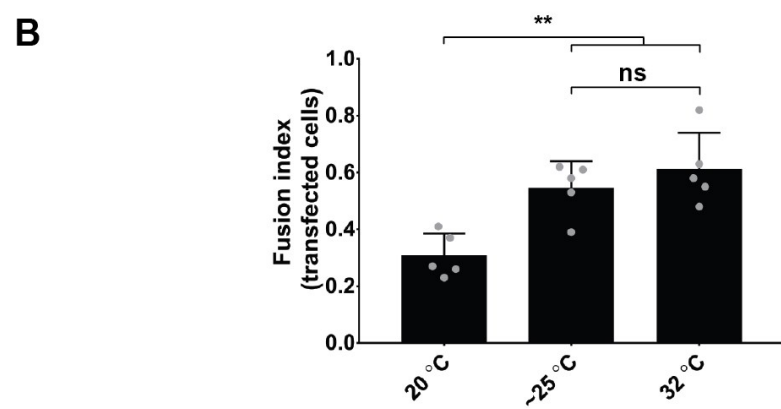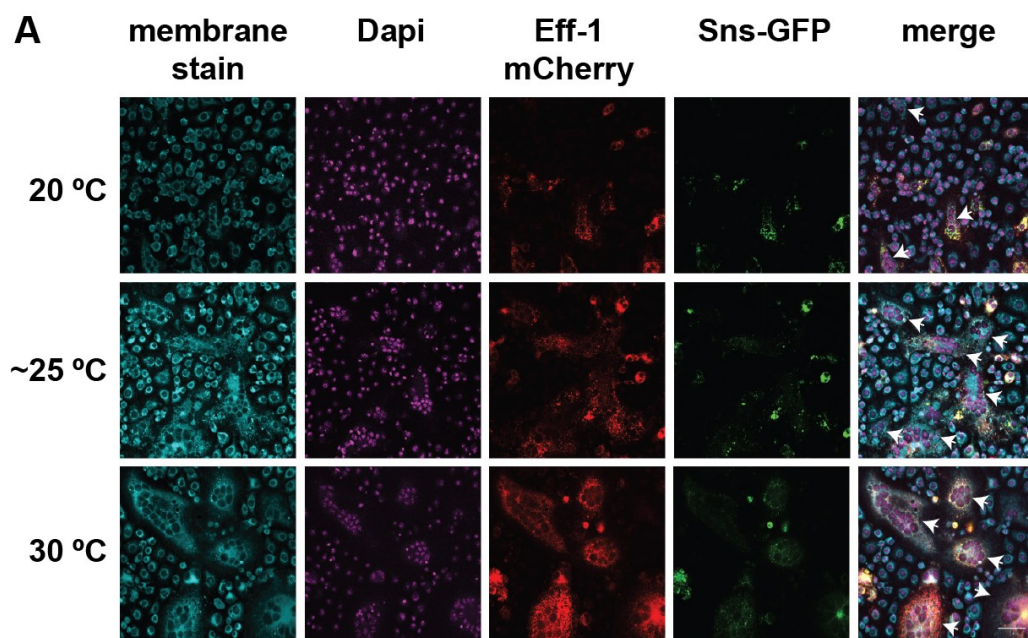
Figure 2.13 S2R+ cells can fuse at permissive and restrictive temperatures

(A) S2R+ cells were cotransfected with Eff-1-mCherry and Sns-GFP and incubated for two

days at 20, 25 or 32 ℃. Then cells were fixed and staining with a membrane dye to

visualize cell boundaries and syncytia. Significant fusion occurred at 25 and 32 ℃. Less

fusion occurred at 20 ℃. It seemed that the total cell count after two days at 20 ℃ was

lower than the other conditions despite similar amount of cells plated probably because of

a slower cell cycle progression at lower temperature. Scale bar 50 μm.

(B) The experiment shown in (A) was quantified for its fusion index. The number of nuclei in

syncytia vs. all transfected nuclei were counted for five different regions for each

condition.

(C) S2R+ cells were transfected and allowed to fuse at different temperatures: cells placed at

18 and 20 ℃ were transfected and left at 25 ℃ for one day and then placed at lower

temperatures for 2 days. Cells didn't fuse at 18 ℃ but cells allowed to fuse for 2 days at

20 ℃ had a fusion index similar to cells fusing at higher temperatures. Cells placed at

34 ℃ for 2 days died. Cells incubated for one day at 25 ℃ followed by one day at 34 ℃

appeared normal and fused well.

(B-C) The bar graph shows the mean and standard deviation. Additionally, the grey dots

show each individual value. Statistical significance analysis was performed with ANOVA

Tukey's multiple comparison test. Adjusted P-values are denoted as follows: * for $p < 0.05$,

** for $p < 0.01$, *** for $p < 0.001$, **** for $p < 0.0001$ and ns for non-significant).
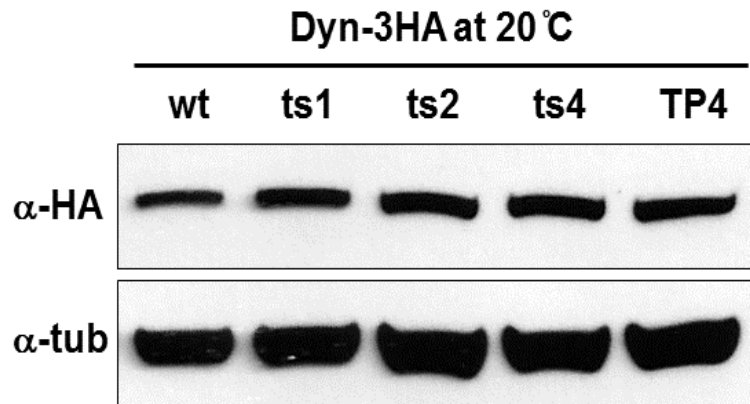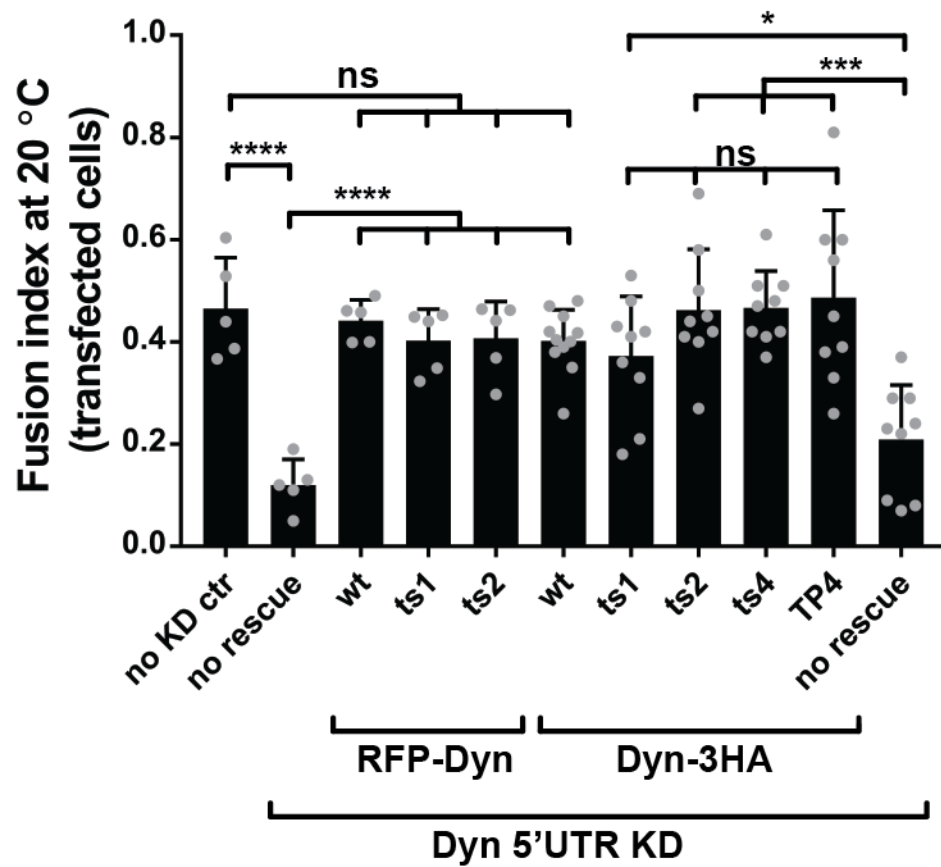
Figure 2.14 *shi^ts* alleles rescue S2R+ fusion at permissive temperature

(A) Dyn-3HA wt and four different ts alleles (*ts1, ts2*, *ts4* and *TP4*) were expressed in S2R+

cells which were cultured at permissive temperature. Their lysates were analyzed by WB

and they show comparable expression levels to wt protein.

(B) Same constructs were probed in their ability to rescue S2R+ fusion defect caused by dsRNA against 5'-UTR of Dyn. All four rescued the fusion defect significantly. The bar graph shows the mean and standard deviation. Additionally, the grey dots show each individual value. Statistical significance analysis was performed with ANOVA Tukey's multiple comparison test. Adjusted P-values are denoted as follows: * for $p<0.05$, ** for $p<0.01$, *** for $p<0.001$, **** for $p< 0.0001$ and ns for non-significant).

A

Dyn-3HA at 32℃

| | - | wt | ts1 | ts2 | ts4 | TP4 |

α-HA

α-tub

α-GFP

B

Dyn-3HA at 32℃

| wt | ts1 | ts2 | ts4 | TP4 |
| 125 | 400 | 100 | 100 | 350 |

α-HA

α-tub

α-GFP
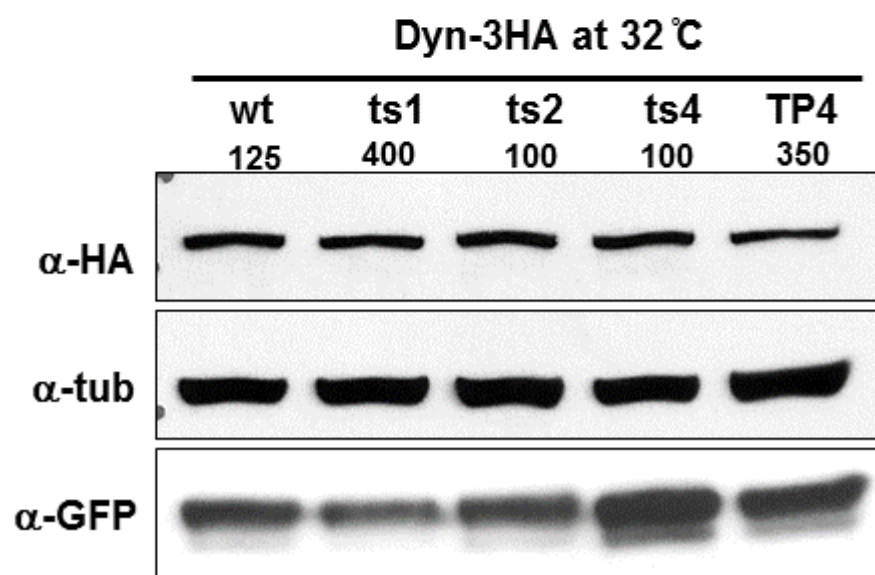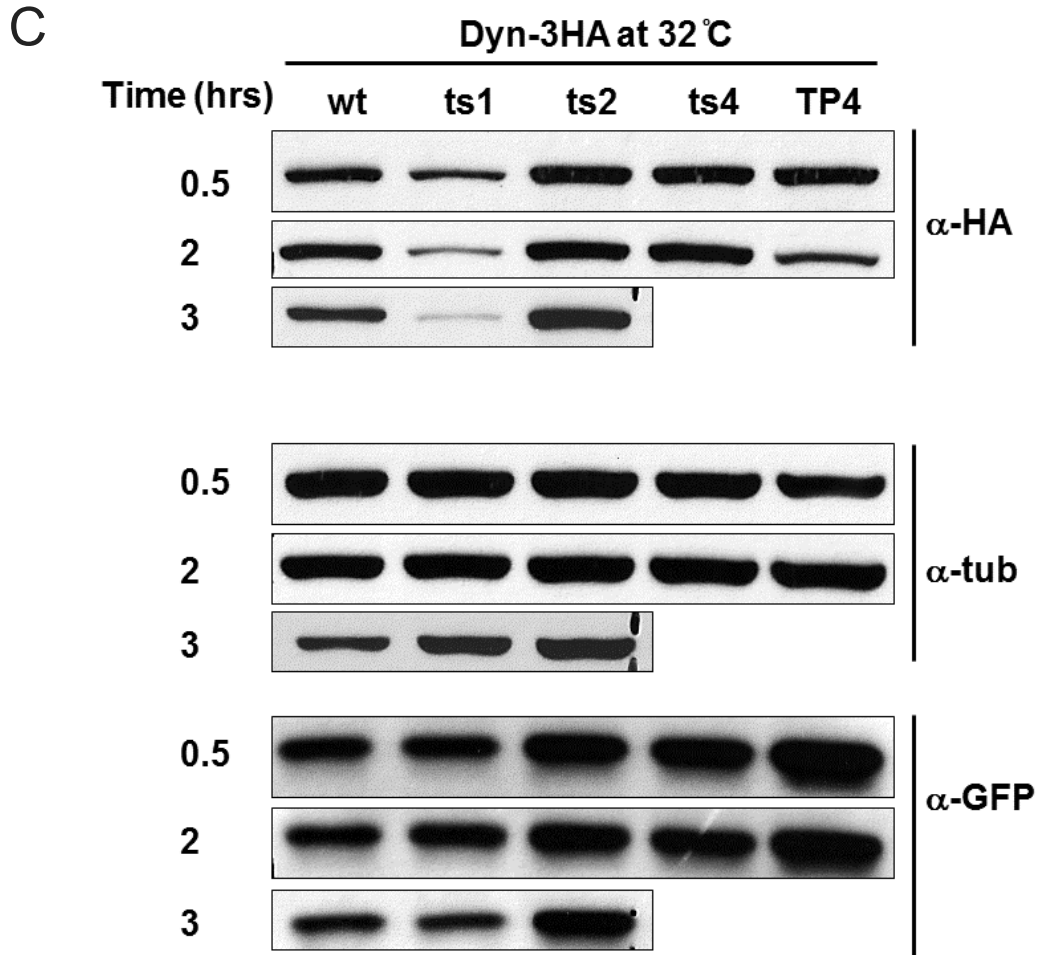
Figure 2.15 *shi*^{ts} alleles have different protein stability when expressed in S2R+ cells at restrictive temperature

(A) Dyn-3HA wt and four different ts alleles (*ts1*, *ts2*, *ts4* and *TP4*) were expressed in S2R+ cells which were cultured at restrictive temperature. Their lysates were analyzed by WB and they show that *ts1* and *TP4* had distinctly lower protein amounts which were not caused by differences in transfections which were assayed by GFP levels.

(B) Amount DNA transfected for *ts1* was adjusted 4 fold to level to achieve protein amounts similar to those observed for *wt*, *ts2* and *ts4*.

(C) An assay was designed to probe for the heat instability of ts1 protein. Dyn ts1 protein amounts decrease drastically within 3 hours of exposure to restrictive temperature.

A
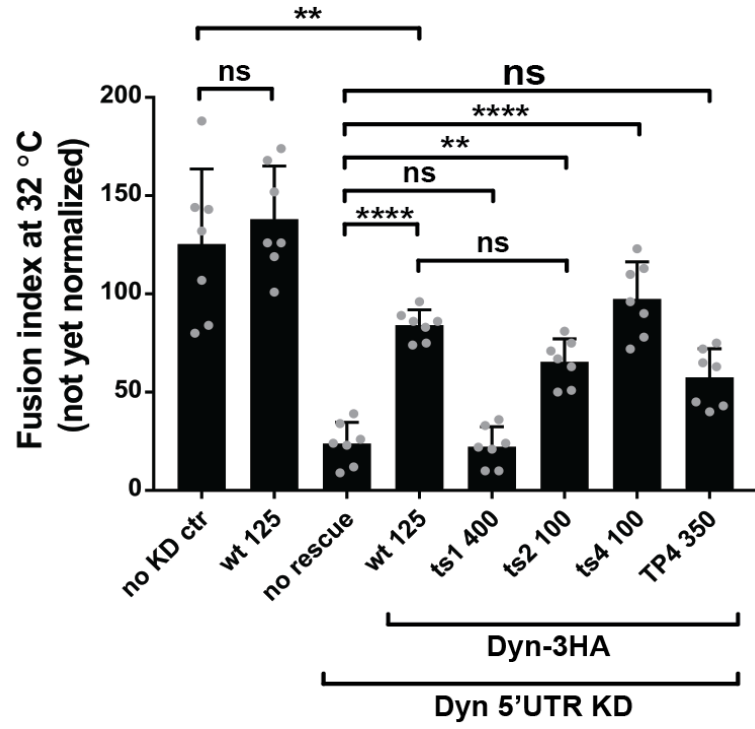
B
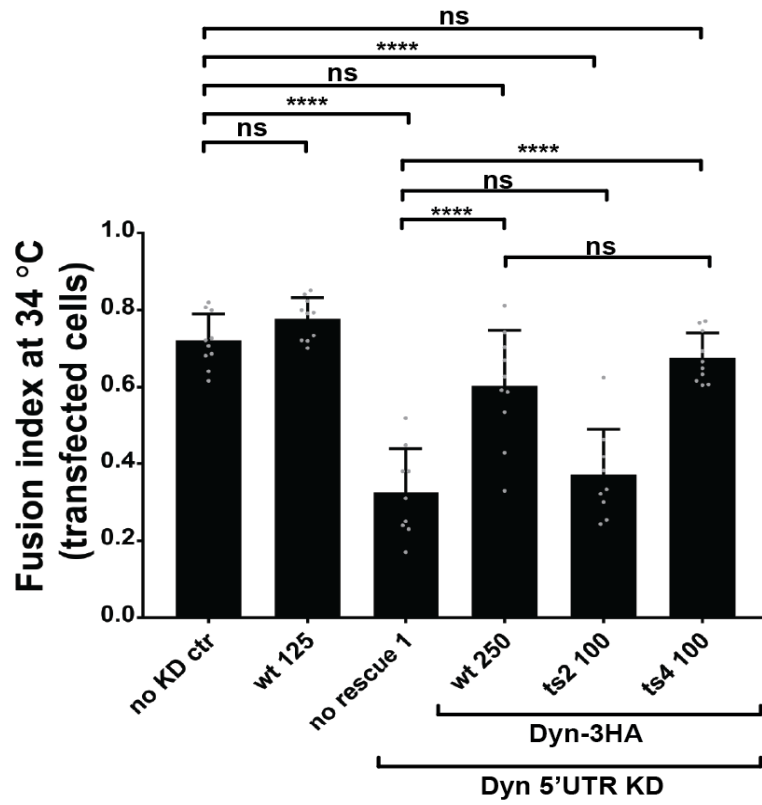
Figure 2.16 Rescue experiments of S2R+ cell-cell fusion using *shi^ts* alleles at restrictive temperatures

(A) At 32℃ *ts 2* and *ts4* but not *ts1 and TP4* were able to rescue the fusion defect caused by Dyn 5'UTR KD in fusing S2R+. Note that transfected plasmids amounts in ng had to be adjusted to compensate for the heat instability of *ts1* and *TP4* protein.

(B) At 34℃ ts4 but not ts2 rescues the fusion defect.

The bar graph shows the mean and standard deviation. Additionally, the grey dots show each individual value. Statistical significance analysis was performed with ANOVA Tukey's multiple comparison test. Adjusted P-values are denoted as follows: * for p<0.05, ** for p<0.01, *** for p<0.001, **** for p< 0.0001 and ns for non-significant).

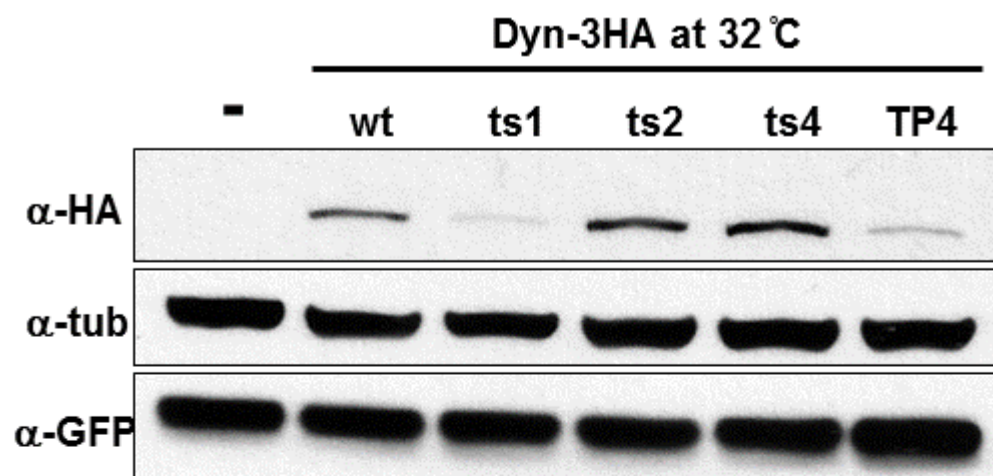As expected all four constructs rescued the fusion defect at permissive temperature. Next I tested the expression of these constructs at restrictive temperature (Figure 2.15 A). At 32℃ the protein levels detected by WB were drastically lower for *ts1* and *TP4* as compared to wt, *ts2* and *ts4*. In order to compare their ability to rescue cell-cell fusion, the amounts of DNA transfected for *ts1* were adjusted to 4 fold of the original amount and those for *TP4* 3.5 fold (Figure 2.15 B) to have comparable protein amounts by WB. Furthermore, I was curious how fast the protein amounts of *ts1* decrease at restrictive temperature, so I expressed wt, *ts1*, *ts, ts4* and *TP4* at 20℃ and then shifted the cells to 32℃ for 0.5-3 hours (Figure 2.15 C). Lower *ts1* proteins amounts were detected starting at 0.5 hours and after 3 hours they were already drastically lower. When assayed for their ability to rescue fusion, *ts4* but not *ts1* and *TP4* were able to rescue cell-cell fusion at 32℃ (Figure 2.16 A). *ts2* rescued at 32℃ (Figure 2.16 A) but not at 34℃ (Figure 2.16 B) which was surprising and may be explained by the presence of small amount of wt Dyn protein showing that *ts2* function at 32℃ in this assay is close to a threshold. I confirmed the expression and localization of the Dyn *ts2* and *ts4* to the F-actin foci in fusing S2R+ cells at restrictive temperature 34℃ (Figure 2.17).

Adult paralysis at restrictive temperature indicated that *ts4* is a severe allele for blocking endocytosis, even though it was not as severe as *ts1* and *ts2*. However, *ts4* was able to rescue cell-cell fusion similar or frequently better to wt protein. I found that very intriguing since it suggested that perhaps this allele can separate the endocytic and non-endocytic functions of Dyn. In order to test this

Sns-GFP	Dyn-3HA	Phalloidin	merge
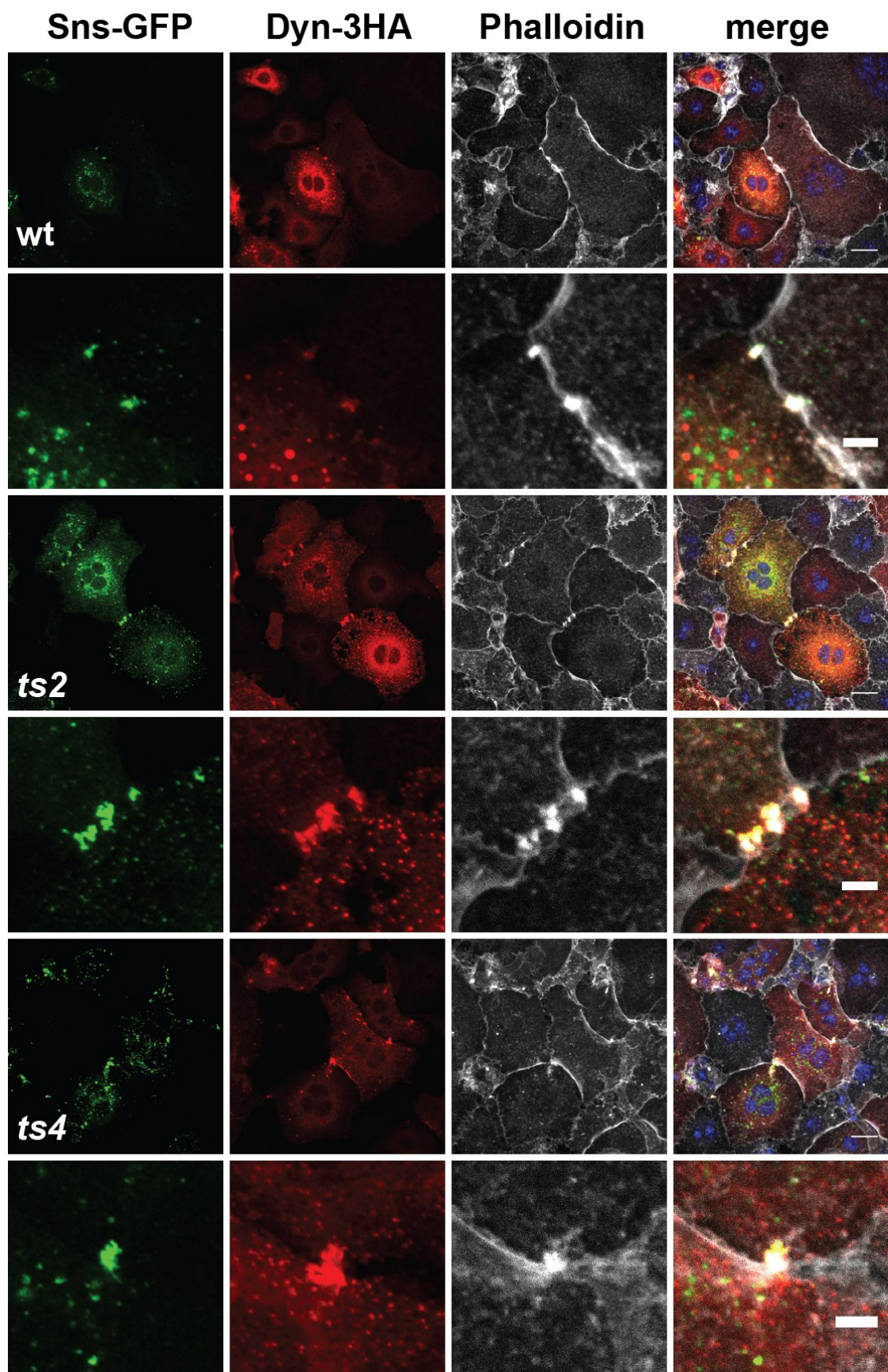
Figure 2.17 *ts2* and *ts4* both colocalize with F-actin foci at restrictive temperature 34 ℃

Mutant alleles were expressed in fusing S2R+ cells and their foci were observed. No obvious

differences in foci morphologies were detected and both mutant proteins localize to the F-

actin foci. Scale bar 20 μm in labeled frames, 2 μm

hypothesis, I performed an endocytosis assay to see if *ts4* is indeed a severe endocytic mutant in S2R+ cells.

Endocytosis assay to determine *shi^ts* allele strength in S2R+ cells

In order to assay the endocytosis in *Drosophila* S2R+ cells we decided to use the Transferrin (Tf) uptake which is a well-studied model for receptor-mediated endocytosis. Even though *Drosophila* has endogenous Tf and its receptor (Yoshiga et al., 1999), we decided to use the mammalian counterpart because of the commercial availability of fluorophore conjugated and iron-loaded Tf. Human Tf receptor was transfected into S2R+ cells and allowed to express for >24 hrs. Alexa488-labled Tf was added to the cells for 5 minutes after which endocytosis was blocked by placing the cells on ice. If endocytosis occurs normally, Tf receptor internalizes upon exposure to iron-loaded transferrin in less than 1 min in S2R+ cells (Gupta *et al*., 2009).

When Dyn mRNA was reduced in S2R+ cells by long dsRNA against Dyn's 5'UTR, it caused a strong inhibition of receptor mediated endocytosis, so the Tf-488 bound by the Tf receptor but was not internalized causing a strong surface staining (Figure 2.18). However, this endocytic defect was rescued upon expression of Dyn3HA wt leading to formation of small endocytic puncta and a drastic decrease of surface bound Tf-488 (Figure 2.18). Next I tested if *ts2* and *ts4* are capable of rescuing the endocytosis at restrictive temperature (34℃). *Ts4* but not *ts2* was able to rescue endocytosis under these conditions. This was
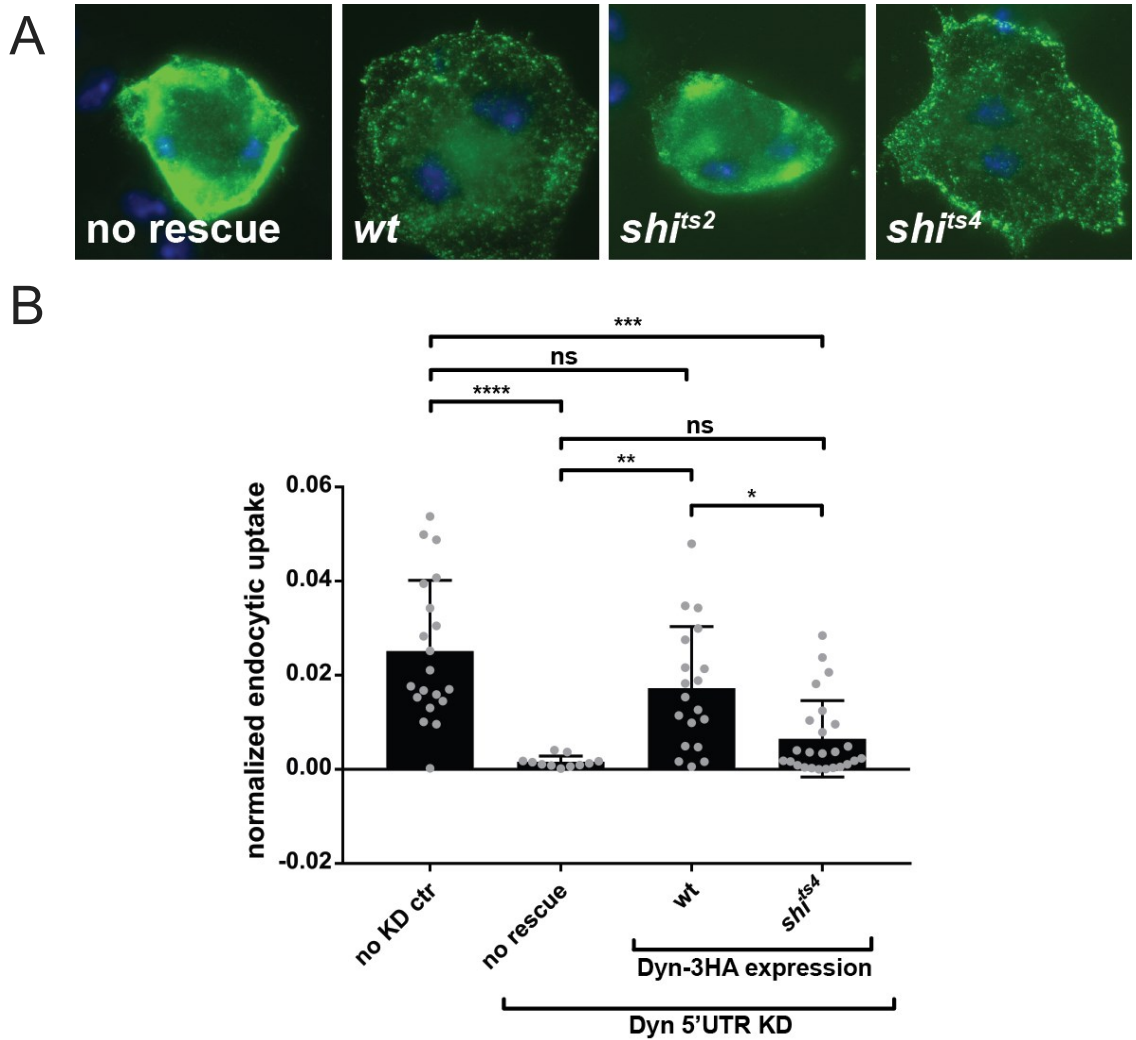
Figure 2.18 Receptor-mediated endocytosis is decreased in Dyn KD cells and can be rescued by either wt Dyn or partially by *ts4* allele at restrictive temperature

(A) S2R+ cells were subjected to Dyn KD using dsRNA against Dyn's 5'UTR and then transfected with mammalian Transferrin receptor and either empty vector or Dyn3HA wt, *ts2*, or *ts4*. These cells were then allowed to internalize conjugated Transferrin-488 (Tf-488, green) for 5 minutes through receptor-mediated endocytosis. Shi KD cells are unable to endocytose the Tf-488, so it remain bound to the receptor on the surface. Dyn3HA wt is able to rescue the endocytosis defect and Tf-488 is internalized by endocytosis into endocytic vesicles. Dyn *ts2* was unable to rescue endocytosis at 34℃. Dyn *ts4* was able to rescue endocytosis at 34℃.

(B) Quantification of the endocytic uptake of Tf-488 in Dyn KD cells vs. no KD control cells. Dyn3HA wt is able to rescue the endocytosis defect at 34℃. Even though Dyn3HA *ts4* was able to qualitatively rescue the endocytosis defect, it is not statistically significant.

The bar graph shows the mean and standard deviation. Additionally, the grey dots show each individual value. Statistical significance analysis was performed with ANOVA Tukey's multiple comparison test. Adjusted P-values are denoted as follows: * for $p<0.05$, ** for $p<0.01$, *** for $p<0.001$, **** for $p< 0.0001$ and ns for non-significant).

surprising since I anticipated that *ts4* would not rescue endocytosis at this temperature (the experiment was done in triplicate). A quantification of the endocytic uptake showed that *ts4* is less efficient in rescuing endocytic uptake than wt Dyn. However, *ts4* always rescued fusion as well or better than wt. This suggest that maybe this allele is able to separate Dyn's endocytosis-dependent and independent function to some extent but more tests are needed to confirm this result since qualitatively *ts4* rescued endocytosis.

Rescue of fusion defect with well-studied alleles of Dyn deficient in specific molecular functions which also act as DN in endocytosis

Dyn is a large GTPase. In cells it is a dimer or tetramer that oligomerize into higher order structures. Several Dyn mutants exist that impair a specific molecular aspect of Dyn's function. When overexpressed in cells, these mutants function as strong dominant-negative (DN) effectors of endocytosis. I wanted to investigate which of Dyn's molecular functions are required for its function in fusion, so I decided to use four GTPase domain and one PH domain mutants in my experiments (Table 5).

Point mutations Q40E, S45N, D180A and K142A are located in the GTPase domain. Similar to wt, they are able to assemble into the higher oligomer structure, bind the membrane and generate curvature. S45N mutation introduces a bulky sidechain of the asparagine residue into the active site and prevents GTP binding; therefore, this mutant no longer hydrolyzes GTP (Marks *et al*., 2001; Chappie *et al*., 2010). In contrast, the basal GTPase activity of Q40E, K142A and

94

Table 5: *Drosophila* homologues of previously characterized DN mammalian Dyn mutants

Mammalian Dyn mutation	Effect	*Drosophila* position
Q40E	Loss of assembly-stimulated enhancement of GTPase activity	Q35
S45N	No GTP binding	S40
K142A	GTP-hydrolysis associated conformational change that alters the pitch of Dyn helix	K137
D180A	Loss of assembly-stimulated enhancement of GTPase activity	D175
I533A	Unable to generate membrane curvature	I527

D180A is similar to wt (Chappie *et al*., 2010). When Dyn assembles into higher order structures, GTPase domains that proximate to each other in adjacent helical turns or rings interact to enhance the GTPase activity. This interaction is mediated by D180 which orients Q40, S41 and G62 in the active site for a more efficient GTP hydrolysis (Chappie *et al*., 2010). Q40E and D180A lack assembly stimulated enhancement of the GTPase activity (Chappie *et al*., 2010). Since K142 has also been shown to be involved in GTPase interactions across helix turns it is hypothesized to also respond to Dyn oligomerization (Chappie *et al*., 2010). Specifically, K142 is thought to mediate GTP-hydrolysis associated conformational change that alters the pitch of Dyn helix which is compromised when mutated (Marks *et a*l., 2001, Feng, 2001).

Dyn's PH domain has a low affinity for phosphatidylinositol 4,5-bisphosphate (PIP_2) that relies on Dyn oligomerization. This interaction is mediated by key residues in the three variable loops (VL) which form a binding pocket for the PIP_2. Additionally, the relatively hydrophobic variable loop 1 (VL1) in the PH domain inserts itself into the acyl chain region of lipid bilayers when PA, PS and phosphoinositides -phosphatidylinositol 4-phosphate (PI_4P) and – are present (Ramachandran and Schmidt, 2008; Burger *et al*., 2010). This VL1 membrane insertion contributes to Dyn's ability to generate curvature upon oligomerization which becomes apparent in experiments utilizing fluid supported bilayer with excess membrane reservoir (SUPER) templates (Pucadyil T.J. and S.L. Schmidt, 2008). In these experiments Dyn in absence of GTP assembles

into spirals and induces membrane tubulation, and upon GTP addition it catalyzes membrane fission and vesicle release.

The residue I533 found at the base of VL1 and is essential for Dyn 1 function and I533A mutant blocks endocytosis at the step of deeply invaginated pits with a constricted neck (Ramachandran *et al*., 2009). SUPER template experiments revealed that I533A mutant is severely impaired in its ability to generate tubules but it can mediate fission on precurved membrane tubes. Therefore, I533A is specifically deficient in membrane curvature generation.

I hypothesized that if one of the mutants would be able to rescue the S2R+ fusion defect generated by 5'-UTR KD of Dyn, it would indicate that that function is not needed for fusion and at the same time it would separate Dyn's role in endocytosis and fusion. I was especially hopeful for I533A's potential to rescue cell-cell fusion. However, even if none of the mutants would rescue cell-cell fusion, they would inform me that these specific molecular functions are required for cell-cell fusion.

First I wanted to confirm that none of these DN Dyn alleles can rescue endocytosis in S2R+ cells (Figure 2.19) which they were not. Next I wanted to test their ability to rescue S2R+ fusion. The expression of these mutants in S2R+ cells confirmed by western blotting (Figure 2.20 A). To test their ability to rescue fusion I knocked down Dyn using dsRNA against its 5'UTR and co-expressed Eff1, Sns, and Dyn-HA wt or mutant. None of the DN Dyn alleles were able to rescue fusion and several of them seemed to function as DN alleles in fusion, too.

A

Dyn-3HA	Tf-488	TfR	merge+Dapi

no KD ctr

5'UTR

5'UTR + wt

Dyn-3HA | Tf-488 | TfR | merge+Dapi

5'UTR + S45N

5'UTR + K142A

5'UTR + D180A
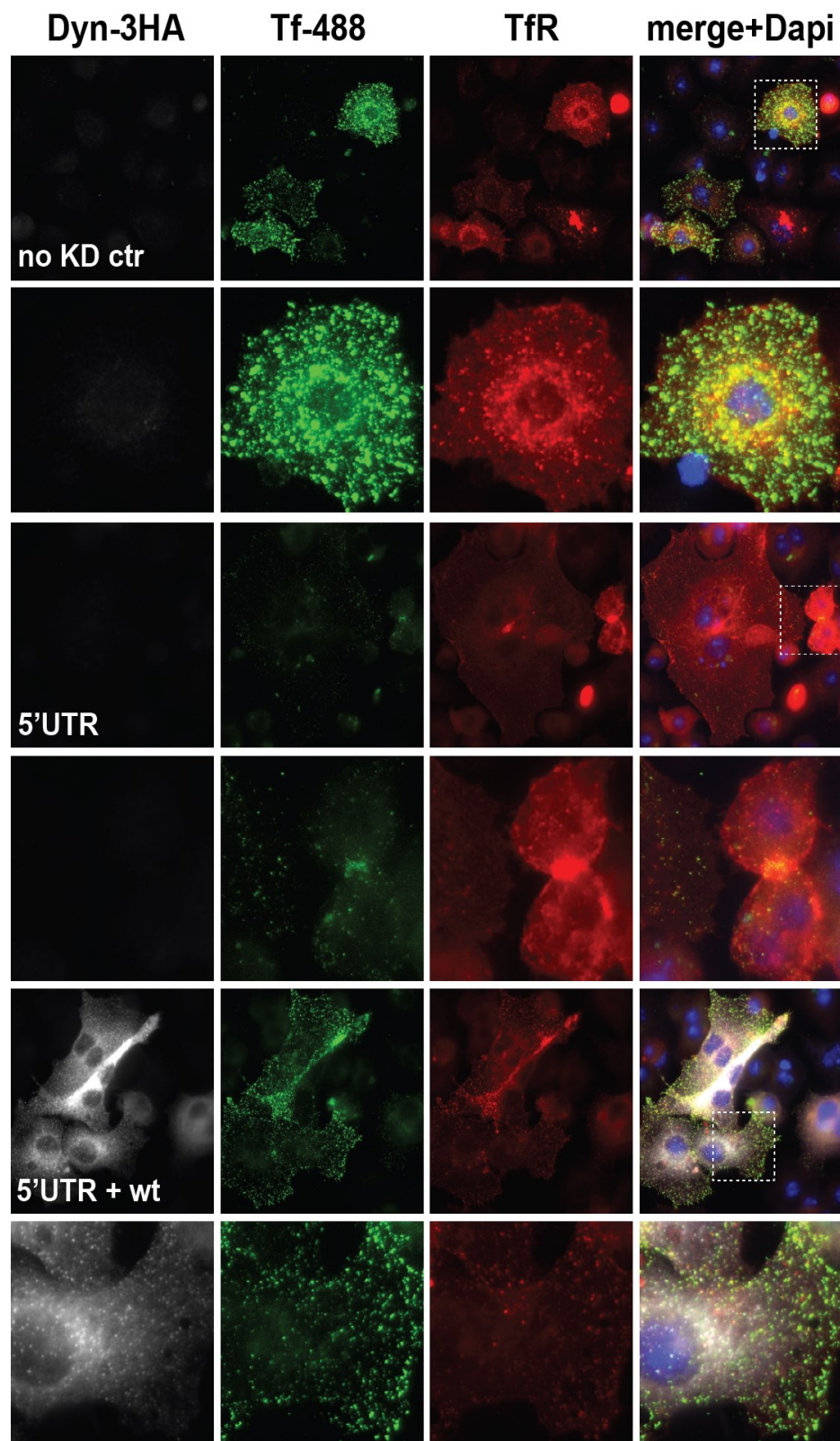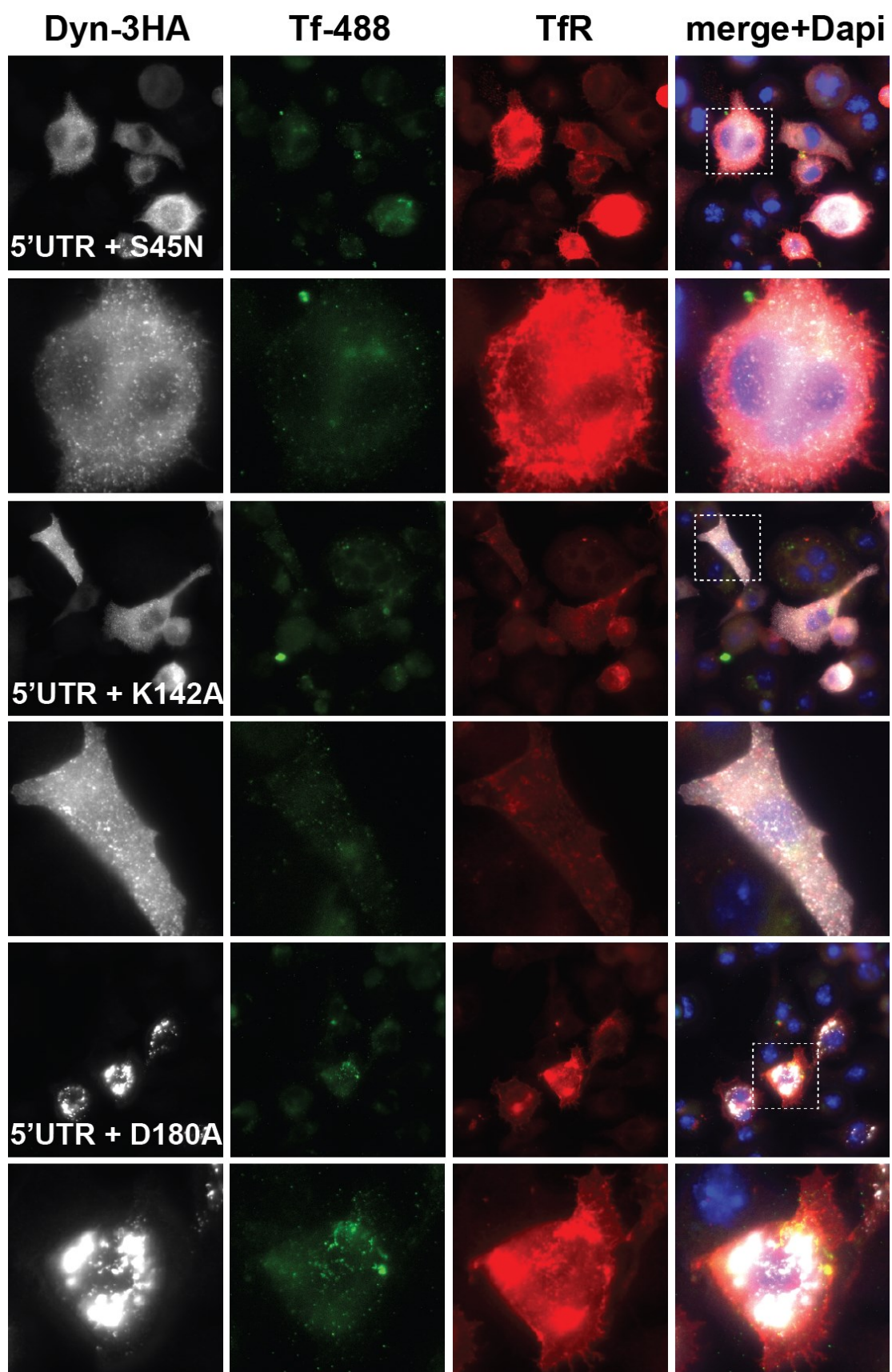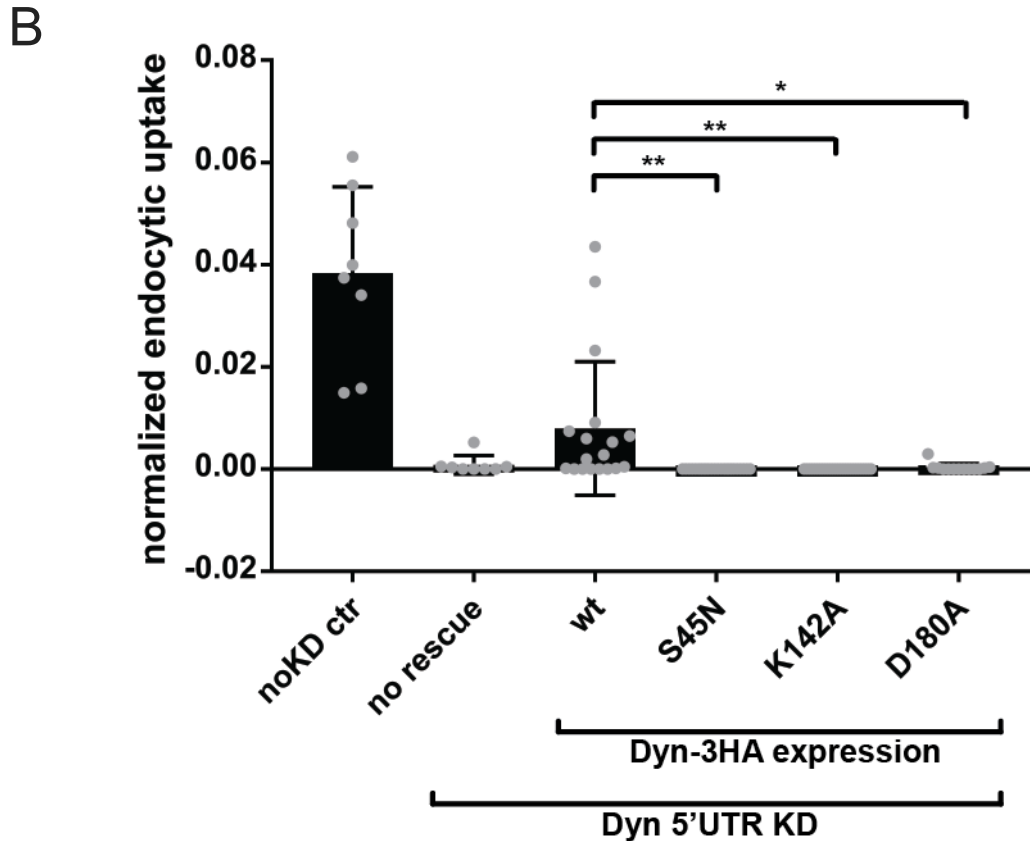
Figure 2.19 Homologues of mammalian endocytic DN Dyn alleles failed to rescue receptor-mediated endocytosis in S2R+ cells

(A) S2R+ cells were subjected to Dyn KD using dsRNA against Dyn's 5'UTR and then transfected with mammalian Transferrin receptor (TfR, red) and either empty vector or Dyn3HA wt or several point mutants (grey). These cells were then allowed to internalize conjugated Transferrin-488 (Tf-488, green) for 5 minutes through receptor-mediated endocytosis. Then the cells were subjected to an acid wash which removes all surface bound Tf-488 from the cells. Dyn KD cells are unable to endocytose the Tf-488, so it remained bound to the receptor on the surface and washed away by the acid wash. Dyn3HA wt is able to rescue the endocytosis defect and Tf-488 is internalized by endocytosis into endocytic vesicles to some extent (it is not clear why it didn't rescue to levels seen in noKD ctr.) None of the Dyn point mutants was able to rescue the endocytic defect.

(B) The endocytic uptake of Tf-488 in (A) was quantified and confirms that the point mutants can't rescue the endocytic defect caused by dsRNA against Dyn's 5'UTR.

The bar graph shows the mean and standard deviation. Additionally, the grey dots show each individual value. Statistical significance analysis was performed with ANOVA Tukey's multiple comparison test. Adjusted P-values are denoted as follows: * for $p<0.05$, ** for $p<0.01$, *** for $p<0.001$, **** for $p< 0.0001$ and ns for non-significant).
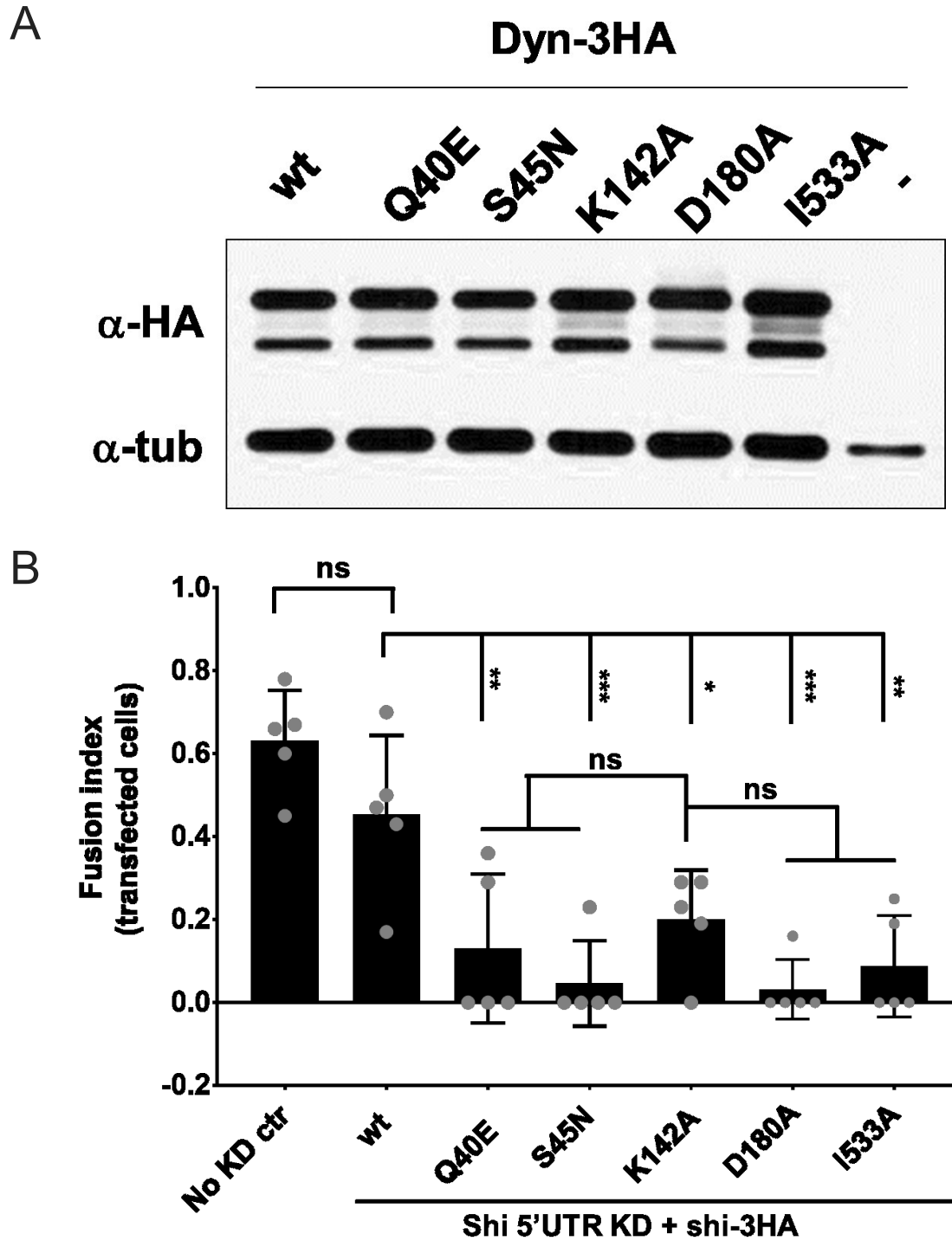
Figure 2.20 Homologues of mammalian endocytic DN Dyn alleles failed to rescue cell-cell fusion in S2R+ cells

(A) Expression of several Dyn point mutants was confirmed by western blotting.

(B) None of the Dyn point mutants were able to rescue cell-cell fusion defect caused by dsRNA against Dyn's 5'UTR.

The bar graph shows the mean and standard deviation. Additionally, the grey dots show each individual value. Statistical significance analysis was performed with ANOVA Tukey's multiple comparison test. Adjusted P-values are denoted as follows: * for $p<0.05$, ** for $p<0.01$, *** for $p<0.001$, **** for $p< 0.0001$ and ns for non-significant).

A

Dyn-3HA	Tf-488	TfR	merge + Dapi

K142A

D180A

I533A
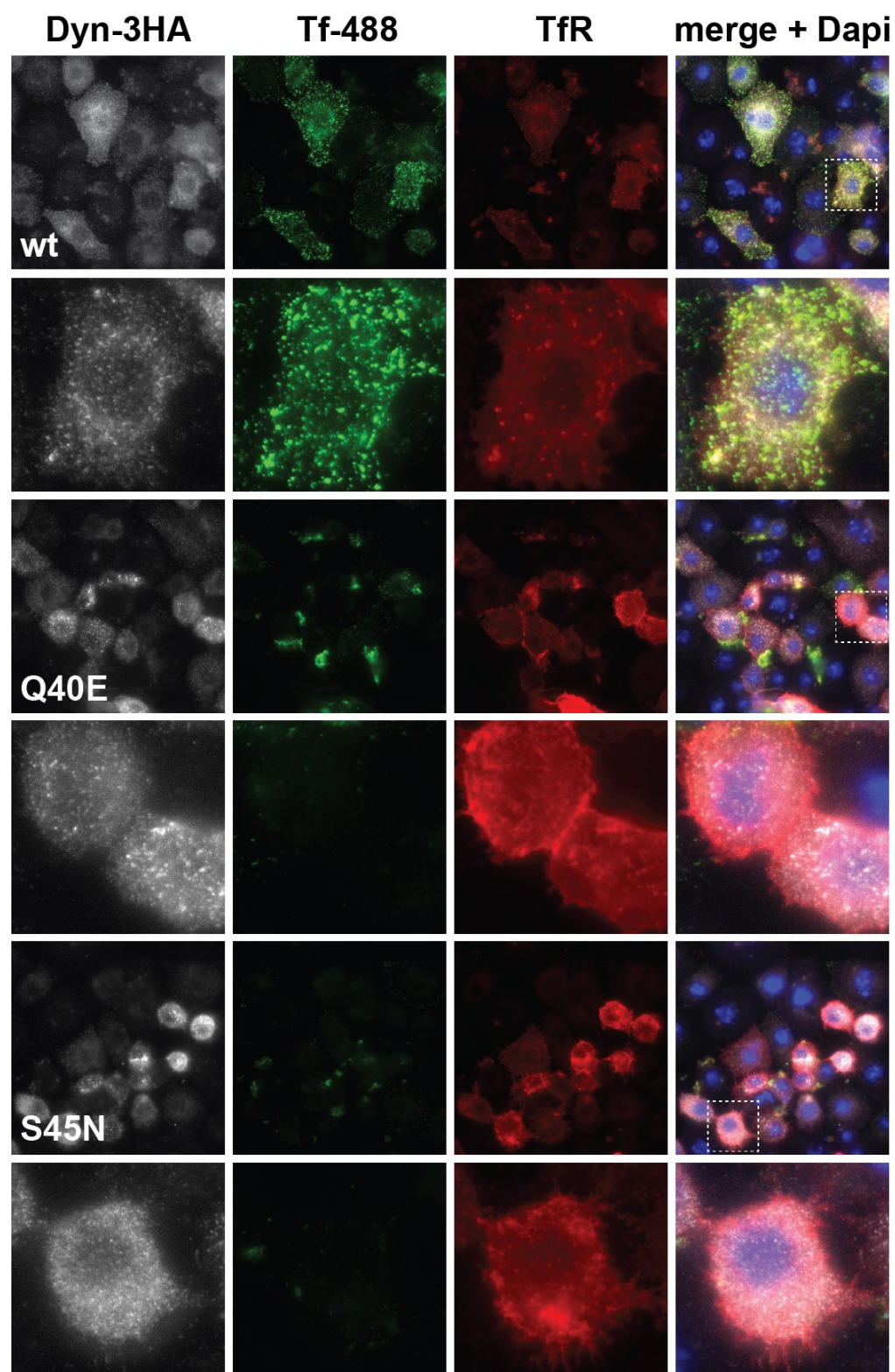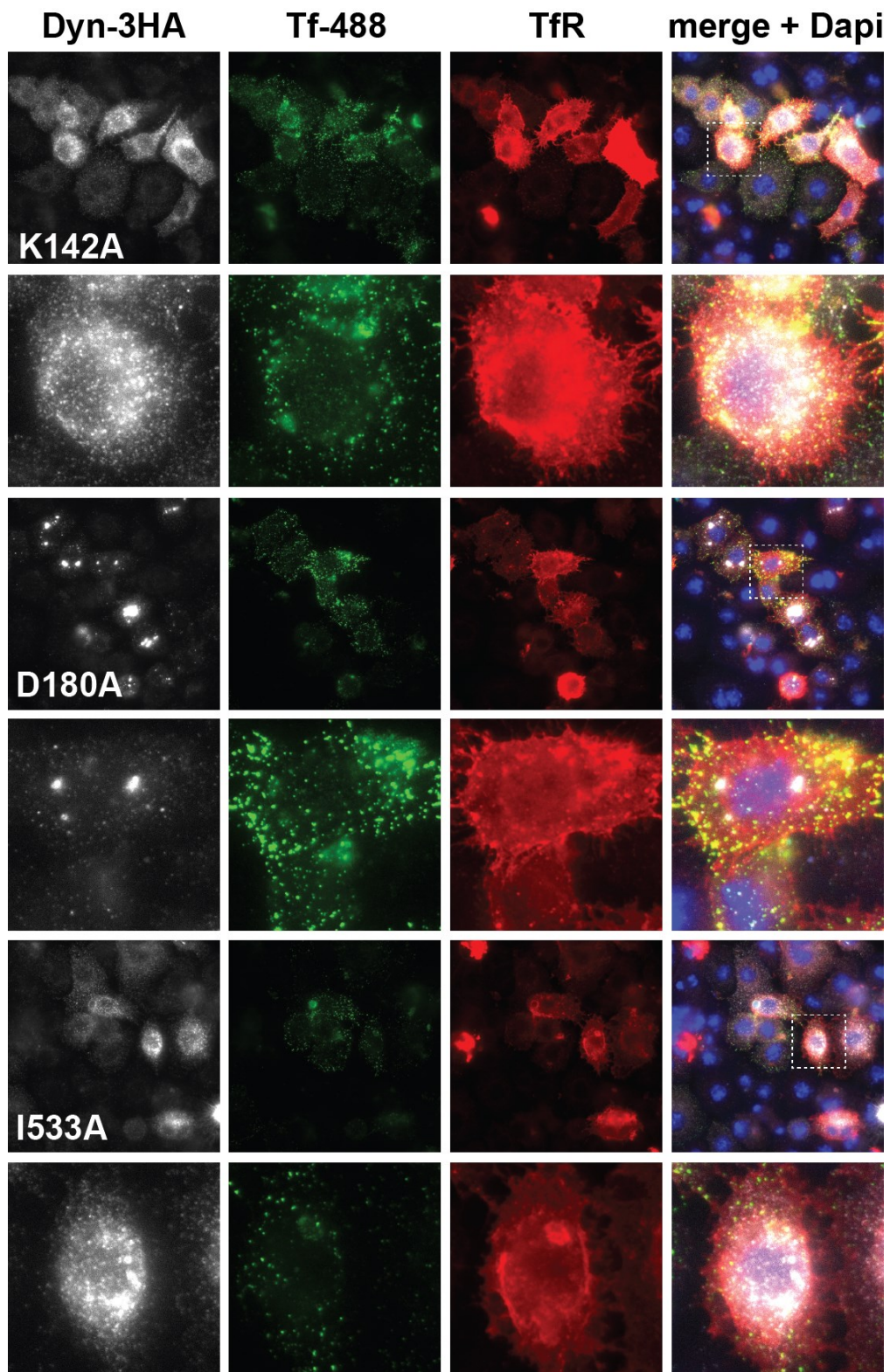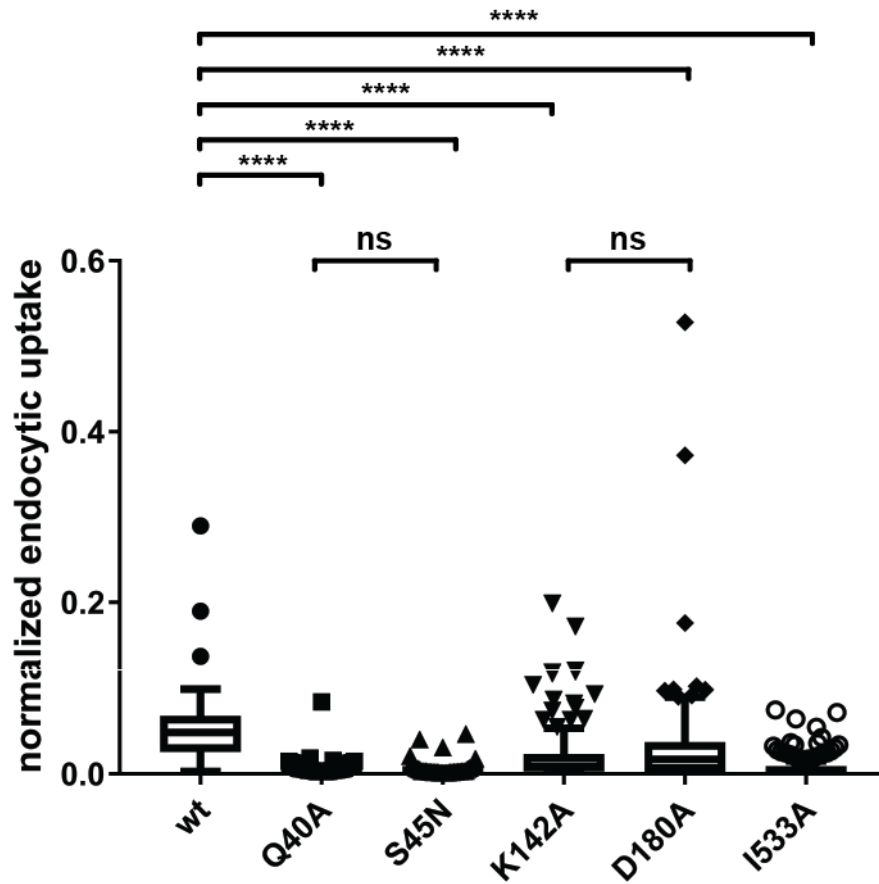
Figure 2.21 Confirmation that homologues of mammalian Dyn mutants function as DN in receptor-mediated endocytosis when overexpressed in S2R+ cells

(A) S2R+ cells were transfected with mammalian Transferrin receptor (TfR, red) and either empty vector or Dyn3HA wt or several point mutants (grey). These cells were then allowed to internalize conjugated Transferrin-488 (Tf-488, green) for 5 minutes through receptor-mediated endocytosis. Then the cells were subjected to an acid wash which removes all surface bound Tf-488 from the cells. In cells unable to endocytose the Tf-488, it remained bound to the receptor on the surface and washed away by the acid wash. All but Dyn3HA K142A and D180A mutants functioned as strong DN endocytic alleles.

(B) The endocytic uptake of Tf-488 in (A) was quantified and confirms that the point mutants function as strong DN endocytic alleles.

Data is displayed using the Tukey box and whiskers plot. Statistical significance analysis was performed with ANOVA Tukey's multiple comparison test. Adjusted P-values are denoted as follows: * for p<0.05, ** for p<0.01, *** for p<0.001, **** for p< 0.0001 and ns for non-significant).
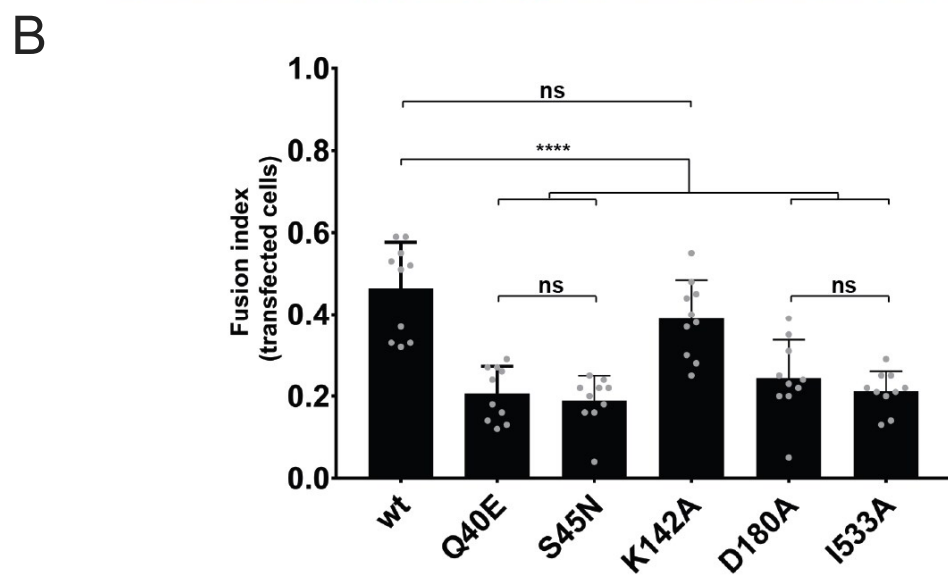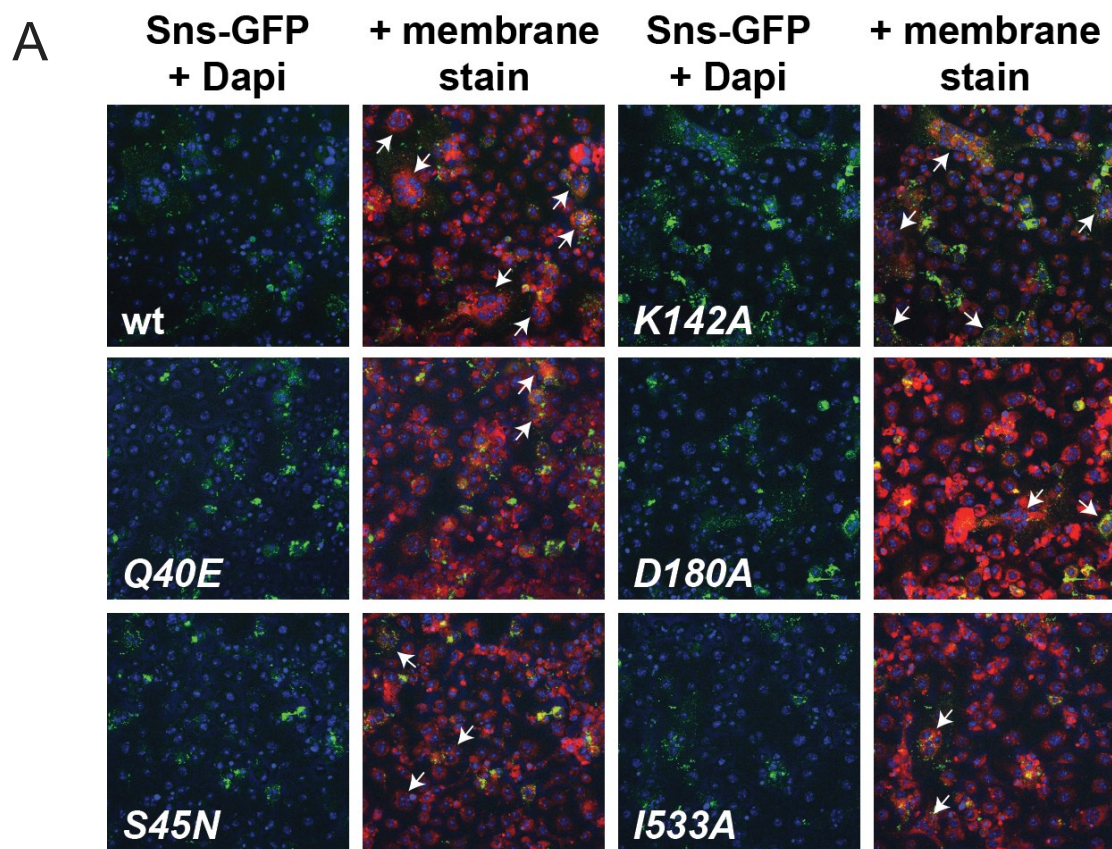
Figure 2.22 Homologues of DN endocytic Dyn alleles also function as DN in cell-cell fusion when overexpressed in S2R+ cells

(A) S2R+ cells were co-transfected with Eff1, Sns, and Dyn (wt or DN mutant alleles) and allowed to fuse for 2 days. All mutants except K142A decreased cell-cell fusion.

(B) S2R+ fusion was quantified and confirm the qualitative observations in (A).

The bar graph shows the mean and standard deviation. Additionally, the grey dots show each individual value. Statistical significance analysis was performed with ANOVA Tukey's multiple comparison test. Adjusted P-values are denoted as follows: * for $p<0.05$, ** for $p<0.01$, *** for $p<0.001$, **** for $p< 0.0001$ and ns for non-significant).

Phalloidin	Dyn-3HA	Sns-GFP	merge+Dapi
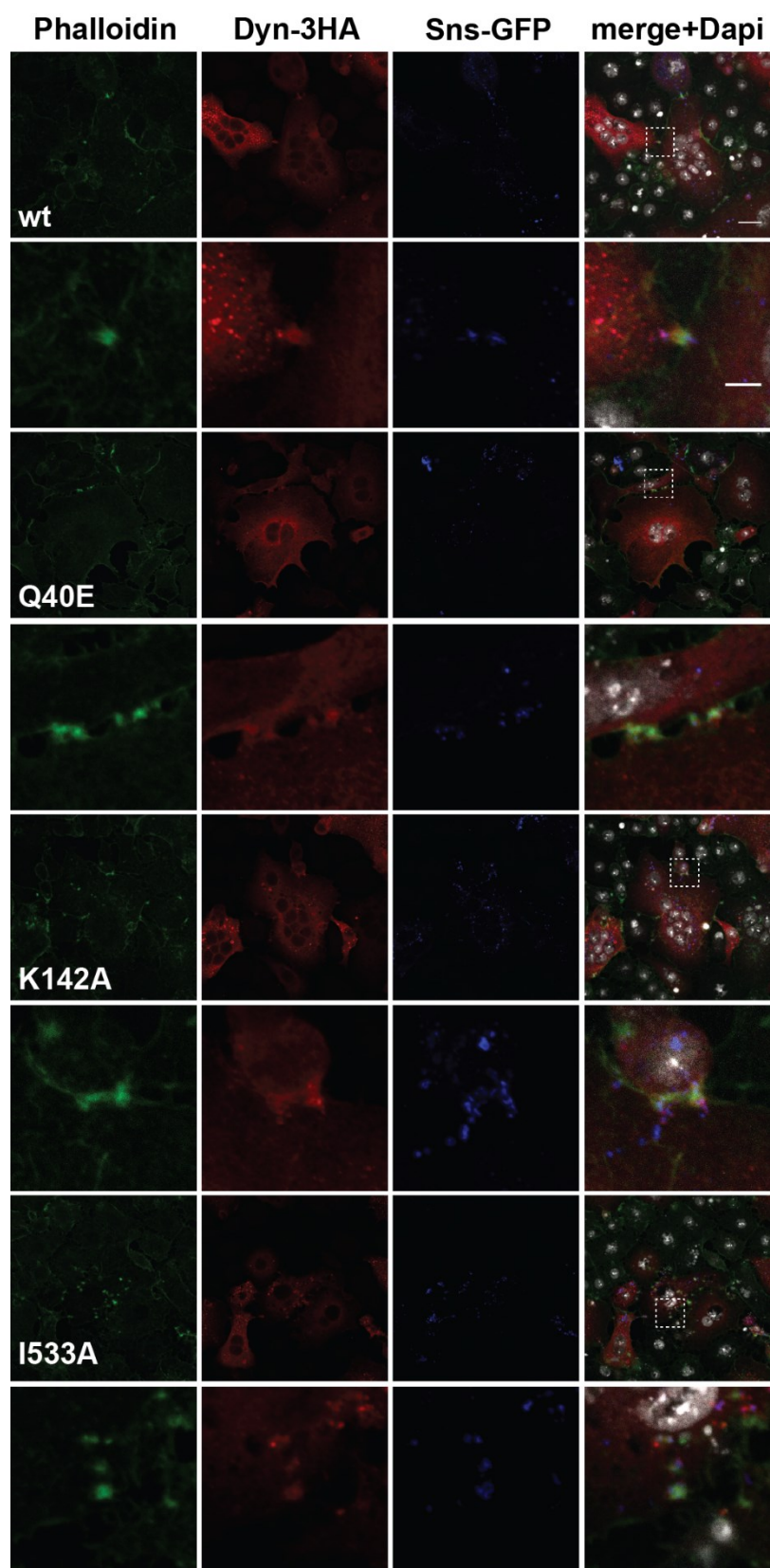
Figure 2.23 Dyn DN alleles localize to F-actin foci with no apparent differences in F-actin foci morphologies

The F-actin foci morphologies for S2R+ cells expressing several different DN Dyn alleles were observed and no apparent differences were discovered Scale bar 20 μm in large images, 5 μm in close-up below.

Table 6 Summary of experiments using Dyn DN alleles

DM homologue of Dyn mutant	S2R+ Fusion		S2R+ Endocytosis	
	Rescues 5'UTR KD fusion defect?	Overexpression causes a defect?	Rescues 5'UTR KD endocytosis defect?	Overexpression causes a defect?
(wt)	YES	NO	YES	(NO)
Q40E	NO (DN)	YES	-	YES (strong DN)
S45N	NO (DN)	YES	NO	YES (strong DN)
K142A	NO	NO	NO	Yes (weak DN)
D180A	NO	YES	NO	Yes (weak DN)
I533A	NO (DN)	YES	-	YES (strong DN)

This DN effect of these mutants was be further investigated in fusing S2R+ cells with no KD. I confirmed that they function as DN in endocytosis (Figure 2.21) and cell-cell fusion (Figure 2.22) when overexpressed in S2R+ cells. Surprisingly, K142A was not a strong DN in endocytosis and not statistically different from wt in cell-cell fusion. Furthermore, I examined the F-actin foci of fusing S2R+ cells that express these mutants and did not see any gross differences (Figure 2.23).

In summary, the effect of DN Dyn alleles on endocytosis and cell-cell fusion are highly correlated in S2R+ cells (Table 6). This may indicate that Dyn's diverse molecular function is required in both processes. Alternatively, it could mean that the observed fusion defect may be due to endocytic defect.

I have attempted to disrupt endocytosis by a Dyn-independent way through a knock down of clathrin (clathrin light chain and clathrin heavy chain) and rab5. First I confirmed a successful KD clathrin light and heavy chain by dsRNA (Figure 2.24 A). Knock down of these leads to a statistically significant fusion defect (Figure 2.24 B,C). However, it is hard to know if the effect of cell-cell fusion is direct.

Rescue of fusion defect using mutants of Dyn reported to be diminished in their ability to bind F-actin directly

Dyn's F-actin binding ability was mapped to the middle domain of Dyn, specifically to several positively charged amino acids (marked red in Figure. 2.25 D, Gu *et al*., 2014).

A

B

| Phalloidin | Eff-1-mCherry | Sns-GFP | merge |

ctr

CLC KD

CHC KD
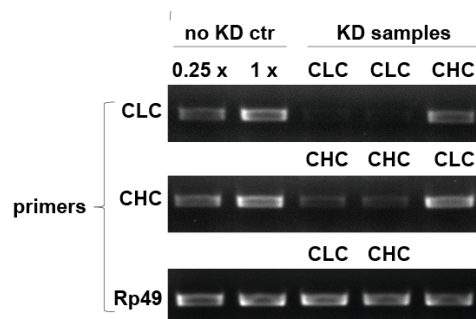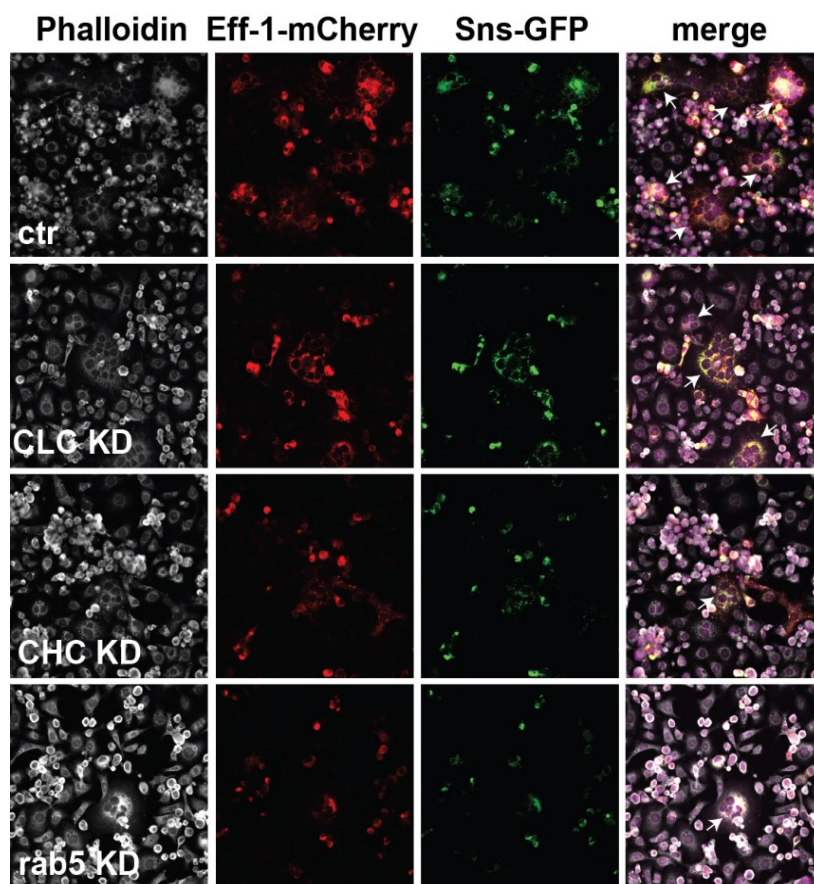
rab5 KD

C
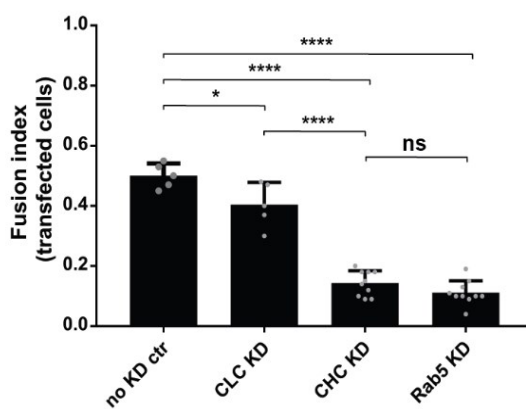
Figure 2.24 Knock down of clathrin and rab5 causes a fusion defect in S2R+ cells

(A) RT-PCR was used to confirm successful KD of Clathrin Light Chain (CLC) and Clathrin Heavy chain (CHC). Rab5 KD was also successful but not shown here.

(B) KD of CHC caused a noticeable fusion defect. rab 5 KD cells looked unhealthy.

(C) Quantification of the fusion defect observed in (B). KD of CLC causes a small but statistically significant fusion defect.

The bar graph shows the mean and standard deviation. Additionally, the grey dots show each individual value. Statistical significance analysis was performed with ANOVA Tukey's multiple comparison test. Adjusted P-values are denoted as follows: * for $p<0.05$, ** for $p<0.01$, *** for $p<0.001$, **** for $p< 0.0001$ and ns for non-significant).

A

| | Phalloidin | Dyn-3HA | Sns-GFP | merge + Dapi |

no KD ctr + wt

no rescue

wt

5xAKE

5xABD

2xAEK
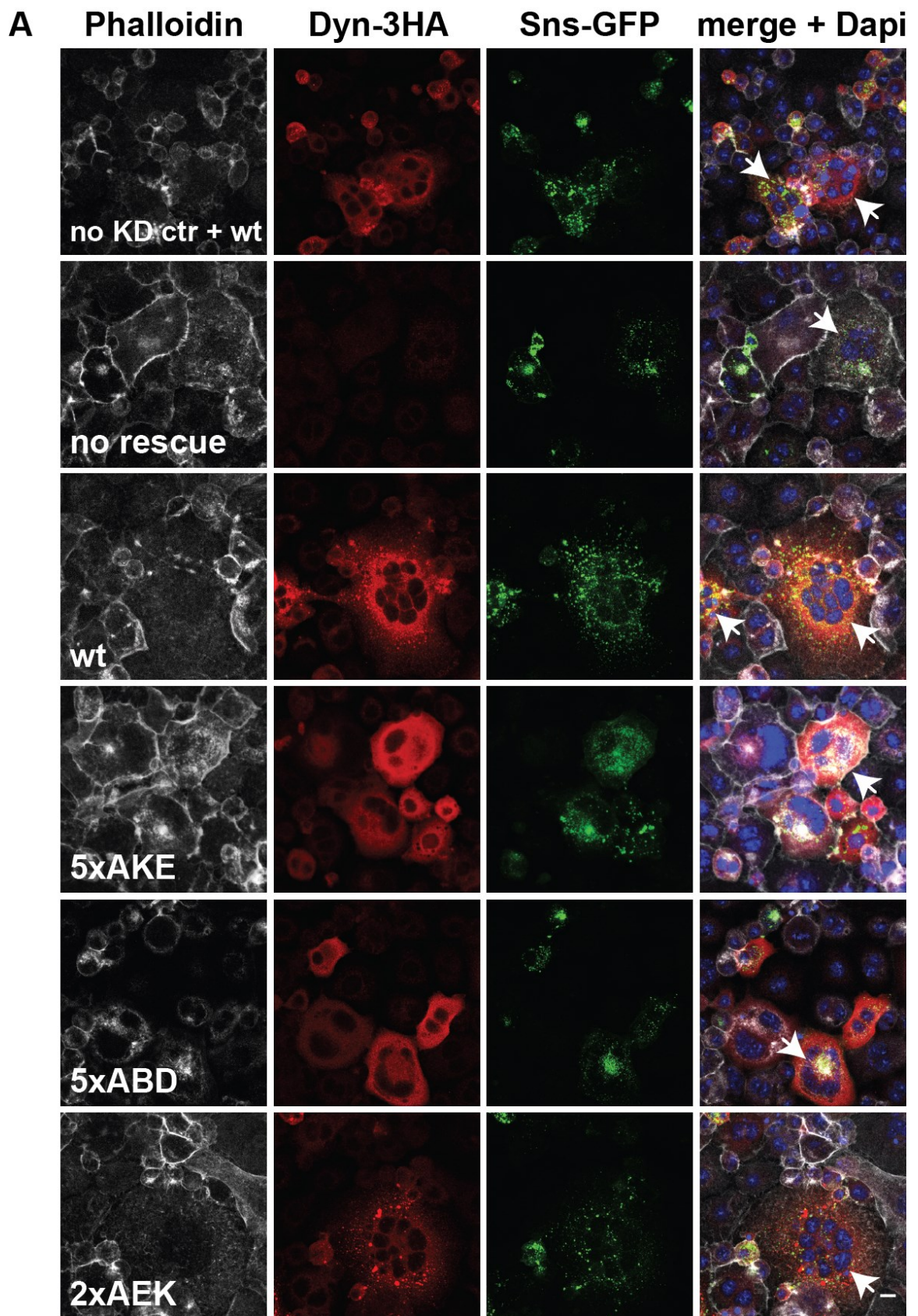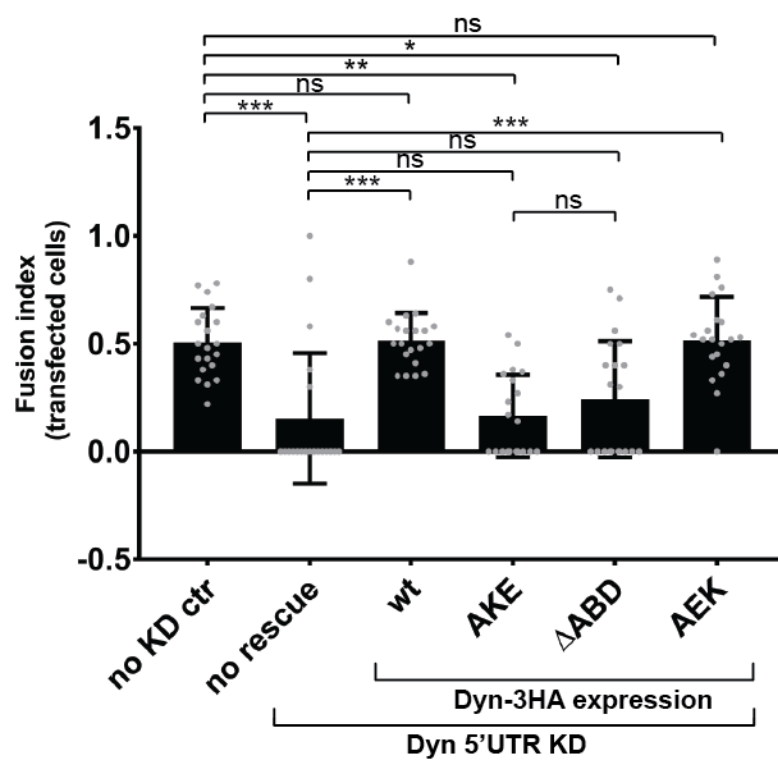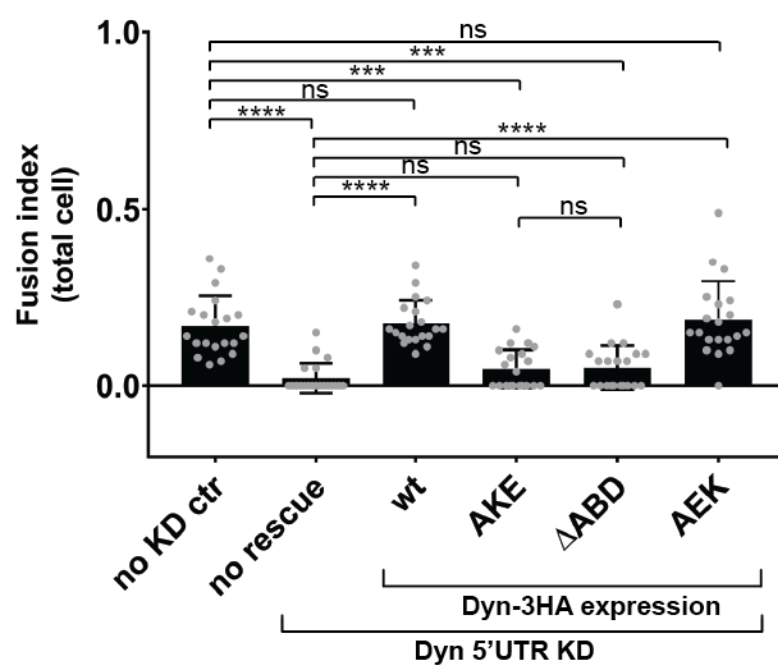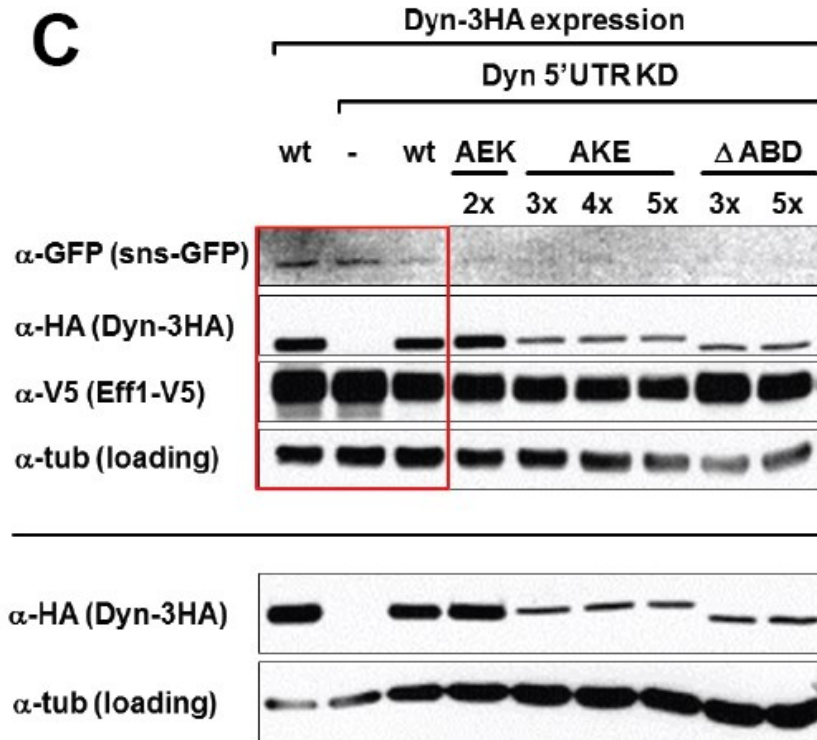
Figure 2.25 Dyn mutants reported to be deficient in their F-actin binding ability fail to rescue S2R+ fusion defect caused by 5'UTR KD

(A) S2R+ cells were treated with dsRNA against Dyn's 5'UTR and co-transfected with Eff1 and Sns and well as wt and mutant Dyn. Both actin binding mutants (AKE and ∆ABD) failed to rescue S2R+ fusion. Note: Sns-GFP transfer didn't work well, but the first two lanes shown that there are similar levels of sns-GFP in no KD ctr with wt shi-3HA expression and Dyn KD cells no rescue (inside the red rectangle). Also note that tubulin

loading lane transfer is uneven in corners. These technical difficulties do not change the interpretation of the data.

(B) Quantification of S2R+ fusion observed in (A). Same data is shown normalized to transfected cells (B) and total cells (B') both are shown because data in (B) may appear like a bimodal distributions but instead is a result of a smaller imaging frame. The bar graph shows the mean and standard deviation. Additionally, the grey dots show each individual value. Statistical significance analysis was performed with ANOVA Tukey's multiple comparison test. Adjusted P-values are denoted as follows: * for $p<0.05$, ** for $p<0.01$, *** for $p<0.001$, **** for $p< 0.0001$ and ns for non-significant).

(C) Western blot analysis of the expression of the different contracts. The actin binding mutants have a much lower expressed protein amounts even after the input vector amount was increased up to 5 fold

(D) .Location of the residues mutated in actin binding mutants.

Table 7 *Drosophila* homologues of previously characterized F-actin binding Dyn mutants

Mammalian Dyn mutation	Effect	*Drosophila* position
AKE	diminished actin binding	K410, R411, K417, K422 to E
AEK	Increased actin binding	E418 and 430 to K
ΔABD	diminished actin binding	ΔF362-A440 (insertion of KL between I394-K441)

A

Dyn-3HA	Tf-488	TfR	merge+Dapi

no rescue

wt

3xAKE

Dyn-3HA	Tf-488	TfR	merge+Dapi

5xAKE

5xΔABD

2xAEK

B

C
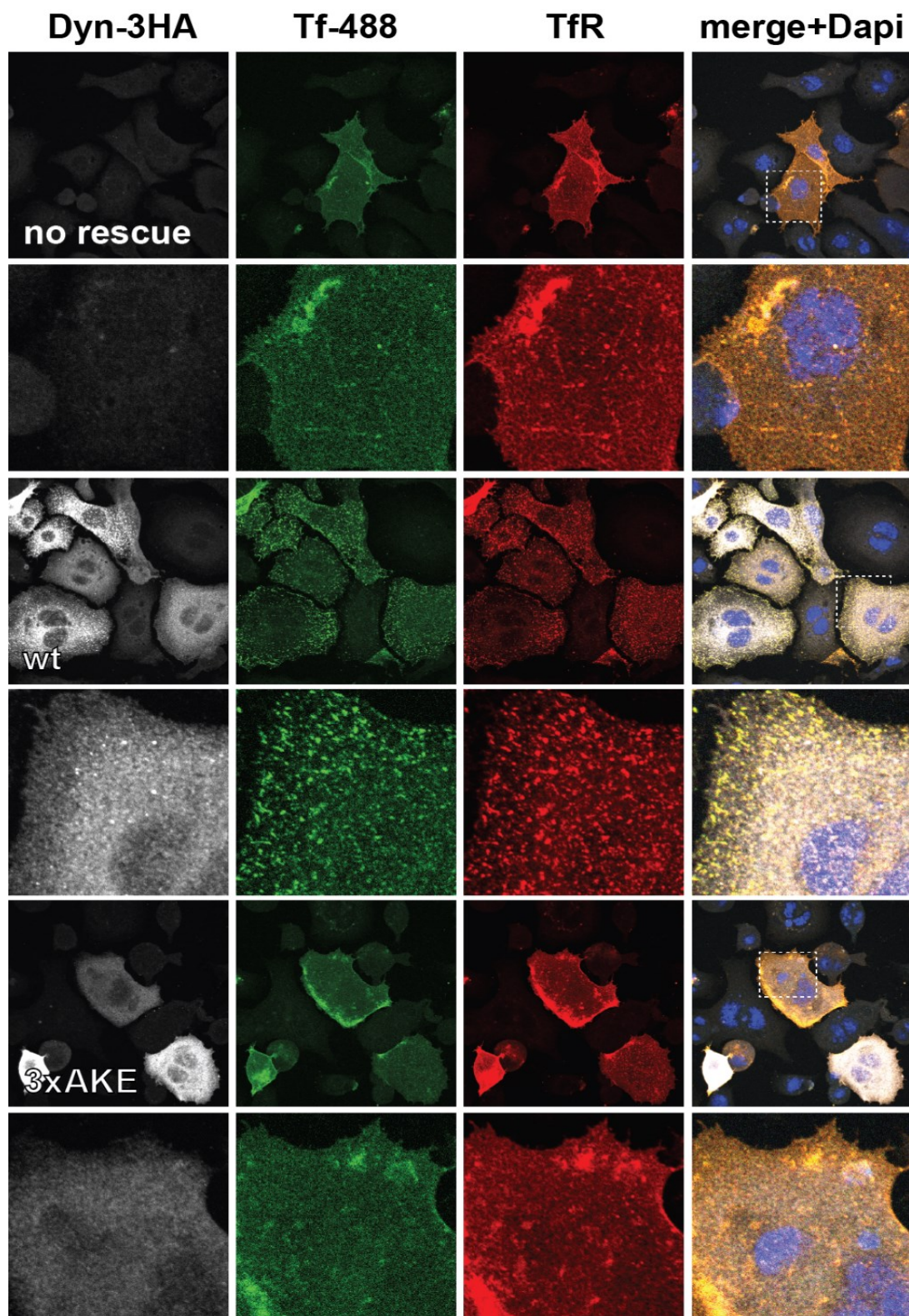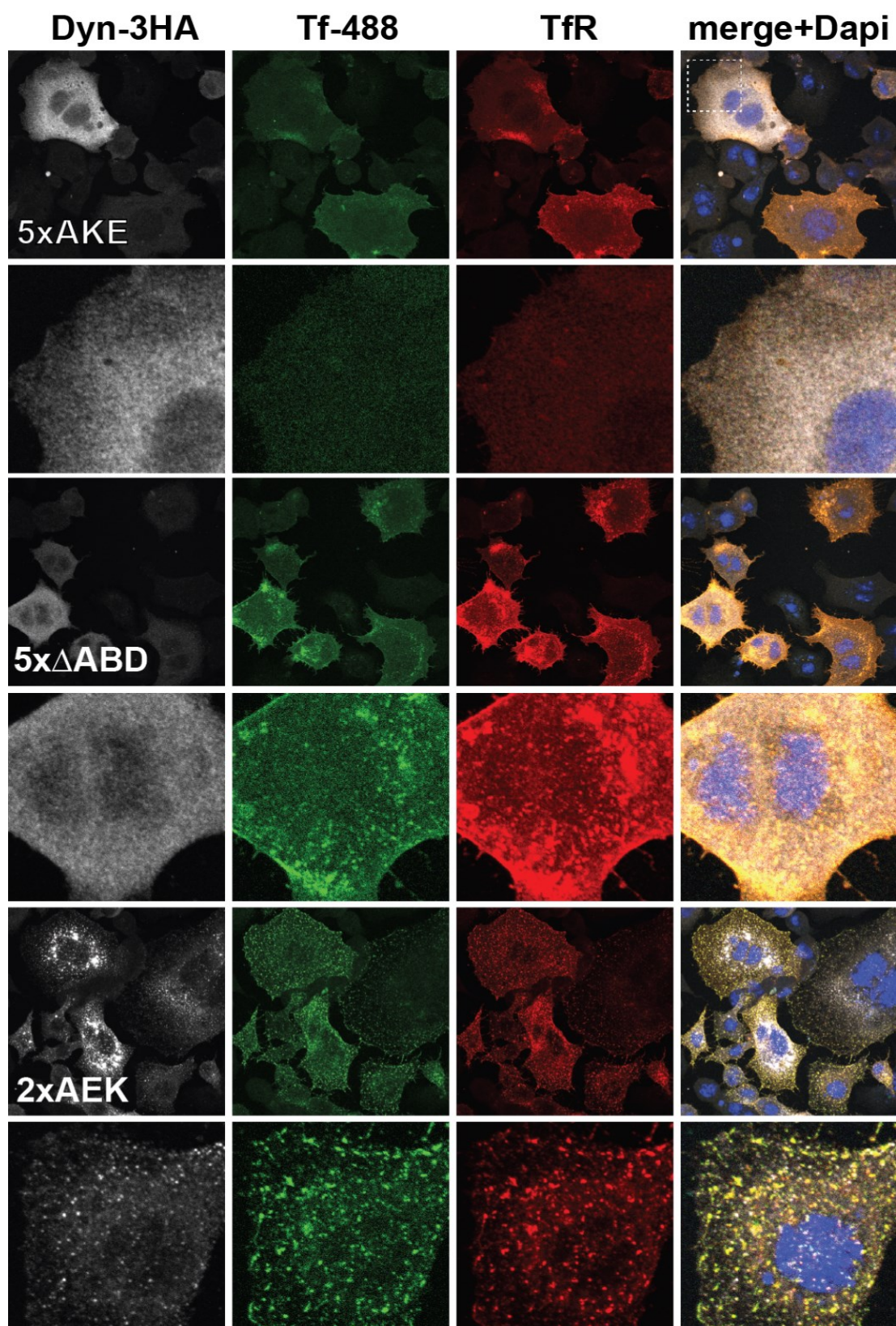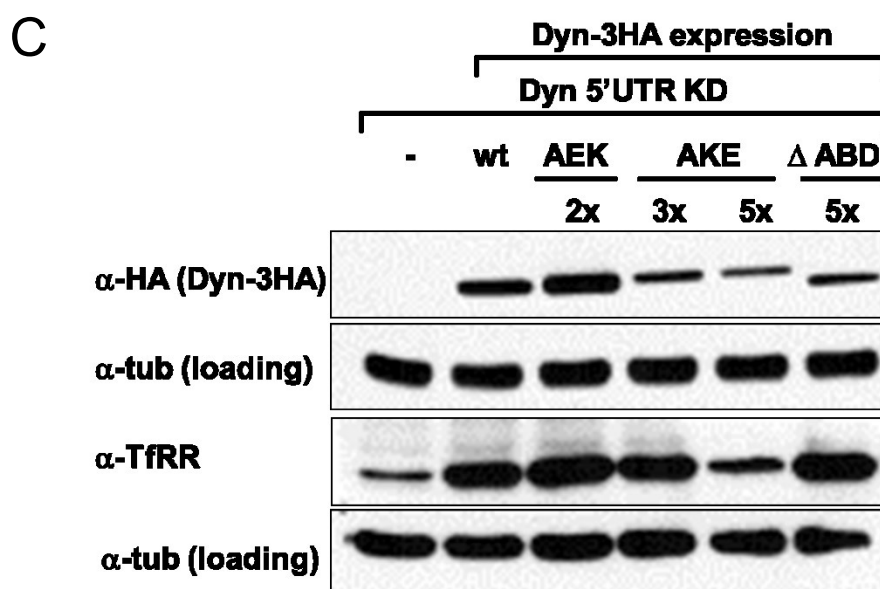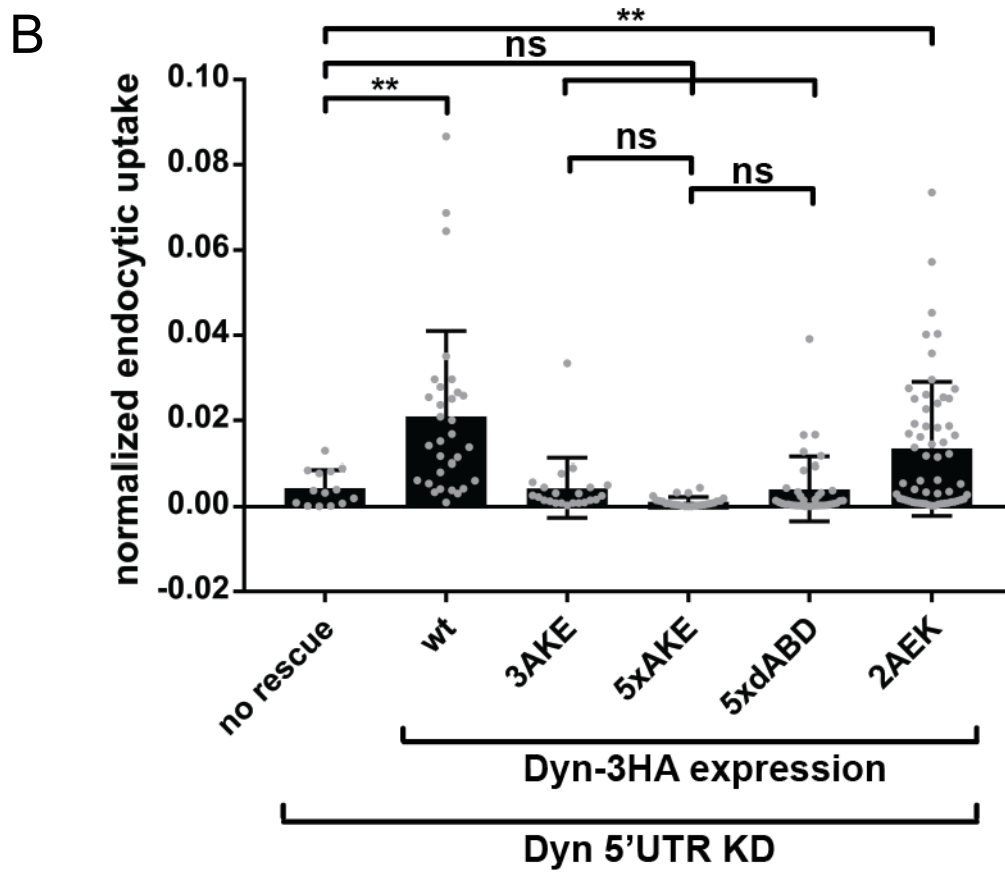
Figure 2.26 Dyn mutants reported to be deficient in their F-actin binding ability fail to rescue S2R+ endocytosis defect caused by 5'UTR KD

(A) S2R+ cells were subjected to Dyn KD using dsRNA against Dyn's 5'UTR and then transfected with mammalian Transferrin receptor (TfR, red) and either empty vector or Dyn3HA wt or several point mutants (grey). These cells were then allowed to internalize conjugated Transferrin-488 (Tf-488, green) for 5 minutes through receptor-mediated endocytosis. Then the cells were subjected to an acid wash which removes all surface bound Tf-488 from the cells. Dyn KD cells are unable to endocytose the Tf-488, so it remained bound to the receptor on the surface and washed away by the acid wash. Dyn3HA wt is able to rescue the endocytosis defect and Tf-488 is internalized by endocytosis into endocytic vesicles. Both actin binding mutants (AKE and ΔABD) failed to rescue S2R+ endocytic defect.

(B) The endocytic uptake of Tf-488 in (A) was quantified and confirms that AKE and ΔABD mutants can't rescue the endocytic defect caused by dsRNA against Dyn's 5'UTR.

The bar graph shows the mean and standard deviation. Additionally, the grey dots show each individual value. Statistical significance analysis was performed with ANOVA Tukey's multiple comparison test. Adjusted P-values are denoted as follows: * for $p < 0.05$, ** for $p < 0.01$, *** for $p < 0.001$, **** for $p < 0.0001$ and ns for non-significant).

| Dyn-3HA | Tf-488 | TfR | merge+Dapi |
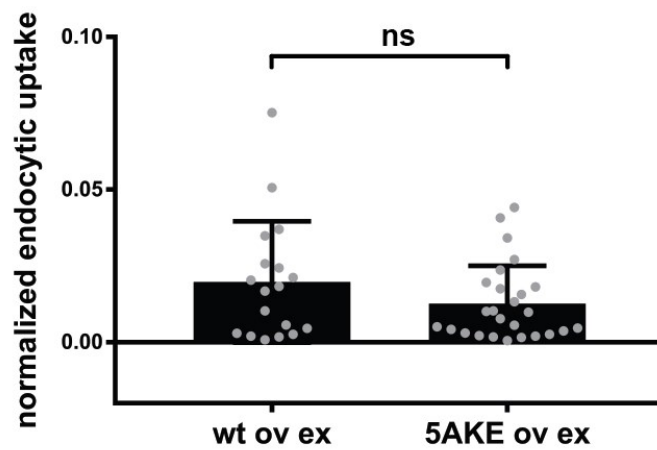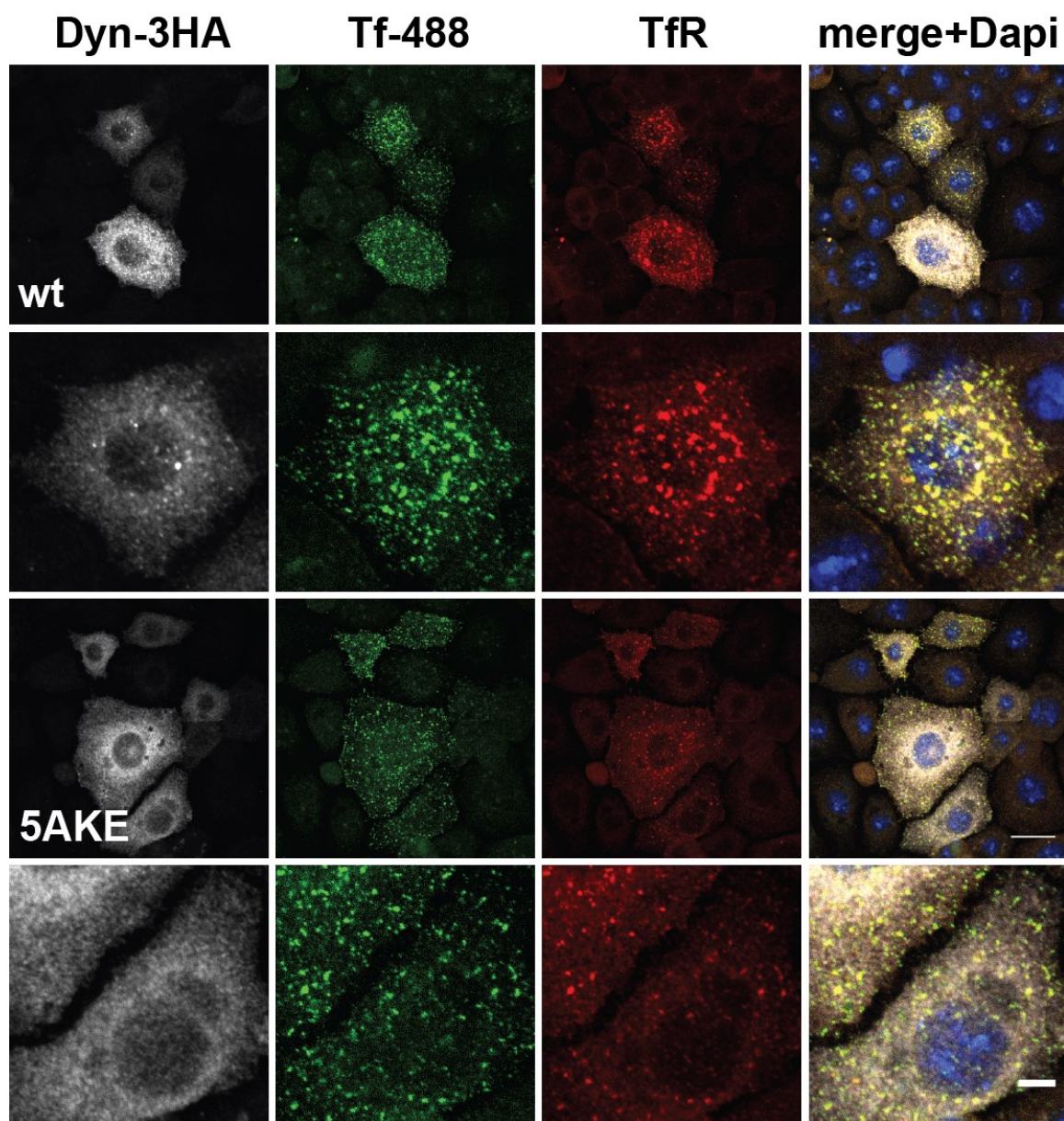
Figure 2.27 Dyn mutant deficient in its ability to bind F-actin does not function as a DN in endocytosis when overexpressed in S2R+ cells

Actin binding mutant AKE was overexpressed in S2R+ cells and assayed for its ability to function as a DN in S2R+ cells endocytosis. AKE is not a DN allele.

The bar graph shows the mean and standard deviation. Additionally, the grey dots show each individual value. Statistical significance analysis was performed with ANOVA Tukey's multiple comparison test. Adjusted P-values are denoted as follows: * for $p<0.05$, ** for $p<0.01$, *** for $p<0.001$, **** for $p< 0.0001$ and ns for non-significant).

Upon site-directed mutagenesis of these residues to negatively charged residues (All K to E, AKE), Dyn's F-actin binding ability was reported to be lost. A second Dyn mutant replace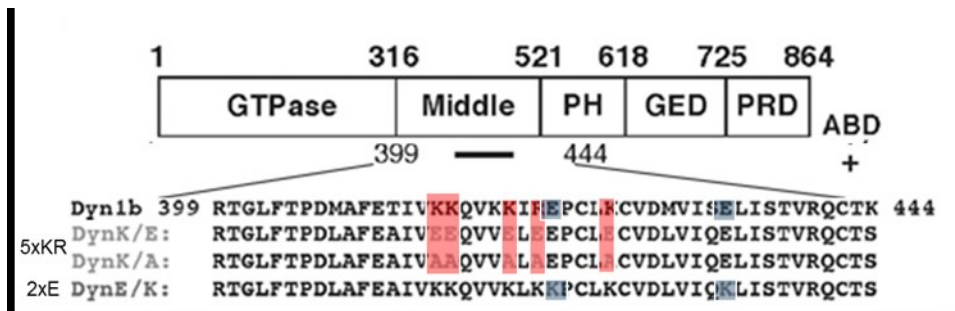d negatively charged residues in the actin-binding domain to positively charged residues (marked blue in Figure. 2.25 D, Gu et al., 2014; All E to K, AEK; Table 7), which had a higher affinity for F-actin. Additionally, same study reported that these mutants do not affect endocytosis when they are overexpressed in mammalian cells.

We wanted to test the *Drosophila* equivalent of these mutants in our system. First, I checked the protein amounts of these mutants when expressed in S2R+ cells using WB. AKE and ΔABD protein amounts were significantly lower. I increased the amount of DNA transected to 3-5 fold and still observed a much lower amount of these mutants (Figure 2.25 C). Despite that I tested their ability to rescue cell-cell fusion when Dyn knocked down using its 5'UTR. AEK but not AKE and ΔABD were able to rescue cell-cell fusion (Figure 2.25 A, B, B'). Next I tested their ability to rescue S2R+ endocytosis. AEK but not AKE or ΔABD rescued endocytosis (Figure 2.26 A, B). I also wanted to confirm that AKE indeed doesn't function as a DN in endocytosis as was reported in Gu et al, 2014 which was the case (Figure 2.27).

The actin binding mutants were unable to separate Dyn's endocytosis-dependent and –independent functions as I initially hoped. This data corroborates my finding with the DN alleles that Dyn's function in endocytosis and cell-cell fusion is correlated.

Part 2.3: FRAP of F-actin focus in *shi^{ts2}* embryos at restrictive temperature

Previous studies in our lab have used fluorescence recovery after

photobleaching (FRAP) to measure the changes in F-actin dynamic at the

fusogenic synapse. The F-actin foci can be visualized when mRFP-Actin is

expressed with *twi*-Gal4 driver. The F-actin foci recover within 5 minutes after

FRAPing (Jin *et al*., 2011) and the several parameters can be extracted from a

modeling the recovering behavior such as $t_{1/2}$ or the time it takes the signal to

recover to half of its end intensity and immobile fraction or what percentage of

original signal doesn't recover. I have measured these values for *w^{1118}* and *shi^{ts2}*

at 32℃ and detected no statistical difference (Figure 2.28). Therefore, it appears

that there is no difference in actin dynamics at the fusogenic synapse in the

Drosophila embryo.
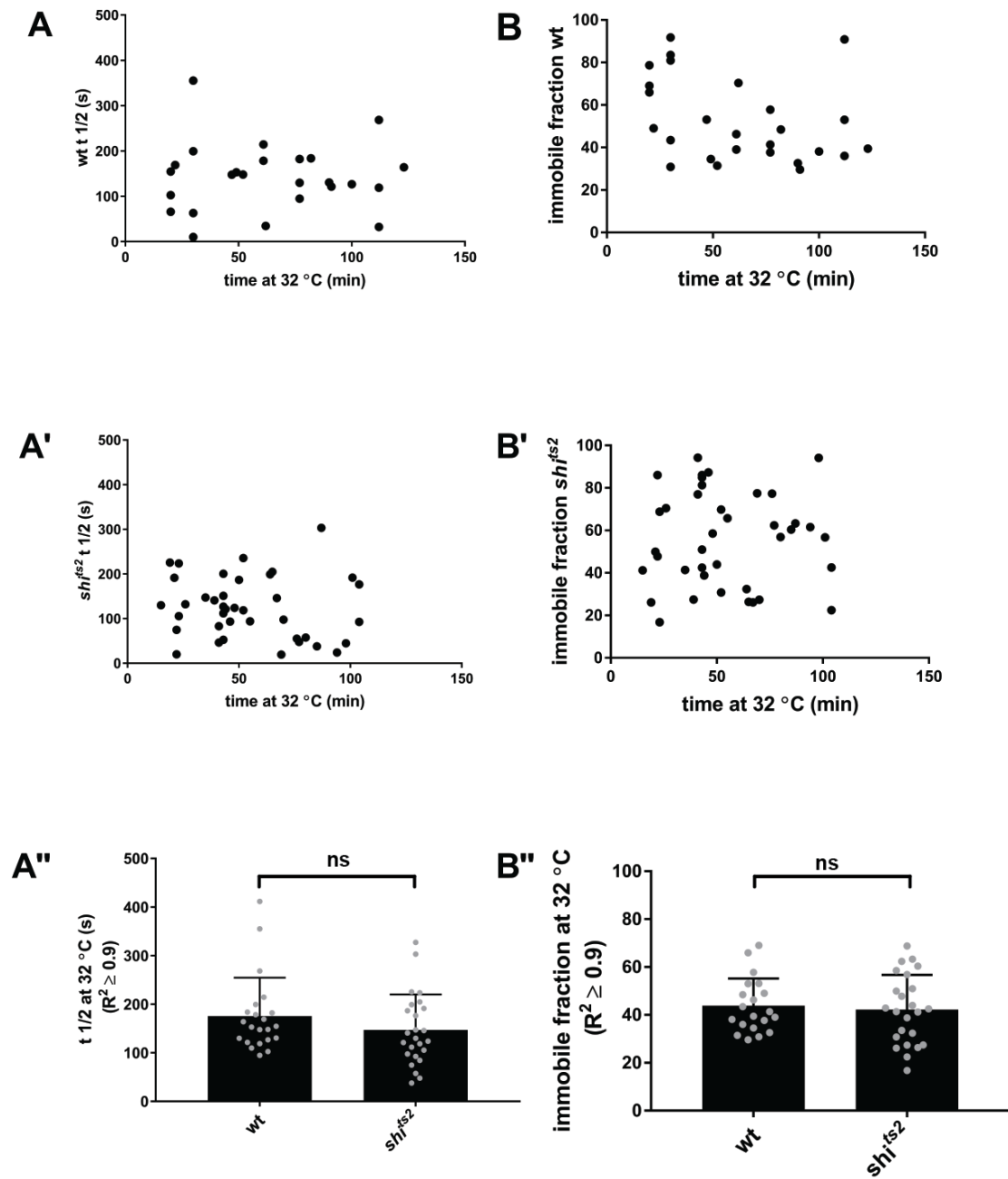
Figure 2.28 No differences in F-actin dynamics were detected in *shi^{ts2}* F-actin foci at restrictive temperature

RFP-actin was expressed in the *Drosophila* mesoderm using *twi*-Gal4 driver and F-actin foci were observed using live-imaging in E14 and early E15 embryos. F-actin foci were bleached and

allowed to recover. The intensity of the F-actin focus was quantified and fitted to determine $t_{1/2}$ and immobile fraction.

(A, A') $t_{1/2}$ values for w^{1118} and shi^{ts2} were plotted over time the embryo was exposed to 32℃. It appears that there was a linear relationship.

(B, B') immobile fraction values for w^{1118} and shi^{ts2} were plotted over time the embryo was exposed to 32℃. It appears that there was a linear relationship.

(A", B") These was no statistical difference in $t_{1/2}$ or immobile fraction between w^{1118} and shi^{ts2} embryos at 32℃. The bar graph shows the mean and standard deviation. Additionally, the grey dots show values whose R^2 value is equal or great to 0.9. Statistical significance analysis was performed with Student's T-Test.

Part 2.4 Gelsolin

Mammalian Dyn has the ability to antagonize Gelsolin's (Gls) binding to barbed ends of F-actin (Gu *et al*., 2010). I wanted to test if Dyn effect on cell-cell fusion was Gls-dependent. If Dyn causes a fusion defect by no longer preventing capping by Gls, knocking down Gls in *shi*^*ts2* embryos at restrictive temperature would decrease the fusion defect. However, when I knocked-down (Gls) in *shi*^*ts2* embryos there was no change in the DA1 count (data not shown). F-actin foci are very dynamic structures, so one would anticipate that if Gls is involved, that a loss of Gls would also lead to a fusion defect, since many more barbed ends would be uncapped. I examined the body-wall musculature of Gls deficiency line and saw no fusion defect despite low maternal loading (FlyBase; data not shown). Furthermore, I checked for an enrichment of Gls at the F-actin focus using α–Gls antibody in wt and Gls deficiency lines and saw a signal in both genotypes. Since it is likely that the Gls does not have a large maternal contribution this would indicate that the staining is non-specific but this conclusion needs further testing. I also knocked down Gls in S2R+ cells and saw no change in the fusion index. In summary, while my data does not exclude Gls as a contributor to cell-cell fusion, it is suggesting that it may not be a major component.

Part 2.5 Conclusion

I have shown that Dyn localizes to the fusogenic synapse in *Drosophila* embryo and fusing S2R+ cells. Furthermore, Dyn disruption (ts alleles in *Drosophila* or

Dyn KD in S2R+ cells) significantly and drastically decreases fusion. The F-actin foci in the heat shocked *shi*^{ts2} embryos have an aberrant morphology and decreased invasiveness. We think that this defect is caused by Dyn's endocytosis-independent functions based on Dyn striking colocalization with F-actin which hold true through its dynamic life-cycle. Additionally, we do not see an enrichment of clathrin at the fusogenic synapse and see no enrichment of clathrin coated pits at the fusogenic synapse in the EM images of the *shi*^{ts2} embryos at restrictive temperature. I also used the S2R+ cell-cell fusion to investigate the mechanism of Dyn's function and also see a colocalization with F-actin foci in the attacking cells.

Dyn is dimer/tetramer that assembles into higher order oligomer for its function. Dyn is also a GTPase and its catalytic activity is highly enhanced upon assembly. Furthermore, Dyn is able to use the energy from GTPase hydrolysis to perform conformational changes throughout the molecule. Structure-function studies showed that Dyn has a highly correlated function between cell-cell fusion and endocytosis. This is consistent with Dyn's array of intra- and intermolecular function being similar in both processes. However, based on my data exclusively, I cannot rule out endocytosis a cause or contributor to the observed fusion defect. However, these is some suggestion that *shi*^{ts4} may separate Dyn's endocytosis dependent and –independent function but this needs further investigation.

Part 2.6 Dyn biochemical studies implicate its direct binding to F-actin as a probable mechanism for cell-cell fusion

Ruihui Zhang, a postdoctoral fellow in our lab has conducted a series of experiments with purified Dyn. He has shown that Dyn binds and bundles F-actin in co-sedimentation assays and negative stain EM and that this binding is concentration dependent. Using negative stain EM he has shown that Dyn forms regularly spaced repeated units around the F-actin bundle which are likely to be Dyn rings of roughly 31 nm diameter. Addition of GTP leads to a disassembly of these Dyn rings.

Furthermore, he has shown that ts mutants and the endocytic mutants are also capable of bundling F-actin. However, the GTP-dependent disassembly is significantly impaired in these mutants suggesting that Dyn oligomer disassembly may contribute to the fusion defect. Furthermore, when Ruihui tested the ability of Dyn wt or mutants to affect Arp2/3-mediated branch formation on existing F-actin filaments he observed that Dyn ts2 prevented branch formation which is a possible mechanism leading to the aberrant F-actin foci morphology of the *shi*[ts2].embryos.

Discussion

I found that Dyn's function in cell-cell fusion and endocytosis is highly correlated in my S2R+ experiments. Dyn dimers/tetramers assemble into oligomers that use energy released by the GTP hydrolysis. GTPase domain mutants (Q40E, S45N, K142A, D180A) interfere with Dyn's ability to bind GTP, experience the oligomerization-based enhancement of GTPase activity and to transmit this energy via conformational changes throughout the Dyn oligomer. It makes sense that these mutants would affect both processes. Similar to endocytosis, Dyn forms an oligomer and performs GTP-dependent mechanical work. However, unlike in endocytosis, Dyn does not form a ring around membrane neck of the vesicle but instead on an F-actin bundle.

We initially hypothesized based on the striking colocalization of Dyn and F-actin at foci that Dyn's function in cell-cell fusion will be independent of Dyn's ability to bind and affect the cell membrane. I533A is in the variable loop that inserts into and destabilizes the plasma membrane. At first it was very surprising that the Dyn's PH domain mutant I533A was not able to rescue cell-cell fusion and had a DN effect. We do not yet understand the effect of this mutant especially because the PH domain is not involved in F-actin binding. A more detailed understanding of Dyn's F-actin binding may provide insight into this mutant.

Additionally, it is interesting that K142A functions as a weak DN in *Drosophila* endocytosis but does not have a DN effect in cell-cell fusion, especially considering that it is a strong DN in the mammalian system. It would

134

seem that similar to the *ts4* alleles, it shows a slight mismatch between the mutants effect on endocytosis and cell-cell fusion. Both mutants may prove to be interesting for further investigation.

The main support for our hypothesis that Dyn's function in cell-cell fusion is independent of endocytosis comes from the striking effect of Dyn on the F-actin foci invasiveness and the lack of endocytic pits at the fusogenic synapse in the *Drosophila* embryo. This interpretation is further strengthened by the biochemical assays placing Dyn as a direct modulator of F-actin. Super-resolution and EM images in our lab have shown that Dyn oligomer indeed accumulated on F-actin bundles in S2R+ foci further strengthening this interpretation.

Taken together, these results lead us to formulate the following model. Duf and Sns engagement upon attachment of founder cells/myotubes and FCM leads to the activation of Sns and the phosphorylation of its cytosolic tail. This in turn recruits SH2-SH3 adaptor proteins in the FCM – based on our S2R+ data we postulate that Crk, Drk and Dock will be recruited. These in turn (or at least drk and dock) recruit Dyn via its PRD. The adaptor proteins are also recruiting in parallel the F-actin regulatory machinery which ultimately leads to the initiation of the F-actin formation. We postulate that while the initial F-actin focus formation does not require Dyn, the focus maturation requires Dyn oligomerization at the fusogenic synapse. Dyn oligomer will undergo cycles of assembly and disassembly and bundle F-actin in some areas of the focus. This is required for the invasiveness of the focus and successful fusion. In *shi^{ts2}* mutant the GTP-

dependent disassembly is inhibited and that prevents Arp2/3 from finding new binding sites and continue to make branches. This in turn leads to an aberrant morphology of the Foci and a decreased invasiveness and ultimately a fusion defect.

Dyn has been implicated in mammalian cell-cell fusion (Shin *et al*., 2014). The investigators proposed a mechanism in which actin-rich protrusions in the attacking cell and clathrin-coated pits in the receiving cell mediate cell-cell recognition leading to cell-cell fusion. It is possible that Dyn's F-actin bundling function is required in *Drosophila* and mammals, but in mammals Dyn also acquired an additional role in the receiving cell that is endocytosis-dependent. Further investigations are needed to confirm this hypothesis.

Chapter 3: Materials and Methods

Fly genetics

Fly stocks were obtained from the Bloomington Stock Center (Bloomington, IN), except for the following: sns-GAL4 (Kocherlakota et al., 2008); rP298-GAL4 (Menon and Chia, 2001). Additionally, shi^4, shi^{TP1}, shi^{TP4}, shi^{TP5}, shi^{TP9}, shi^{TP12} were a gift from M. Ramaswami.

Adult paralysis assays at restrictive temperatures

I wanted to confirm the temperature sensitivity of shi^{ts} alleles by exposing adult flies to restrictive temperatures (32 and 37 C). 10 flies were placed into an empty vial (with small holes drilled into it to allow faster equilibration of temperature) and put into an incubator. The amount flies paralyzed (no longer standing on their feet and typically lying belly up at the bottom of the vial.) was recorded over time. Each genotype was tested either in triplicate or quadruplicate for each gender. For shi^{ts1} and shi^{ts2} there was no difference and there was a small difference for shi^{ts4} between males and females at 32 and 37℃, so both genders were combined for analysis since this is also the case in the embryo fusion defect experiments.

Fusion defect detection at restrictive temperature

Detection of the fusion phenotype in temperature-sensitive *shibire* alleles was done with the following protocol: embryos were collected for 1 hour at 20℃ and allowed to proceed with embryogenesis at 18℃ for 15-16 hours upon which they were heat-shocked or 4 hours at 32 or 34℃. For some experiments, this

protocol was slightly modified as follows: 1. in order to determine if heat-shocking more carefully staged embryos would lead to a more severe phenotype egg collection was done for 30 min and embryogenesis was allowed to proceed for 13-16 hours with 30 min intervals. 2. For some experiment egg collection was done for 2 hours (my data showed that collecting embryos for 1 hour and incubating from 15 hours or 16 hours was not statistically different, so I collected eggs for 2 hours and incubated for 15 hours in later experiments). Experiments involving the detection or measurement of F-actin foci were done with the same protocol as the detection of fusion defect except that the heat shock was only 2 hours long. The embryos were transferred into 1.5 mL tubes and placed into a myBlock Mini Digital Dry Bath (Benchmark) for the heat shock. Washing and dechlorination was done on warm heating block with pre-warmed reagents.

Fixation and devitalization protocol

The heat-shocked embryos were dechlorinated with 50% bleach for 2 minutes and thoroughly rinsed before being incubated in 1:1 heptane/4% formaldehyde in PBS buffer for 20 min with vigorous shaking. The mixture was allowed to stand for the phases to separate and the lower phase was removed using a pipette. Next, the embryos were devitalized by addition of equal volume of methanol and a short vigorous shake. The embryos were washed in methanol and transitioned into a PBS butter containing 0.2% BSA and 0.1%Triton (PBST) in preparation for staining.

Alternatively, the embryos were fixed in formaldehyde-saturated heptane (1:1 mix of 37% formaldehyde and heptane, shaken well and left overnight) for 1 hour at room temperature and transferred onto double sided tape in a plastic petri dish for hand-devitalization. This protocol was necessary for phalloidin staining and a preferred protocol for fusion defect detection because it allowed to visually confirm embryo staging through embryo morphology.

Immunohistochemistry

Primary and secondary antibodies were added and incubated either for 1-2 hours at room temperature or overnight at 4℃.

The following antibodies were used: rabbit anti-muscle myosin heavy chain (1:1000; Kiehart and Feghali, 1986); rat anti-TM (1:1000); rabbit anti-Sns (1:400; Galletta *et al*., 2004); rabbit anti-Dmef2 (1:800; Nguyen *et al*., 1994); rabbit anti-Lmd (1:800; Duan *et al*., 2001); rabbit anti-Eve (1:30; Developmental Studies Hybridoma Bank, Iowa City, IA); rabbit anti-Ants (1:2000; Chen and Olson, 2001); rabbit anti-GFP (1:500; Invitrogen); chicken anti-GFP (1:5000; Invitrogen); rabbit anti-HA (1:500 ThermoFischer Cat # 715500)

The secondary antibodies used at 1:200 were: Alexa-488, -568, and 647 (Invitrogen) and biotinylated antibodies (Vector Laboratories) made in goat. Vectastain ABC kit (Vector Laboratories) and the TSA system (Perkin Elmer) were used to amplify fluorescent signals.

For staining of F-actin, embryos were fixed and hand devitalized, followed by incubation with FITC/Alexa-488/orAlexa-647-conjugated phalloidin (1 mg/ml) (Sigma) at 1:200 for 1 hour at room temperature.

Confocal imaging of fixed samples

Images were obtained as described in Sens *et al*., 2010. Namely using a LSM 700 Meta confocal microscope (Zeiss), acquired with LSM Image Browser software (Zeiss) and Zen software (Zeiss), and processed using ImageJ.
 All samples were mounted in Vectashield (Vector Laboratories) and imaged at room temperature.

Electron microscopy

The high-pressure freezing and freeze substitution (HPF/FS) method was used to fix fly embryos as described (Sens et al., 2010; Zhang and Chen, 2008). Briefly, a Bal-Tec device was used to freeze stage 12-14 embryos. Freeze-substitution was done with 1% osmium tetroxide, 0.1% uranyl acetate in 98% acetone and 2% methanol on dry ice. After embedding embryos in Epon (Sigma-Aldrich), thin sections (70 nm) were cut with an ultramicrotome (Ultracut R; Leica), mounted on copper grids, and post-stained with 2% uranyl acetate for 10 min and Sato's lead solution (Sato, 1968) for 1 min to improve image contrast. Images were acquired on a transmission electron microscope (CM120; Philips).

FRAP experiments in the *Drosophila* embryo

FRAP experiments were done as described in Jin *et al*., 2011. Embryos were collected, dechorionated with 50% bleach, thoroughly washed, and gently aligned onto the acid-free double-sided tape (Therm O Web), which keeps embryos from rolling and drifting. Subsequently, embryos were covered with a thin layer of Halocarbon oil 700/27 (2:1; Sigma), which allows oxygen exchange and keeps embryos alive. Fluorescent mRFP-actin foci (transgene driven by *twi*-Gal4) were visualized by a Zeiss AxioObserver with 780-Quasar confocal module & FCS. The solid 561 nm laser output was set to 2% to avoid photobleaching and phototoxicity. The pinhole was set to 1.0 AU and four frames were averaged per scan. Five to six prebleached images were first acquired to record the original intensity of the foci. Regions of interest (ROI) (randomly selected actin foci) were identified manually and quickly bleached to around 20% of original intensity. Alternatively, the foci were denoted by regions and photo-bleached using the options provided in the Zen software. Subsequent images were acquired every 30 s. The fluorescence intensity of the pre- and postbleach ROIs was determined using a fixed-size ROI. In addition to ROI, the fluorescence intensity of two regions outside of foci was measured and used to normalize the ROI values to imaging-associated photobleaching. The the half-time (t1/2) of recovery and the immobile fraction (% of original signal intensity that didn't recover) were calculated from the fitted curves by the Prism software.

Reconstitution of cell-cell fusion in cultured cells

S2R+ were cultured in Schneider's medium (Gibco) supplemented with 10%. S2R+ fusion was induced as described by Shilagardi *et al*., 2013. Namely, 1.2×10^6 cells were plated onto 6-well plates and allowed to attach for minimum of 30 min (up to several hours).

Cells were transfected with DNA using the Effectene transfection reagent (QIAGEN) according to manufacturer's instructions which are as follows: to DNA constructs (up to 600 ng) was added the Buffer EC to a final volume of 100 μl. Next 3.2 μl of Enhancer was added, the solution was vortexed for 1 s and incubated at room temperature for 2-5 minutes. To this DNA-Enhancer mixture was added 10 μl of Effectene Transfection Reagent, the solution was vortexed for 10 seconds and incubated at room temperature for 5 to 10 minutes. The transfection solution was then added dropwise to the cells. The transfected constructs were allowed to express for 48 -72 hrs (depending of the apparent cell-cell fusion efficiency which was assessed using a light microscope)

Knock-down experiments

Knockdown of gene transcripts were done using long dsRNA generated by MEGAscript T7 Transcription Kit (Ambion). Synthesized dsRNA were purified using NucAway Spin Columns (Ambion).

Soaking protocol: S2R+ cells were first incubated with 3 μg/ml of dsRNA for 2 days. On the second day a new dose of dsRNA was added to the wells (3 μg/ml) and cells were incubated for another day or two. One day 3 or the cells

were plit, plated, and transfected with tagged Eff-1, Sns (to induce fusion) and Dyn constructs (to assay their ability to rescue cell-cell fusion). Cells were then allowed to fuse for 48 to 72 hours. One day after transfection, an additional dose of dsRNA was added to the wells (3 μg/ml).

Transfection protocol: S2R+ cells (1.2×10^6 cell/well) were plated and allowed to adhere for minimum 30 minutes. Then cells were transfected with Eff-1, Sns, and 100 ng dsRNA (for some experiments the amount of dsRNA was increased) and allowed to fuse for 48 to 72 hours.

Knock down efficiency was monitored using RT-PCR. The total RNA was extracted from cells using RNeasy mini kit (QIAGEN) following the manufacturer's instructions (see protocol in the appendix). Then, 5 μg or 1 μg of total RNA was used to generate cDNA using either SuperScript First-Strand Synthesis System for RT-PCR (Invitrogen) or iScript cDNA Synthesis kit (BIO-RAD), respectively, following the manufacturer's instructions. Then transcript specific primers were used to assay the knock down efficiency and primers specific for ribosome protein 49 (rP49) were used as loading controls. In order to detect PCR over amplification of transcripts that would prevent detection of knockdown a ¼ dilution of the no knock-down control was used.

Coimmunoprecipitation (Co-IP) experiments

Co-IP experiments were done as described in Jin *et al*., 2011. Namely, expression constructs were transfected in S2R+ cells. Cells were harvested, washed with PBS, and incubated in NP40-Triton buffer (10mMTris [pH 7.4],

150mMNaCl, 1mMEDTA, 1% Triton X-100, and 0.5% NP40) containing 1mM

PMSF and protease inhibitor cocktail (Roche) for 30 min at 4℃ with agitation.

After centrifugation, the cleared supernatants were subjected to

immunoprecipitation (IP) followed by western blot. Antibody used for IP: Rabbit

α-GFP (1:1,000); for western blot: rabbit α-HA (1:1000; ThermoFischer Cat #

715500), mouse a-V5 (1:1000; Invitrogen), mouse α-tubulin (1:1000;

Developmental Studies Hybridoma Bank, Iowa City, IA). Secondary anobodies

used for wester blots: α-rabbit/mouse-HRP (1;10,000; Invitrogen) or α-chicken-

HRP (1:20,000, Invitrogen).

Tf-488 uptake experiments

S2R+ cells were transfected with 100 ng human TfR and either empty vector or

respective Dyn construct and allowed to express the construct for >36 hrs. Then

the cells were washed and incubated in PBS containing Ca^{2+}, Mg^{2+}, Glucose and

BSA (called PBS^{4+}) for 30 min. Than the cells were incubated with 5 µg/ml

Transferrin-Alexa-488 (Molecular Probes T-13342) for 5 minutes. Afterwards the

reagent was immediately removed and cells were placed on ice and washed with

cold PBS and acid wash while remaining on ice. Then the cells were fixed with

4% formaldehyde and stained for TfR and Dyn. For detailed protocol see

Appendix.

The images for each condition were acquired using the same settings and

images were analyzed using automatic quantification macro in ImageJ (see

Appendix).

Generation of Shi mutants for S2R+ experiments

Table 8 pAc-shi-3HA was used as the backbone for site-directed mutagenesis. These primer

pairs were used to introduce the appropriate mutation.

Mutation name	Dm position		Primer sequence
ts1	G268D	fw	CCGACCGTCTC**GAC**ACCCCCTACTTGCAG
		rv	CTGCAAGTAGGGGGT GTCGAGACGGTCGG
ts2	G141S	fw	GACAAAGGTGGCCATT**AGC**GATCAACCGGTGGATATTGAGC
		rv	GCTCAATATCCACCGGTTGATCGCTAATGGCCACCTTTGTC
ts4	P171S	fw	GGCTGTGACC**TCG**GCCAATACGGATCTGGC
		rv	GCCAGATCCGTATTGGCCGAGGTCACAGCC
TP4	P133L	fw	CCCTGATCGATTTG**CTC**GGCCTGACAAAGGTGG
		rv	CCACCTTTGTCAGGCCGAGCAAATCGATCAGGG
Q40E	Q35	fw	GTG GTC GGT GGC **GAG** TCA GCT GGC AAG AGT TC
		rv	GA ACT CTT GCC AGC TGA CTC GCC ACC GAC CAC
S45N	S40	fw	CAG CTG GCA AG**A AT**T CCG TTT TGG AGA
		rv	TCT CCA AAA CGG AAT TCT TGC CAG CTG
S45N	S40	fw	GCC AGT CAG CTG GCA AG**A AT**T CCG TTT TGG AGA ACT TTG TGG
		rv	CCA CAA AGT TCT CCA AAA CGG AAT TCT TGC CAG CTG ACT GGC
K142A	K137	fw	CAGGCCTGACA**GCG**GTGGCCATTGGCGATCAACC
		rv	GGTTGATCGCCAATGGCCACCGCTGTCAGGCCTG
D180	D175	fw	ACC CCG GCC AAT ACG **GCC** CTG GCC AAT TCG GAT GCC
		rv	GGC ATC CGA ATT GGC CAG GGC CGT ATT GGC CGG GGT
I533A	I527	fw	CATGGTCATCCAGAACCTTGGA**GCC**ATGAAAGGTGGATCGC
		rv	GCGATCCACCTTTCATGGCTCCAAGGTTCTGGATGACCATG

146

Chapter 4: References

Abrams J.M., Lux A., Steller H. and M. Krieger (1992). Macrophages in
Drosophila embryos and L2 cells exhibit scavenger receptor-mediated
endocytosis. . *Proc. Natl. Acad. Sci*. **89**: 10375-1379.

Antonny B., Burd C., De Camilli P., Chen E., Daumke O., Faelber K., Ford M.,
Frolov V.A., Frost A., Hinshaw J.E., Kirchhausen T., Kozlov M.M., Lenz M.,
Low H.H., McMahon H., Merrifield C., Pollard T.D., Robinson P.J., Roux A.
and S. Schmidt (2016). Membrane fission by dynamin: what we know and
what we need to know. *EMBO*. **35**: 2270-2284.

Artero R.D., Castanon I., and M.K. Baylies (2001). The immunoglobulin-like
protein Hibris functions as a dose-dependent regulator of myoblast fusion
and is differentially controlled by Ras and Notch signaling. *Development*.
128: 4251-4264.

Bataillé L. Delon I., Da Ponte J.P., Brown N.H. and K. Jagla (2010). Downstream
of identity genes: muscle-type-specific regulation of the fusion process. *Dev.
Cell.* **19**: 317-328.

Bate, M. (1990). The embryonic development of larval muscles in *Drosophila*.
Dev. **110**. 791-804.

Baylies M.K. and M. Bate (1996). *twist*: A myogenic switch in *Drosophila*.
Science. **722**: 1481-1484.

Bitoun M., Maugenre S., Jeannet P.Y., Lacène E., Ferrer X., Laforêt P, Martin
J.J., Laporte J., Lochmüller H., Beggs A.H., Fardeau M., Eymard B., Romero
N.B. and P. Guicheney (2005). Mutations in dynamin 2 cause dominant
centronuclear myopathy. *Nat Genet.* **37**:1207–1209.

148

Bour B.A., Chakravarti M., West J.M. and S.M. Abmayr (2000). *Drosophila* SNS, a member of the immunoglobulin superfamily that is essential for myoblast fusion. *Genes Dev*. **14**(12): 1498-1511.

Burger K.N.J., Demel R.A., Schmid S.L. and B. de Kruijff (2000). Dynamin is membrane-active: lipid insertion is induced by phosphoinositides and phosphatidic acid. *Biochemistry*. **39**: 12485-12493.

Chappie J.S., Acharya S., Liu Y., Leonard M., Pucadyil T.J. and S.L. Schmid (2009). An intramolecular signaling element that modulates dynamin function *in vitro* and *in vivo*. *Mol. Biol. Cell*. **20**: 3561-3571.

Chappie J.S., Acharya S., Leonard M., Schmid S.L. and F. Dyda (2010). G domain dimerization controls dynamin's assembly-stimulated GTPase activity. *Nature*. **465**: 435-441.

Chen E.H. and E.N. Olson (2001). Antisocial, and intracellular adaptor protein, is required for myoblast fusion in *Drosophila. Dev. Cell*. **1**: 705-715.

Chen E.H. and E.N. Olson (2004). Towards a molecular pathway for myoblast fusion in *Drosophila*. *Trends Cell Biol*. **14**(8): 452-460.

Chen E.H. and E.N. Olson (2005). Unveiling the mechanisms of cell-cell fusion. *Science*. **308**: 369-373.

Desai C.J., Garrity P.A., Keshishian H., Zipursky L. and K. Zinn (1999). The *Drosophila* SH2-SH3 adapter protein Dock is expressed in embryonic axons and facilitates synapse formation by the RP3 motoneuron. *Dev*. **126**: 1527-1535.

Destaing O., Ferguson S.M., Grichine A., Oddou C., De Camilli P., Albiges-Rizo C. and B. Roland (2013). Essential function of dynamin in the invasive properties and actin architecture of v-Src induced podosomes/invadosomes. *PLoS ONE*. **8**(12): e77956.

Dohrmann C, Azpiazu N. and M. Frasch (1990). A new *Drosophila* homeo box gene is expressed in mesodermal precursor cells of distinct muscles during embryogenesis. *Genes Dev*. **4**: 2098-2111.

Durieux A., Prudhon B., Guicheney P. and M. Bitoun (2010). Dynamin 2 and human diseases. *J. Mol. Med*. **88**: 339-350.

Erickson M.R.S., Galetta B.J. and S.M. Abmayr (1997). *Drosophila* myoblast city encodes a conserved protein that is essential for myoblast fusion, dorsal closure, and cytoskeletal organization. *J. Cell Biol*. **138**(3): 589-603.

Feng H. (2001). Picture story. The separator. *Nat. Struct. Bio*. 8 (4):301-301.

Geisbrecht E.R., Haralalka S., Swanson S.K., Florens L., Washburn M.P. and S.M. Abmayr (2007). *Drosophila* ELMO/DEC-12 interacts with Myoblast city to direct myoblast fusion and ommatidial organization. *Dev. Bio*. **314**: 137-149.

Grigliatti T.A., Hall L., Rosenbluth R. and D.T. Suzuki (1973). Temperature-sensitive mutations in *Drosophila* melanogaster. *Mol. Gen. Genet*. **120**: 107-114.

Guha A., Sriram V., Krishnan K.S. and S. Mayor (2003). *shibire* mutations reveal distinct dynamin-independent and –dependent endocytic pathways in primary cultures of *Drosophila* hemocytes. *J. Cell Sci*. **116**: 3373-3386.

Gupta G.D. Swetha M.G., Kumari S., Lakshminarayan R., Dey G. and S. Mayor (2009). Analysis of endocytic pathways in *Drosophila* cells reveals a conserved role for GBF1 in internalization via GEECs. PLoS ONE. 4(8): e6768. doi:10.1371.

Hakeda-Suzuki S., Ng J., Tzu J., Dietzl G., Sun Y., Harms M., Nardine T., Kuo L. and B.J. Dickson (2002). Rac function and regulation during *Drosophila* development. *Nature*. **416**: 438-442.

Jin P., Duan, R., Luo F., Zhang G., Hong S.N. and E.H. Chen (2011). Competition between Blown Fuse and WASP for WIP binding regulates the dynamics of WASP-dependent actin polymerization *in vivo*. *Dev. Cell*. **20**: 623-638.

Kaipa B.R., Shao H., Schäfer G., Trinkewitz T., Groth V., Liu J., Beck L., Bogdan S., Abmayr S.M. and S. Önel (2012). Dock mediates Scar- and WASp-dependent actin polymerization through interaction with cell adhesion molecules in founder cells and fusion-competent myoblasts. J. Cell Sci. **126**: 360-372.

Kesper D.A., Stute C., Buttgereit D., Kreisköther N., Vishnu S., K. Fischbach and R. Renkawitz-Pohl (2007). Myoblast fusion in *Drosophila* melanogaster is mediated through a fusion-restricted myogenic-adhesive structure (FuRMAS). *Dev. Dyn*. **236**: 404-415.

Kiehart D.P. and R. Feghali (1986). Cytoplasmic myosin from *Drosophila melanogaster*. *J. Cell. Biol*. **103**(4): 1517-1525.

Kim J.H., Peng J., Duan R. and E.H. Chen (2015). Mechanisms of myoblast
fusion during muscle development. *Curr. Opin. Genet. Dev*. **32**: 162-170.

Kim S., Shilagardi K., Zhang S., Hong S.N., Sens K.L., Bo J., Gonzalez G.A. and
E.H. Chen (2007). A critical function for the actin cytoskeleton in targeted
exocytosis of prefusion vesicles during myoblast fusion. *Dev. Cell*. **12**: 571-
586.

Koenig J.H. and K. Ikeda (1989). Disappearance and reformation of synaptic
vesicle membrane upon transmitter release observed under reversible
blockage of membrane retrieval. *J. Neurosci*. **9**(11): 3844-3860.

Kosaka T. and K. Ikeda (1982). Possible temperature-dependent blockage of
synaptic vesicle recycling induced by a single gene mutation in *Drosophila.
J. Neurobiol*. **14**(3): 207-225.

Lee E. and P. De Camilli (2001). Dynamin at actin tails. *. Proc. Natl. Acad. Sci*.
99(1): 161-166.

Loebrich S. (2014). The role of F-actin in modulating Clathrin-mediated
endocytosis: Lessons from neurons in health and neuropsychiatric disorder.
Commun. Integr. Biol. **7**: e28740.

Lu M and K.S. Ravichandran (2006). Dock180-ELMO cooperation in Rac
activation. *Methods Enzymol*. **406**: 388-402.

Marks B., Stowell M.H.B., Vallis Y., Mills I.G., Gibson A., Hopkins C.R. and H.T.
McMahon (2001). GTPase activity of dynamin and resulting conformation
change are essential for endocytosis. *Nature*. **410**: 231-235.

Massarwa R., Carmon S., Shilo B.Z. and E.D. Scheiter (2007). WIP/WASp-based actin-polymerization machinery is essential for myoblast fusion in *Drosophila*. *Dev. Cell*. **12**(4): 557-569.

Mayor S., Parton R.G. and J.G. Donaldson (2014). Clathrin-independent pathways of endocytosis. *Cold Spring Harb. Perspect. Biol*. **1**(1): 1-20.

McNiven M.A., Baldassarre M. and R. Buccione (2004). The role of Dynamin in the assembly and function of podosomes and invadopodia. *Front. Biosci*. **9**: 1944-1953.

Nguyen H.T., Bodmer R., Abmayr S.M., McDermott J.C. and N.A. Spoerel (1994). D-mef2: a *Drosophila* mesoderm-specific MADS box-containing gene with a biphasic expression profile during embryogenesis*. Proc. Natl. Acad. Sci*. **91**(16): 7520-7524.

Nolan K.M., Barrett K., Lu Y., Hu K., Vincent S. and J. Settleman (1998). Myoblast city, the *Drosophila* homolog of DOCK180/CED-5, is required in a Rac signaling pathway utilized for multiple developmental processes. *Genes Dev*. **12**: 3337-3342.

Ochoa G.C., Slepnev V.I., Ringstad N., Takei K., Daniell L., Kim W., Cao H., McNiven M., Baron R. and P. De Camilli (2000). A functional link between dynamin and the actin cytoskeleton at podosomes. *J. Cell Biol*. **150**(2): 377-389.

Orth J.D., Krueger E.W., Cao H. and M.A. McNiven (2002). The large GTPase dynamin regulates actin comet formation and movement in living cells. . *Proc. Natl. Acad. Sci*. **99**(1): 167-172.

Özkan E., Chia P.H., Wang R.R., Goriatcheva N., Borek D., Otwinowski Z., Walz T., Shen K. and KC. Garcia (2014). Extracellular architecture of the SYG-1/SYG-2 adhesion complex instructs synaptogenesis. *Cell*. **156**: 482-494.

Podbilewicz B., Leikina E., Sapir A., Valansi C., Suissa M., Shemer G., L.V. Chernomordik (2006). The *C. elegans* developmental fusogen EFF-1 mediates homotypic fusion in heterologous cells and *in vivo*. *Dev. Cell*. **11**: 471-481.

Pollitt A.Y. and R.H. Insall (2009). WASP and SCAR/WAVE proteins: the drivers of actin assembly. *J. Cell Sci*. **122**: 2575-2578.

Poodry C.A. (1990). Shibire, a neurogenic mutant of Drosophila. *Dev. Biol*. **138**: 464-472.

Pucadyil T.J. and S.L. Schmidt (2008). Real-time visualization of dynamin-catalyzed membrane fission and vesicle release. *Cell*. **135**: 1263-1275.

Ramachandran R. and S.L. Schmidt (2008). Real-time detection reveals that effectors couple dynamin's GTP-dependent conformational changes to the membrane. *EMBO*. **27**: 27-37.

Richardson B.E., Beckett K., Nowak S.J. and M.K. Baylies (2007). SCAR/WAVE and Arp2/3 are crucial for cytoskeletal remodeling at the site of myoblast fusion. *Development*. **134**: 4357-4367.

Rozelle A.L., Machesky L.M., Yamamoto M., Driessens M.H.E., Insall R.H., Roth M.G., Luby-Phelps K., Marriott G., Hall A. and H.L. Yin (2000). Phosphatidylinositol 4,5-bisphosphate induces actin-based movement of raft-enriched vesicles through WASP-Arp2/3. *Cur. Bio*. **10**(8): 311-320.

Ruiz-Gomez M., Coutts N., Price A., Taylor M.V., and M. Bate (2000). *Drosophila* Dumbfounded: a myoblast attractant essential for fusion. *Cell*. **102**: 189-198.

Schäfer G., Weber S., Holz A., Bogdan S., Schumacher S., Müller A., Renkawitz-Pohl R. and S. Önel (2007). The Wiskott–Aldrich syndrome protein (WASP) is essential for myoblast fusion in *Drosophila*. *Dev. Bio*. **304**: 664-674.

Schröter R.H., Lier S., Holz A., Bogdan S., Klämbt C., Beck L. and R. Renkawitz-Pohl (2004). *kette* and *blown fuse* interact genetically during the second fusion step of myogenesis in *Drosophila*. *Development*. **131**(18): 4501-4509.

Sens K.L., Zhang S., Jin P., Duan R., Zhang G., Luo F., Parachini L., and E.H. Chen (2010). An invasive podosome-like structure promotes fusion pore formation during myoblast fusion. *J. Cell Biol.*, **191**(5): 1013-1027.

Sever S., Chang J. and C. Gu (2013): Dynamin rings: not just for fission. *Traffic*. **14**: 1194-1199.

Shelton C., Kocherlakota K.S., Zhuang S. and S.M. Abmayr (2009). The immunoglobulin superfamily member Hbs functions redundantly with Sns in interactions between founder and fusion-competent myoblasts. *Development*. **136**: 1159-1168.

Shin N.S., Choi H., Neff H., Wu Y., Saito H., Ferguson S.M., De Camilli P. and R. Baron (2014). Dynamin and endocytosis are required for the fusion of osteoclasts and myoblasts. *J. Cell Biol*. **207**(1): 73-89.

Shpetner H.S. and R.B. Vallee (1989). Identification of dynamin, a novel mechanochemical enzyme that mediates interactions between microtubules. *Cell*. **59**(3): 421-432.

Strünkelnberg M., Bonengel B., Moda L.M., Hertenstein A., de Couet G., Ramos R.G.P. and K.F. Fischbach (2001). Rst and its paralogue kirre act redundantly during embryonic muscle development in *Drosophila*. *Development*. **128**: 4229-4239.

Takei K., McPherson P.S., Schmidt S.L. and Pietro De Camilli (1995). Tubular membrane invaginations coated by dynamin rings are induced by GTP-γS in nerve terminals. *Nature*. **374**(9): 186-190.

Windler S.L. and D. Bilder (2010). Endocytic internalization routes required for delta/notch signaling. *Curr. Bio*. **20**(6): 538-543.

Yoshiga T., Georgieva T., Dunkov B.C., Harizanova N.., Ralchev K. and J.H. Law (1999). *Drosophila* melanogaster transferrin cloning, deduced protein sequence, expression during the life cycle, gene localization and up-regulation on bacterial infection. *Eur. J. Biochem*. **260**: 414-420.

Chapter 5: Appendix

RNA isolation for RT-PCR from S2R+ cells

(Adapted with no changes from Qiagen RNeasy mini kit)

Protocol:

1. S2R+ cells were grown in to confluency in 6well
2. Before start, **add 10 μL of β-mercaptoethanol (ME) to 1 mL buffer RLT in a fume hood** (mix stable at RT for up to 1 month) here 6.5 uL/650 uL buffer RLT
3. Aspirate medium
4. Disrupt cells by adding **600 ul/well of Buffer RLT (WITH β-ME)**, swirl the plate
5. Pipet lysate directly into a QIAshredder spin column placed in 2 ml collection tube, centrifuge for 2 min at full speed, discard insert
6. Add 1 volume of 70% ethanol (600 uL/well) to the collection tube, mix well by pipetting (viscous).
7. Transfer up to 700 uL into RNeasy spin column (including any precipitate that may have formed) placed in 2 ml collection tube, centrifuge for 15s >/= 10,000 rpm, discard the flow-through
8. On-column DNase Digestion
   a. Add 350 uL of Buffer RW1 to the RNeasy spin column, spin 15s at 10,000 rpm, discard flow through
   b. Add 10 uL DNase I stock sol to 70 uL Buffer RDD, mix gently by inverting the tube
   c. Add the 80 uL DNase I incubation mix directly to spin column and place on bench top for 15 min
   d. Add 350 uL buffer RW1 to spin column, spin for 15s at 10,000 rpm, discard flow through.
9. If don't do DNase, wash 700 uL RW1 wash, spin for 15s at 10,000 rpm, discard flow through
10. Change the collection tube
11. Add 500 uL of Buffer RPE to the RNeasy spin column, spin for 15s at 10,000 rpm, discard flow through
12. Add 500 uL of Buffer RPE to the RNeasy spin column, spin for 2 min at 10,000 rpm, discard flow through
13. Spin once with empty column
14. Place the RNeasy spin column in a new 1.5 ml collection tube. Add 30-50 uL of RNeasy-free water (right in the middle) directly to spin column membrane, spin for 1min at 10,000 rpm to elude the RNA
15. Measure the RNA conc. By nano drop, use RNA-40 settings

Tf-488 uptake experiments

- Let cells grow (>36 hours) at 25°C
- Gently wash cells 3 times in PBS.

Solution	PBS ++++ for uptake experiments (1x)		▾
Desired Volume	500	ml ▾	Reset

Ingredient	Stock	For 1 Liter	For Desired Volume
PBS	liquid	1000 ml	500 ml
IMPORTANT: add CaCl2.2H2O always first!			
CaCl2.2H2O (1 mM final)	solid	147.0 mg	73.5 mg
MgCl2.6H2O (1 mM final)	liquid	203.3 mg	101.65 mg
BSA (0.2 % final)	solid	2000 mg	1000 mg
Glucose (i.e. dextrose; 5 mM final)	solid	900.8 mg	450.4 mg
verify that pH is at 7.4			
alternatively, prepare solution from 1 M MgCl2, CaCl2 and glucose stocks => diluted 1000x and 200x respectively			

- Add 600 µl of PBS^{++++}
- Incubate in PBS++++ for 30 min (because there is transferrin in the serum used in media)
- Prepare 2x solution of ligands (i.e. 10 µg/ml):
  - Tfn-Alexa488 (stock 5 mg/ml, 1:500 dilution): 4.8 µl of stock into 2400µl PBS^{++++}
- Add 750µl of 2x ligand solution to cells and incubate for 5 minutes (i.e. 5 µg/ml):
- When pulse is over, dump medium and place cells on ice – wash immediately with ice-cold PBS (3 times).
- rinse cells with ice-cold acetic acid x3 (0.2M acetic acid, 0.2M NaCl, pH 2.5) to remove surface bound Tf.
- Finally, wash cells twice in ice-cold PBS.
- Fix cells in paraformaldehyde (4 %) for 10 min. (stock is 20%)
- Continue with regular S2R+ staining protocol

ImageJ Macro used to quantify endocytic uptake in S2R cells

```
//put numbers of threshold you'd like to use for analysis

MinThresh = "625";

MaxThresh = "5000";

//Method" NA in your case

Method = "Triangle";

Automatic = false;


dir = getDirectory("Choose a Directory ");

//setBatchMode(true);

OpenList(dir);


function OpenList(dir) {

    list = getFileList(dir);

    for (i=0; i<list.length; i++) {

      if (endsWith(list[i], "/")){

         OpenList(""+dir+list[i]);}

       else {

for (i = 0; i<list.length; i++){

        if (endsWith(list[i], ".tif")){

open(dir+list[i]);

getDimensions(width, height, channels, slices, frames);

}

}}}}


ids = newArray(nImages);

for (j=0; j < ids.length; j++){

selectImage(j+1);

title = getTitle();
```

```
ids[j] = title;}


for (j=0; j < ids.length; j++){

                selectImage(ids[j]);

                imagedir = getDirectory("image");

                z = getTitle;

                run("Set Measurements...", "area redirect=None decimal=2");

                //Point to the slice (i.e. channel) you'd like to remove - currently, we remove Dapi
(channel 3) and HA(channel 1)

                run("Slice Remover", "first=3 last=3 increment=1");

                run("Slice Remover", "first=1 last=1 increment=1");

                run("Split Channels");

                run("Threshold...");

                setAutoThreshold("Huang dark");

                b = getTitle;


                run("Analyze Particles...", "size=20-Infinity show=Outlines display clear
summarize");

                saveAs("jpeg", imagedir+z+"_surfaceAreaTfnR.jpg");

                close();

                selectWindow("Results");

                saveAs("txt", imagedir+z+"_nuclei.txt");

                close ("Results");

                close(z);

                close(b);
}


File.makeDirectory(dir+File.separator+"Results");

selectWindow("Summary");

saveAs("txt", dir+File.separator+"Results"+File.separator+"surfaceAreaTfnR.txt");

run("Close");

run("Clear Results");
```

```
run("Set Measurements...", "area mean redirect=None decimal=2");

ids = newArray(nImages);

for (j=0; j < ids.length; j++){

selectImage(j+1);

title = getTitle();

ids[j] = title;}


for (j=0; j < ids.length; j++){

                selectImage(ids[j]);

                a = getTitle;

                filename = split(a, "-");

                Name1 = filename[0];

                Name2 = filename[1];

                run("Threshold...");

                if (Automatic == true){

                        setAutoThreshold(""+Method+" dark");

                setOption("BlackBackground", true);

                }


                if (Automatic == false){

                setThreshold(MinThresh, MaxThresh);

                setOption("BlackBackground", true);

                }


                b = getTitle;

                run("Set Measurements...", "area mean median limit display redirect=None
decimal=2");

                run("Analyze Particles...", "size=0.07-3.1415  circularity=0.40-1.00
show=Outlines display clear summarize");

                saveAs("jpeg", imagedir+Name2+"_"+Name1+".jpg");

                close(a);

                close(b);
```

```
                }

//setBatchMode(false);

selectWindow("Summary");

saveAs("txt", dir+File.separator+"Results"+File.separator+"Intensities.txt");

run("Close");

selectWindow("Threshold");

run("Close");

if (isOpen("Results")) {selectWindow("Results"); run ("Close");}

while (nImages>0) {

        selectImage(nImages);

        close();}
```

CURRICULUM VITAE

The Johns Hopkins University School of Medicine

Nathalie Gerassimov   April 2019

Educational History:

Ph.D.	2019	Program in Biochemistry, Cellular and Molecular Biology	Johns Hopkins School of Medicine
		Mentor: Elizabeth E. Chen, Ph.D.	
B.A.	2010	Biochemistry	Smith College
A.S.	2008		Cottey College

Other Professional Experience:

Intern	2018-2019	Milken Institute, Washington, D.C. 6 months internship
Intern	2018	MedImmune, Gaithersburg, MD 3 months internship
Research Rotation	2012	Laboratory of Doug Robinson, Ph.D. at Johns Hopkins School of Medicine
Research Rotation	2012	Laboratory of Andrew Feinberg, Ph.D. at Johns Hopkins School of Medicine
Research Assistant	2010-2012	Laboratory of Gudrun Ihrke, Ph.D. At Uniformed Services University of the Health Sciences, Bethesda, MD
Intern	2011	Laboratory of Ma Namboodiri, Ph.D. At Uniformed Services University of the Health Sciences, Bethesda, MD
Undergraduate researcher	2008-2010	Laboratory of Adam Hall, Ph.D. At Smith College, Northampton, MA

Scholarships and Fellowships

2016-2018   American Heart Association Predoctoral Fellowship

2012-2013   Thomas J. Kelly and Mary L. Kelly Young Scholar Award

2009   HHMI Undergraduate Research Fellowship - Smith College

Academic and other Honors

2015   Outstanding journal club presentation award
Department of Molecular Biology and Genetics
Johns Hopkins School of Medicine

2010   B.A. from Smith College, *summa cum laude*

2010   Hellman Award in Biochemistry for outstanding achievement in the second semester of biochemistry, Smith College

2008   All-Missouri First Academic Team, Cottey College

Posters and Abstracts

.N. Gerassimov, S. Kim, A. Mercado Perez, T. Tran, D. Luvsanjav, E.H. Chen. "Dynamin regulates actin cytoskeletal organization during cell-cell fusion."

Platform talk at Annual Drosophila Research Conference, 2017.

Poster presentation at the American Society of Cell Biology Meeting, 2016.

Publications

Nathalie Gerassimov, Ruihui Zhang, Donghoon Lee , John Jimah , Sangjoon Kim , Delgermaa Luvsanjav , Jonathan Winkelman , Marcel Mettlen , Michael Abrams , Raghav Kalia , Peter Keene , Pratima Pandey , Benjamin Ravaux , Ji Hoon Kim , Jonathon Ditlev , Guofeng Zhang , Michael Rosen , Adam Frost , Neal Alto , Margaret Gardel , Sandra Schmid , Jenny Hinshaw, and Elizabeth Chen. The mechanisms of dynamin-actin interaction. *Manuscript submitted for publication.*

Science Communication Experience

2017-2019   Volunteer writer for ASBMB Today
Monthly print and online publication distributed to the 32,000 members of the American Society
for Biochemistry and Molecular Biology
- Wrote ten articles (500-900 words) to highlight research in several scientific fields and the accomplishments of selected scientists

Service Experience

2016   Mentor, Reading Partners

2013   Tutor, Incentive Mentoring Program Baltimore, MD

Teaching and Mentoring Experience

2013 – 2018   **Genetics lecturer** for Summer Academic Research Experience (SARE) program
- Gave an annual lecture to introcude genetics to high

school students

2015-2017   **Research mentor**
- Supervised and trained 2 junior students in their independent research

2013 - 2016   **Teaching assistant**
Fundamentals of Genetics and Macromolecular Structure and Analysis graduate level classes
- Designed and graded a problem set
- Held teaching hours to review subject matter